

Manipulating the Subcellular Localisation of Cell Cycle
Regulators to Break Cell Size Dependency in the
Arabidopsis Root



School of Biosciences, Cardiff University

A thesis submitted in partial fulfilment of the requirements for the
degree of Master of Philosophy, August 2023

Emma Williams

Acknowledgements

First and foremost, I would like to sincerely thank my supervisor, Dr Angharad Jones, for the extensive amount of time and support she has given during, and after the four years of my employment. She has been an incredibly supportive mentor, both in my professional and personal development, and it has been a privilege to be her first employee, and watch her group grow. I am very grateful to my co-supervisor, Professor Jim Murray, who has provided valuable insights and suggestions relating to this project, and who has always been extremely encouraging of my work. I would additionally like to recognise colleagues in Dr Jones' group. Firstly, Dr Billy Tasker-Brown for sharing his research and knowledge as we collaborated on the project, collecting valuable data in the early hours of the morning during his first year of fatherhood. I would also like to thank newer members such as Dr Ashwinie Nagarajah, who was always happy to give advice during the writing process, answering many questions. Additionally, Matthew de Guzman who continued the project by performing a very technical and time-consuming replicate of an experiment in this study. I would like to thank our collaborators Professor Leah Band and Dr Daniel Williamson for providing, and importantly, explaining computational modelling data.

I would also like to express my gratitude to the wider members of the Jim Murray lab. It is a supportive environment, and it has been a pleasure to watch the group change and develop over the years. Specifically, I would like to mention Dr Tamara Lechon Gomez. She is an incredibly talented and hardworking researcher who deserves the utmost recognition. She has helped me immensely during my project, answering technical questions and importantly, being a supportive friend. Additionally, I am very grateful to Ms Jo Kilby, who throughout this time has provided an extensive degree of practical assistance to the entire lab, and who has always looked out for my wellbeing. It has been a pleasure to see her recently finish her Doctor of Philosophy. I would also like to thank Dr Walter Dewitte. He is an incredibly knowledgeable and insightful researcher, who has given me excellent advice in terms of life, science and with regards to my further direction in life.

I would also like to thank Professor Peter Morgan, for his invaluable assistance with my statistical analysis. He went out of his way to think about my data outside of his working hours and consolidate my knowledge of R, helping me select the best statistical models. I appreciate his commitment to the lifelong acquisition of knowledge, in all fields.

Lastly, I would like to profusely thank my parents and sister, for the overwhelming amount of practical and emotional help gave me, particularly during the final stages of my writing. I am incredibly fortunate to be surrounded by such caring and kind people, and acknowledge their direct and indirect roles in helping me complete this work.

Summary

Cell growth and cell division are fundamental processes that govern the size and specialised functions of individual cells and multi-cellular organisms. Regulation occurs at two transitions in the plant cell cycle: G1/S and G2/M. These checkpoints are controlled by proteins which coordinate a sequence of phosphorylation events, eliciting transcriptional changes required for DNA synthesis and mitosis. Cell size control in *Arabidopsis thaliana* has been demonstrated at G1/S, where a molecular mechanism involving the dilution of a cell cycle inhibitor's concentration facilitates cell cycle progression and corrects asymmetric cell size divisions. This is termed "sizer" cell size control. However, the existence of a similar mechanism at G2/M in plants is unproven. This study presents a strategy to experimentally test the relationship between protein concentration and cell cycle progression, with an aim to identify potential G2/M sizer proteins.

To test the effect of changing the concentration of potential sizer proteins on cell size, an inducible dexamethasone (DEX) system was implemented. GLUCOCORTICOID RECEPTOR (GR) reporter proteins, fused to GFP in both the N and C terminal position were constructed to determine the optimal expression cassette design. Six Genes of Interest (GOIs) with potential sizer roles at G2/M were successfully cloned into the system, one of which, (MYB3R3) was analysed in detail. Five homozygous inducible MYB3R3 lines were optimised for induction and examined for changes in root length and cortex cell size. Results revealed that p35s::MYB3R3-GFP-GR roots induced at 100 μ M DEX for 4 days had significantly larger cell sizes compared to their non-induced counterparts, as well as wildtype and reporter control plants. Further, after 15 days, reductions were seen in the biomass of roots and leaves. These results imply a role in cell size control for MYB3R3 where its concentration must dilute below a threshold for division. Overall, this approach provides a system for identifying GOIs with sizer functions, with future applications in elucidating effects on cell cycle progression and gene expression correlated to cell size.

Table of Contents

1. Introduction	1
1.1 The plant cell cycle and cell size	1
1.2 Regulation of the cell cycle in <i>Arabidopsis thaliana</i>	4
1.3 Mechanisms of cell size control	11
1.4 Cell cycle control at the G2/M transition	15
1.5 The use of a GR inducible system to translocate hypothetical “sizer” proteins from the cytoplasm into the nucleus, to break their dependency on cell size	20
1.6 Aim and objectives of the study	24
2. Materials and Methods	25
2.1 Gel electrophoresis	25
2.2 Polymerase chain reaction (PCR) of DNA using Phusion	26
2.3 Purification of DNA from PCR and agarose gels	26
2.4 <i>Escherichia coli</i> transformation	27
2.5 Colony PCR	28
2.6 Plasmid purification	28
2.7 Design of inducible GFP GR reporter fusion protein cassette in both orientations	29
2.8 Reporter and control plasmid constructions using Golden Gate Modular Cloning (MoClo)	30
2.9 NEBuilder HiFi DNA Assembly Strategy	42
2.10 DNA extraction	46
2.11 Genomic DNA Extraction and primer design for GOIs	46
2.12 Sequencing	54
2.13 <i>Agrobacterium tumefaciens</i> transformation	56
2.14 Floral dipping	56
2.15 Plant growth conditions	57
2.16 Fluorescence microscopy	57
2.17 Confocal microscopy	57
2.18 DEX Induction	58
2.19 Root Length Analysis	59
2.20 Cortex Cell length Analysis	59
2.21 Graphs and statistical analysis	60
2.22 Fluorescence Intensity Measurements	61
3. Results	62
3.1 The position of GR within the fusion protein affects functionality in <i>Arabidopsis thaliana</i>	62
3.2 Segregating <i>p35s::GFP-GR</i> transgenics displayed a range of expression, with and without DEX	68
3.3 Selection of reliable homozygous <i>p35s::GFP-GR</i> reporter lines for use as induction controls	73
3.4 Functional expression of genes of interest in the GR inducible system is sequence dependent	78
3.5 Five <i>p35s::MYB3R3-GFP-GR</i> homozygous lines displayed consistent DEX induction	84
3.6 The five homozygous <i>p35s::MYB3R3-GFP-GR</i> lines showed differential responses to DEX induction in terms of root growth	89

3.7 Induction of MYB3R3 resulted in an increase in cortex cell size	94
3.8 MYB3R3 induction resulted in decreased biomass accumulation over time	104
3.9 Successful cloning of multiple candidate sizer molecules through use of the inducible expression cassette	106
4. Discussion	109
4.1 Golden Gate, a modular cloning strategy for large assemblies was successfully implemented to create a GR-based GFP reporter system	109
4.2 Correct orientation of protein domains and inclusion of linkers are factors in the expression of fusion proteins	112
4.3 While the functionality of the inducible <i>p35s::GFP-GR</i> protein was demonstrated, stability of the expression of the transgenic lines produced was variable	115
4.4 A DEX induction protocol and screening procedures assisted in the selection of an inducible GFP-GR reporter protein, for future optimisation of the system	119
4.5 Profiling of homozygous <i>p35s::GFP-GR</i> T4 population found two lines with consistent GFP expression suitable for further DEX induction experiments	121
4.6 A Gibson-based cloning approach was successful for cloning genes of interest into the inducible expression cassette, in a reusable manner	122
4.7 Inducible <i>p35s::MYB3R3-GFP-GR</i> and <i>p35s::SMR2-GFP-GR</i> , but not <i>p35s::MYB3R4-GFP-GR</i> plants were functional in <i>Arabidopsis thaliana</i>	125
4.8 Five homozygous <i>p35s::MYB3R3-GFP-GR</i> lines were obtained for comparison to and optimisation with <i>p35s::GFP-GR</i>	127
4.9 An upper limit of DEX concentration was determined	129
4.10 No distinct trends were seen for MYB3R3 induction on root growth over a three- day period, however plant biomass was reduced after 15 days	131
4.11 Nuclear translocation of <i>p35s::MYB3R3-GFP-GR</i> increased cortex cell sizes in the root apical meristem	134
4.12 Evaluation of the overall success of the induction system	137
5. Future work and perspectives	140
5.1 Continued optimisation of the DEX system	140
5.2. Optimise cell analysis procedures to determine cell lengths of all of the cells in the root	141
5.3 Elucidate the relationship between large induced MYB3R3 cells and cell cycle length	142
5.4 Further candidate sizer testing using the DEX inducible system	144
References	145
Appendices	164

1. Introduction

1.1 The plant cell cycle and cell size

Cell size is a fundamental property of a multi-cellular organism, dictating its overall size, structure, and function. Cell size must therefore be regulated extremely carefully, accounting for tissue specific differences and environmental cues. The mechanisms behind the control and coordination of cell size and number during the development of tissues and organisms are of great interest, across all multi-cellular organisms (Nomoto et al., 2022). However, in plants, many questions remain as to how these processes are spatially and temporally controlled (D'ario et al., 2021; Jones et al., 2017).

Plants contain two pools of pluripotent stem cells, the shoot apical meristem (SAM) and the root apical meristem (RAM). The SAM and RAM give rise to all above ground mass including primordia, flowers and leaves (Chang et al., 2020), and the intricate underground root network, respectively. As roots are primarily responsible for the uptake of vital nutrients to the plant, it is important that they maintain a degree of plasticity (Nieuwland et al., 2009), to respond to abiotic stresses. Therefore, the processes which couple proliferation and differentiation must be tightly, but flexibly regulated.

The plant mitotic cell cycle is characterised by four distinct phases, Gap 1 (G1), DNA Synthesis (S), Gap 2 (G2) and finally Mitosis (M), during which the cell divides into two daughters (Figure 1.1A). During S phase, the DNA content of the cell doubles, before undergoing cytokinesis in M phase (D'Ario et al., 2021). These active stages are separated by two Gap phases, which enable cellular growth. Often, cell division is asymmetric; daughter cells are of unequal sizes at birth (Figure 1.1B), which creates variation within the population of cells (Jones et al., 2017; Willis et al., 2016; Serrano-Mislata et al., 2015). Modelling data have shown that if these differences are not corrected, lineages beginning from larger cells will continue to get bigger and lineages starting from smaller cells continue to become much smaller over subsequent generations (Figure 1.1B; Jones et al., 2017). The consequences of this

would be severe; smaller cells may be limited by the ability to form vital intercellular components, whereas molecules may diffuse across larger cells at slower rates, hindering essential biochemical processes (Jones et al., 2019). Therefore, to correct for differences in cell size of a population at birth, it has been suggested that cell cycle progression must be linked to cell size, so that smaller cells have more time to accumulate mass comparable to larger counterparts (Jones et al., 2017; Willis et al., 2016). It has been experimentally determined in the model plant species *Arabidopsis thaliana* that larger cells do indeed divide more quickly, in comparison to smaller daughters, in the same population (Jones et al., 2017), meaning that variation in cell size at birth is removed during the cell cycle after each round of stem cell division (D'Ario et al., 2021; Willis et al., 2016). However, how this process is coordinated, with respect to how the cell measures its size and triggers division, has yet to be determined.

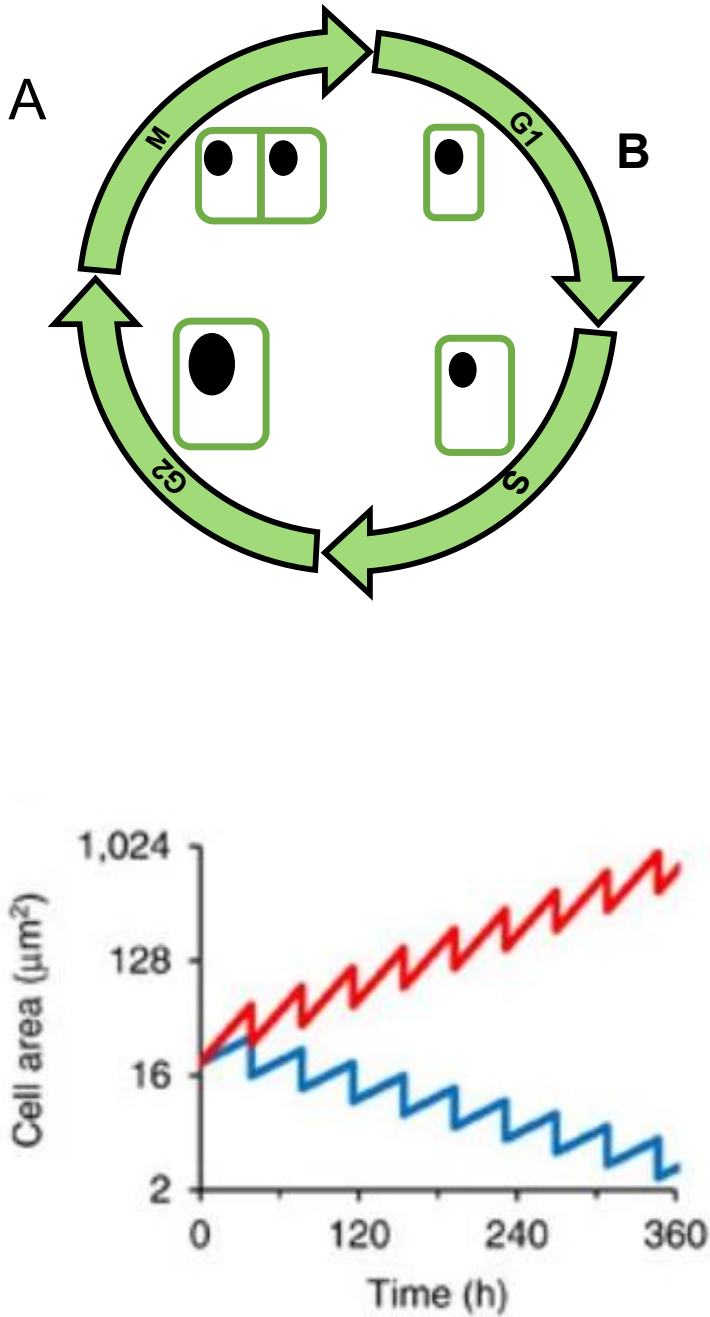


Figure 1.1 The cell cycle and asymmetric divisions in *Arabidopsis thaliana*. A) The four stages of the cell cycle, G1 (Gap 1), S (Synthesis), G2 (Gap 2) and M (Mitosis). A plant cell is shown to start small in G1, start S as a larger cell, double its size and nuclear content during M, before dividing into two symmetrical daughter cells with two nuclei. B) Modelling data showing an uncontrolled asymmetric division over time, where the time taken for a cell to divide is independent on cell size.

1.2 Regulation of the cell cycle in *Arabidopsis thaliana*

How information about cell size is integrated into plant cell cycle progression is not clear. There are two important checkpoints in the cell cycle; the G1/S and the G2/M transitions. Studies using the model plant *Arabidopsis thaliana* have shown that a variety of regulatory proteins govern these checkpoints, with some positively contributing to cell cycle progression, and some acting as repressors (Figure 1.2). Indeed, more than 70 fundamental cell cycle proteins have been identified in *Arabidopsis* (Beemster et al., 2005). Advances have been made in defining the roles of these proteins, including their interactions with each other via transcriptional activation, phosphorylation, and inhibition (Zhao et al., 2012; Boniotti and Gutierrez., 2001; Torres Acosta et al., 2011; Weimer et al., 2016; Yi et al., 2015). Furthermore, the interactions of cell cycle machinery with endogenous developmental hormones have been extensively studied in *Arabidopsis* (Okushima et al., 2018; Magyar et al., 2012; Cruz-Ramírez et al., 2012). This knowledge is fundamental in understanding the spatiotemporal intrinsic regulatory mechanisms which underpin the balance between cell proliferation and differentiation.

Cyclin (CYC) and Cyclin-Dependent Kinase (CDK) complexes are fundamental positive regulators, which propel the cell cycle at both transitions (Boniotti and Gutierrez, 2001; Takatsuka et al., 2009). Research in *Arabidopsis* found that CDKA, a CDK with homology to Cdk1 in mammals could restore functionality to the *cdc28* mutant in yeast (Ferreira et al., 1998), demonstrating that CDK is a highly important protein, conserved across multiple organisms (Porceddu et al., 2001). Its activity is modulated by association with specific cyclins, of which over 50 have been reported in *Arabidopsis thaliana* (Menges et al., 2005). This allows a high number of combinations of CYC/CDK pairs, potentially enabling specificity for different tissues, stages in development and environmental queues. In higher plants, CDKA;1 is expressed throughout the cell cycle, aiding the progression of the cell cycle at both phases (Nowack et al., 2012). Complete loss of CDKA;1 in *Arabidopsis* results in lethality (Nowack et al., 2006), and in tobacco, was shown to inhibit the cell cycle at both G1/S and G2/M transitions, producing larger cells from less frequent cell divisions (Hermerly et al., 1995). This demonstrates a clear role for CDKA in the maintenance of cell division.

Interestingly, higher plants possess a unique set of CDKs; CDKB1;1 and CDKB1;2, which accumulate during late S and M phase, and CDKB2, with expression peaking at the G2/M transition (Menges et al., 2005). The presence of an additional CDK protein, as compared to other organisms, provides further combinations of pairwise CDK/CYC associations, potentially assisting in the high degree of plasticity plants possess in terms of their response to environmental conditions. In contrast to CDKA, the roles of CDKBs in regulation of the cell cycle are less clear. However, a dominant negative mutant study of CDKB1;1 found bigger cells in the SAM with higher DNA content (Boudolf et al., 2004) and micro-RNA depletion of CDKB2 caused defects in the organisation of the SAM (Andersen et al., 2008). Furthermore, in the absence of CDKB1;1, endocycles are promoted (Boudolf et al., 2004), where the DNA content doubles without a division event, resulting in fewer, larger cells. Collectively, these results imply a role for CDKB at promoting entry into mitosis via positive regulation at the G/M transition.

Some CYCs, the activating binding partners of CDKs, have well defined functions in plants, such as the D-Type CYCs which are required for the G1/S transition (Riou-Khamlichi et al. 1999), but functions of many of these CDK partners is still to be determined (Harashima et al., 2013). CYCLIN B1;1 and CYCLIN B1;2 have been shown to form complexes with CDKB, to promote its kinase activity (Figure 1.2), advancing progression through the G2/M transition (Weimer et al., 2016). These complexes are also subject to hormonal regulation (Figure 1.2B). They are heavily influenced by the hormone Auxin, which can directly bind to CYCD, CDKA;1, CDKB1;1, CDKB2;1 and CYCB1;1, reinforcing cell cycle activation throughout the entire cell cycle (Figure 1.2B; Himanen et al., 2002, Okushima et al., 2018). Cytokinin and Brassinosteroid (BR) have also been reported to promote both G1/S and G2/M transitions (Figure 1.2B), via association with CYCD3;1 (Inzé and De Veylder, 2006) and CYC/CDK complexes at both transitions, which also influences the size of the overall meristem (González-García et al., 2011). Further, both stages are negatively regulated by Jasmonate (JA) via suppression of CYCB1;1 and CDKA;1 (Chen et al., 2011), whereas Salicylic Acid (SA) and Ethylene specifically inhibit G2/M via targeting of CYCB1;1 (Pasternak et al., 2019; Street et al., 2015).

Transcriptional regulation of the G1/S checkpoint is well characterised involving RETINOBLASTOMA PROTEIN (RB), CDKA;1's primary target (Nowack et al., 2012), an important cell cycle protein, highly conserved across organisms (Desvoyes et al., 2014); and the E2F transcription factors (De Veylder et al., 2007; Harashima and Sugimoto, 2016). In *Arabidopsis*, at the start of G1/S, RB's homolog RETINOBLASTOMA PROTEIN RELATED (RBR) is in a complex with E2F (Magyar et al., 2012). As cells grow bigger, active CYCD/CDKA;1 complexes increase in number to enable sufficient phosphorylation of RBR, thus triggering dissociation its from E2F (Figure 1.2A). Released E2F is free to dimerise and activate transcription of S-Phase associated genes (Figure 1.2A; Magyar et al., 2012). Hormones also play a role in this process; RBR can inhibit SCARECROW (SCR) – SHORTROOT (SHR), a hormone which assists in the induction of CDKA/CYCD6;1 complexes in an Auxin-dependent manner (Cruz-Ramírez et al., 2012). Auxin additionally activates G1/S phase genes via promotion of E2F activity (Figure 1.2B, del Pozo et al., 2006), by stabilising its interaction with its dimerising partner (not shown for simplicity).

CDK activity during G1/S is modulated by Kip-related proteins (KRPs), important negative regulators of the G1/S transition, of which seven genes have been found in *Arabidopsis* (De Veylder et al., 2001). They provide an extra mode of control through specific inhibition of CDKA;1 (Figure 1.2A; De Veylder et al., 2001) via binding and phosphorylation (Verkest et al., 2005). KRPs are also modulated by hormonal regulation; they can be inhibited via Auxin (Sanz et al., 2011), Gibberellic Acid (GA) (Achard et al., 2009), and Jasmonate (JA) (Chen et al., 2011), whereas their activity is promoted by the DELLA protein GIBBERELIC ACID INSENSITIVE (GAI) (Achard et al., 2009).

Recent research has aimed at elucidating the functions of regulatory proteins at the G2/M checkpoint, a less characterised transition in *Arabidopsis*. Here, a transcriptional network coordinated by members of the R1R2R3-type Myb transcription factor family (Kobayashi et al., 2015) controls entry into M phase. There are five characterised MYB3R proteins (Kobayashi et al., 2015). MYB3R3 and MYB3R5 are repressive MYBs, MYBR4 is an activator, and MYB3R1 has been shown to have dual functionality, working redundantly in complexes of both repressive and activating MYBs (Haga et al., 2007; Haga et al., 2011). Chromatin-

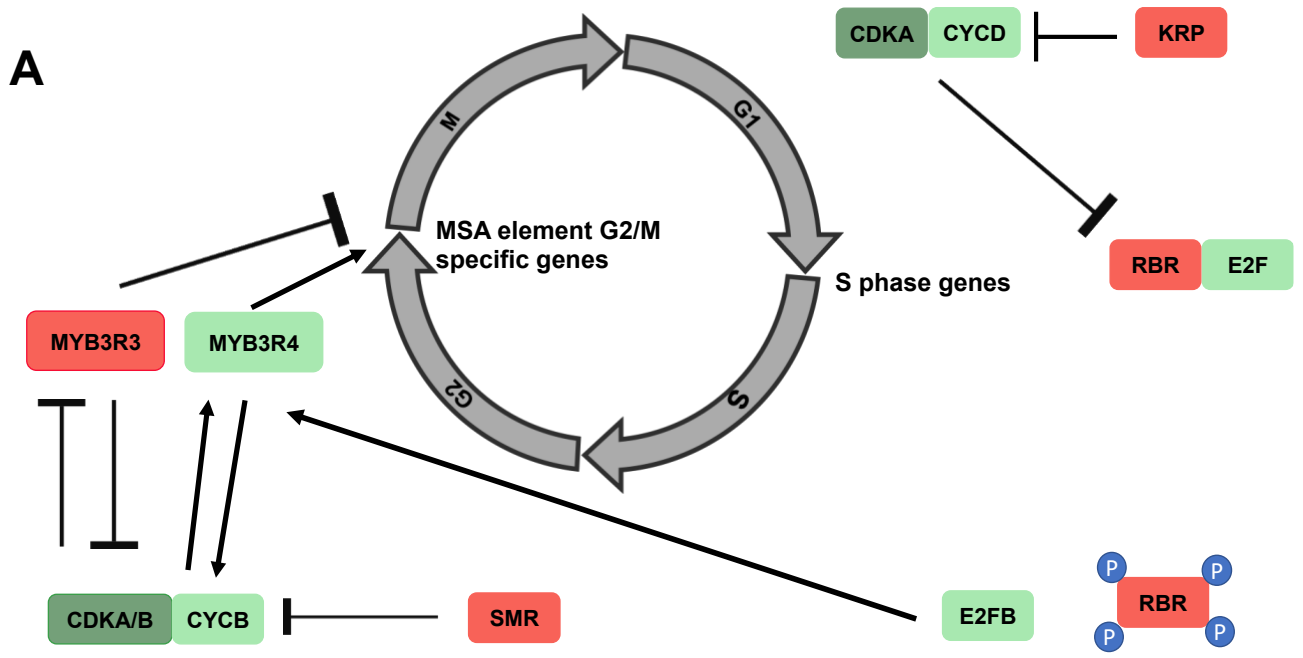
Immunoprecipitation (ChIP) has revealed that these MYBs can bind to the cis regulatory mitosis-specific activator (MSA) elements, characteristic of many genes expressed at G2/M, including CYCLIN B1;2 and KNOLLE (Kobayashi et al., 2015). Therefore, this family of transcription factors plays important, antagonistic roles in the *Arabidopsis* cell cycle.

Regulation of MYB transcription factor activity is achieved by phosphorylation coordinated by CDK; CDK-dependent phosphorylation activates MYB3R4 and inhibits MYB3R3 by targeting it for degradation via the ubiquitin proteolysis pathway (Chen et al., 2017). Thus, the wave of CDK activity at the G2/M transition, specifically produced by CYCB1 and CDKB pairs, is able to initiate the MYB3R mediated transcriptional changes required for the cell to pass through the checkpoint into mitosis (Figure 1.2). As observed at the G1/S transition, CDK inhibitors are also important at the G2/M checkpoint. Members of the SIAMESE-RELATED (SIM/SMR) family are thought to be important negative regulators of the G2/M transition, of which 17 members have been identified in *Arabidopsis* (Kumar et al., 2015). It is believed that some members, SIM (SIAMESE), SMR1, SMR2 and SMR11 can inhibit CDKB1;1 complexes, while the remainder inhibit CDKA;1 (Van Leene et al., 2010; Yi et al., 2015). Similarly to KRP, their activity is promoted hormonally by GAI (Figure 1.2B; Achard et al., 2009). Therefore, KRP and SMR families appear to have distinct inhibitory functions at G1/S and G2/M, respectively (Figure 1.2A).

Throughout the cell cycle, regulatory proteins play fundamental roles in either activating or inhibiting transitions between stages. While studies in *Arabidopsis* have provided information needed to construct a network of both genetic and protein level interactions between cell cycle protein regulators, what remains unclear is how exactly cell cycle transitions are produced as emergent properties of this network, or how cell size information is fed back in. Modelling demonstrates that the relative concentrations of different proteins with respect to one another, the size of the cell, and the phase of the cell cycle are key to producing cell size control behaviours (Williamson et al. 2023). Fluorescently tagged reporter proteins have been useful tools in providing more information on the mass and concentrations of key cell cycle proteins, throughout the cycle (D'Ario et al., 2021; Jones et al., 2017), but further

functional tests are also required to demonstrate the effect of changing protein concentration on both cell size, and length of the cell cycle stages.

To elucidate the answers to these questions, detailed analysis of how the concentrations of these regulatory proteins change throughout the cell cycle, with respect to different cell sizes, is required. Once this information has been obtained, links between regulatory proteins and modes of cell size regulation can be ascertained.



B

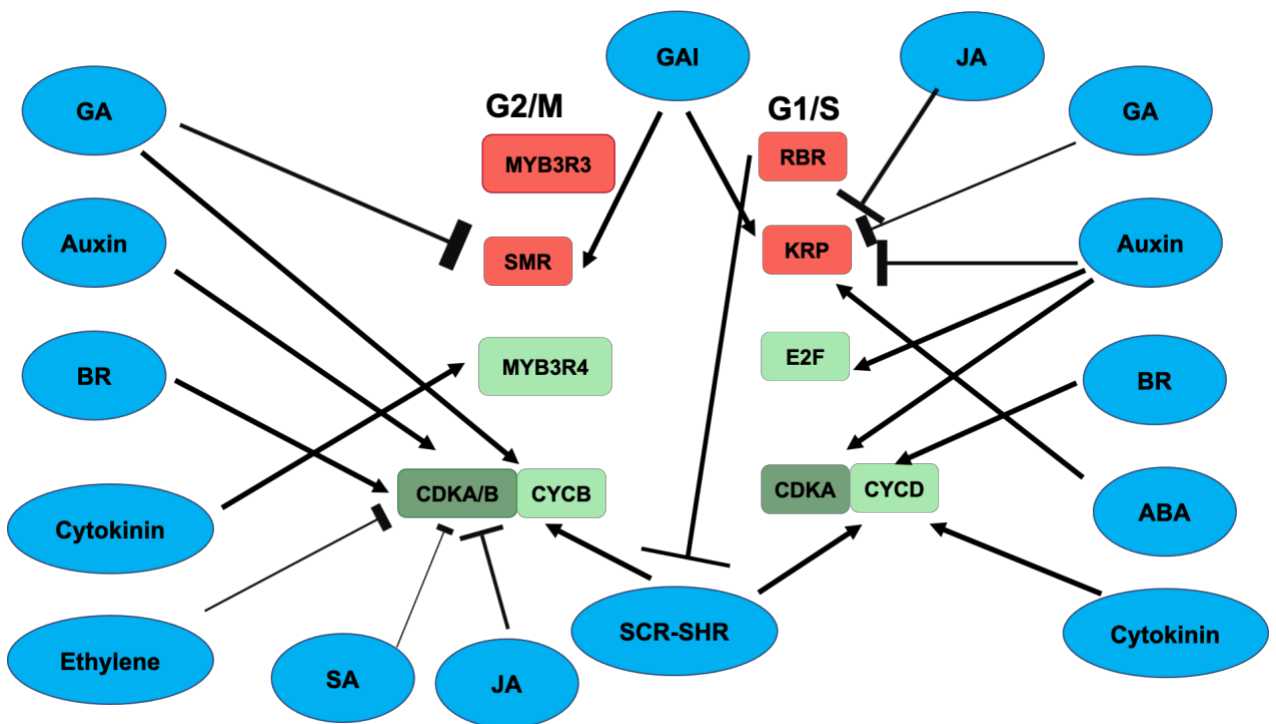


Figure 1.2: The roles of regulatory proteins and hormones in the Arabidopsis cell cycle. In both diagrams, arrows show activation and lines with horizontal bars show inhibition.

Activators of the cell cycle are shown in green. Repressors are shown in red.

A: Schematic of the cell cycle in plants. The four phases are shown by the circular arrows: G1 (Gap 1), S (Synthesis), G2 (Gap 2) and M (Mitosis). S phase genes and MSA element G2/M specific genes are activated at the G1/S and G2/M transitions respectively. At both checkpoints, CYCLIN (CYC) and CYCLIN-DEPENDENT KINASE (CDK) complexes, including CDKA/CYCD at G1/S and CDKA/CYCB at G2/M, drive cell cycle progression. At G1/S, CDKA/CYCD complexes inhibit E2F-bound RETINOBLASTOMA-RELATED PROTEIN 1 (RBR), via phosphorylation which frees E2FB, enabling activation of S phase genes (Boudolf et al., 2004.) KIP RELATED PROTEIN (KRP) complexes can limit this action via inhibition of CYCD/CDKA complexes (Verkest et al., 2005). E2FB promotes the R1R2R3-type Myb MYB3R4, an activator of the G2/M transition, which binds competitively to the MSA element of G2/M specific genes together with an inhibitor, MYB3R3, from the same family of transcription factors (Kobayashi et al., 2015). CDKA/B/CYCB complexes coordinate this phase of the cell cycle, via mutual inhibition and activation of MYB3R3 and MYB3R4, respectively (Kobayashi et al., 2015). SIAMESE-RELATED SMR proteins negatively regulate this transition, via phosphorylation of both CDKA and CDKB, by different family members (Kumar et al., 2015). B: The interaction of Arabidopsis phytohormones (shown by blue ovals) with cell cycle proteins (rectangles), at both G1/S and G2/M. Auxin has roles at both stages of the cell cycle, via inhibition of KRP and promotion of CDK/CYC complexes (Sanz et al., 2011; Himanen et al., 2002, Okushima et al., 2018). GAI activates SMR and KRP, whereas GA inhibits KRP and promotes CYCB activity (Achard et al., 2009). Jasmonate (JA) inhibits KRP at G1/S, and inhibits CDK/CYC complexes at G2/M, showing an opposing role at each cell cycle checkpoint. BR and Cytokinin activate CDK/CYC complexes at both transitions (González-García et al., 2011). SA and Ethylene have repressor functions at G2/M, specifically inhibiting CYCB1;1 (Pasternak et al., 2019; Street et al., 2015). SCARECROW (SCR) – SHORTROOT (SHR) activates CDK/CYC complexes at both transitions, and is inhibited by RBR (Cruz-Ramírez et al., 2012).

1.3 Mechanisms of cell size control

Several mechanisms of cell size control have been proposed across both unicellular and multicellular organisms. “Adders” and “timers” are simple mechanisms, independent of the size of a cell at birth, whereas “sizer” modes of regulations are correlated with cell size (Facchetti et al., 2017). For every cell division, adders incorporate a fixed value onto their cells (Cadart et al., 2018). This is often observed in unicellular organisms such as bacteria and budding yeast (Soifer et al., 2016) and has also been empirically observed in human cells (Cadart et al., 2018). Under timer size control, the length of cell division is always kept constant, again irrespective of cell size heterogeneity in a population. Therefore, this is more suited for cell populations which mostly undergo symmetrical size divisions and unicellular organisms, such as bacteria (Taheri-Aaghi et al., 2015) and budding yeast (Campos et al., 2014), or for specialised functions such as in the *Drosophila* embryo (Clark et al., 2022). Sizers in contrast, have an internal scale, tightly correlated with the size of a cell at birth, which once a threshold is reached, facilitates mitosis (D’Ario et al., 2021; Facchetti et al., 2017). Modelling the behaviour of these mechanisms in terms of size at birth and size at division reveals that of the three, the sizer mode of control is the most efficient to correct for unequal, asymmetric divisions that may take place in the plant meristems (Figure 1.3A; D’Ario and Sablowski, 2019; Williamson et al., 2023). Therefore, this appears to be the most likely mechanism of cell size control, in the meristematic tissues of *Arabidopsis*, which frequently undergo asymmetric cell division (Jonest et al., 2017).

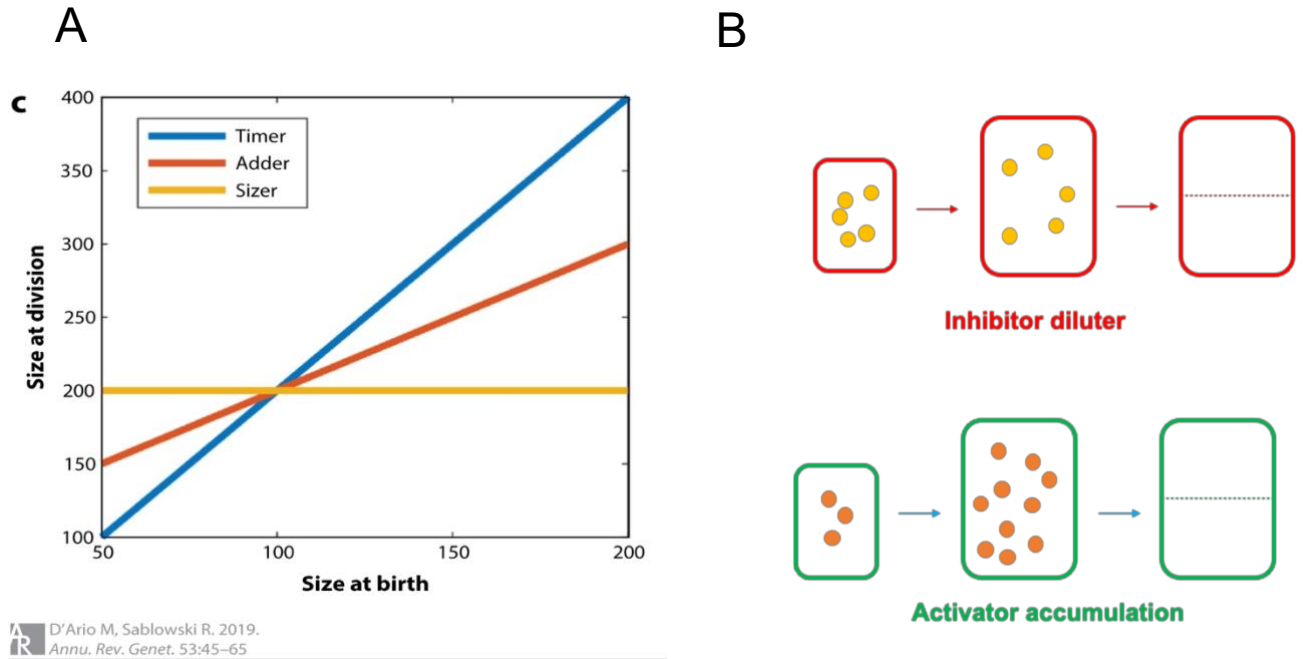
Most sizer mechanisms can be attributed to the concentration of one, or multiple regulatory molecules of the cell cycle. This could be an activator accumulator, where a protein’s concentration rapidly increases as the cell grows and increases its protein synthetic capacity, or an inhibitor dilutor where a fixed mass of protein diminishes in concentration as the cell gets bigger (Figure 1.3B; Williamson et al., 2023). In both cases, cell growth results in a change in protein concentration, reaching a threshold which once overcome, facilitates cell division (Proulix-Giraldeu et al., 2022). Given the large number of positive and negative regulators of the cell cycle at both the G1/S and G2/M transitions, multiple different regulatory proteins (Figure 1.2A) have the potential to act as sizers (Figure 1.3C).

Candidate sizer proteins have been proposed in several organisms. Activator accumulator behaviour has been suggested in fission yeast, where cells shorter at birth undergo a longer cell division, enabling them to elongate to a relatively larger degree prior to division (Fantès et al., 1977). This is due to a well-established positive correlation between the size of a cell and its capacity to synthesise RNA and proteins (Elliott et al., 1979; Sun et al., 2020). Consequently, cells are able to increase the production rate of an activator accumulator as their mass increases, which can then outcompete inhibitory proteins and activate other positive regulators to promote entry through a cell cycle checkpoint (Jones et al., 2017). A recent study in fission yeast used a Förster Resonance Energy Transfer (FRET) approach to show that a CDK, *cdc2*, acts as an activator accumulator at both G1/S and G2/M transitions, by reaching two incrementally higher thresholds (Sugiyama et al., 2023). Similarly, in *Arabidopsis*, modelling data showed that incremental increases in CDK activity at both checkpoints was sufficient to allow progression through the cell cycle (Jones et al., 2017), suggesting it could function as an activator accumulator (Figure 1.3C). However, while CDK concentration can serve as a proxy for the size of a cell at division, its activity could be under the control of another regulatory protein in the cell cycle such as the CYC proteins (Figure 1.2A). Similarly other positive regulators such as E2F and MYB3R4 that promote cell cycle progression through transcriptional control could also facilitate activator accumulator sizer control if they accumulated during the cell cycle (Figure 1.3C).

On the other hand, inhibitor dilution appears to be a more documented route of sizer-mediated control. Here, a protein's mass remains fixed, and its concentration is diminished as the cell increases in size (Figure 1.3B; Williamson et al., 2023). Perhaps the most convincing example of this is in the budding yeast *Saccharomyces cerevisiae*. The protein Whi5, functionally analogous to RBR in plants, has been implicated as an inhibitor dilutor in budding yeast (Schmoller et al., 2015). Here, timelapse experiments were used to quantify the concentration of the Whi5 protein, relative to cell size, finding it to dilute as cells increase in size (Schmoller et al., 2015). Consequently, due to sufficient removal of the Whi5 protein and therefore modulation of its inhibitory effect on the yeast cell cycle, progression through the G1/S checkpoint is facilitated. Whi5 is synthesised just after G1/S, and its rate of

production is related to gene copy number, enabling its concentration to be independent from the rate of its production based on cellular size. This allows it to act as a reliable proxy for cell size at division, where its concentration, rather than mass, can be tightly correlated to the size of the cell (Williamson et al., 2023). This qualifies Whi5 as a sizer protein in budding yeast. The same has been seen in human cells where RB, a homolog of Whi5 and RBR, is synthesised after G1, meaning that, upon division, most RB synthesised is inherited by the daughter cells and diluted based on growing cellular volume (Zatulovskiy et al., 2020). Interestingly, despite its homologs in both yeast and mammals demonstrating sizer capacity, time course data showed that RBR's concentration does not dilute to enable progression through G1/S in *Arabidopsis* (D'Ario et al., 2021), highlighting the differences in cell size homeostasis across species.

Recently, the inhibitor KRP4 has been proposed to control the G1/S transition (D'Ario et al., 2021). Here, KRP4 is bound to chromatin, while free KRP4 in the cell is degraded by F-BOX LIKE 17 (FBL17). Thus, during cytokinesis, when chromatids are split KRP4 is equally inherited by the two daughters. In the case of an asymmetric division, larger cells will have a lower concentration of KRP4 and can therefore divide again quicker, and the reverse is true for smaller cells. This mechanism of sizer control is specifically linked to the chromatin capacity of the cell, and implies a sizer role for KRP4 as an inhibitor dilutor (Figure 1.3C). Further, as KRP is a known CDK inhibitor (Figure 1.2A; Verkest et al., 2005), its dilution could facilitate the cell size proportional accumulation of CDK observed at the G1/S transition (Jones et al., 2017). While the coordination of the G1/S transition is beginning to become clearer, it is unknown as to whether there is a protein subject to the same mechanisms at G2/M, however proteins with positive and negative regulatory roles at this checkpoint (Figure 1.2A; Figure 1.3C) could act as sizers.



C

Protein	Mode	Checkpoint
CDKA	AA	G1/S
CYCD2	AA	G1/S
RBR	ID	G1/S
MYB3R3	ID	G2/M
MYB3R4	AA	G2/M
KRP	ID	G1/S
E2FA	AA	G1/S
CDKB1;1	AA	G2/M
CYCB1;1	AA	G2/M

Figure 1.3: A: Model of timer (blue), adder (red) and sizer (yellow) control, with regards to the relationship of size of a cell at birth to size at division (D'Ario and Sablowski, 2019). B: Hypothetical "sizer" mechanisms, showing the behaviour of an internal protein in the cell (yellow and orange circles) which then divides. Red cells show the proposed mechanism of inhibitor dilution, the green cells show the accumulation of an activator (Image courtesy of Billy Tasker-Brown). C: Table of regulatory cell cycle proteins, hypothesised to be potential sizers in the Arabidopsis cell cycle. AA – activator accumulator, ID – inhibitor dilutor.

1.4 Cell cycle control at the G2/M transition

In light of recent findings at the G1/S transition, the question remained: how is cell size and cell cycle progression controlled at G2/M? Advances in answering these questions have been made via the collection of empirical data using a novel cell cycle marker, *H4::DB-VENUS* (Jones et al., 2017). This enabled live cell imaging to be conducted to track entire cycles, where the length of the cell cycles and phases could be directly measured, and subsequently correlated to cell size. Here, cells in G1 could be separated from actively dividing cells, in S/G2/M. Therefore, the relationship between length and size in both the entire cell cycle, and the lengths of G1, followed by S/G2/M could be determined. Data collected from *in vivo* time courses using these markers showed that larger cells at birth in the SAM exhibited shorter cell cycles, and vice versa (Jones et al., 2017). This phenomenon seen at the later checkpoint was especially pronounced in younger primordia (Jones et al., 2017). The implication of size control at G2/M is consistent with observations in other species; *S. pombe* has been evidenced to have biphasic CDK activity, meeting two incrementally higher checkpoints for cell cycle progression (Coudreuse and Nurse, 2010; Sugiyama et al., 2023) and RB's size activity in humans also occurs at G2/M (Zatulovskiy et al., 2020). Further, modelling experiments have suggested that organisms with a longer G1 and a shorter G2/M are more likely to undergo size corrections, as opposed to a relatively longer G2/M phase, which appears to favour adder control (Proulx-Giraldeau et al., 2022).

The empirical finding of Jones and Colleagues has been explored further by a recent computational model (Figure 1.4) (Williamson et al., 2023) of the protein network that accounts for the transcriptional and translational networks elucidated in previous studies (Kobayashi et al., 2015; Chen et al., 2017). These simulations were carried out to address whether it was necessary to have control in *Arabidopsis* at G2/M (Figure 1.4B and C) in light of robust cell size control demonstrated at G1/S (D'Ario et al., 2021; Jones et al., 2017), and whether it is theoretically possible to generate size dependent progression through G2/M using the known regulatory proteins and components (Figure 1.2B; Figure 1.3C). Following this, regulators which appeared to have potentially important roles in cell size control at G2/M could then be identified and selected for further study. Interestingly, results demonstrated that cell size

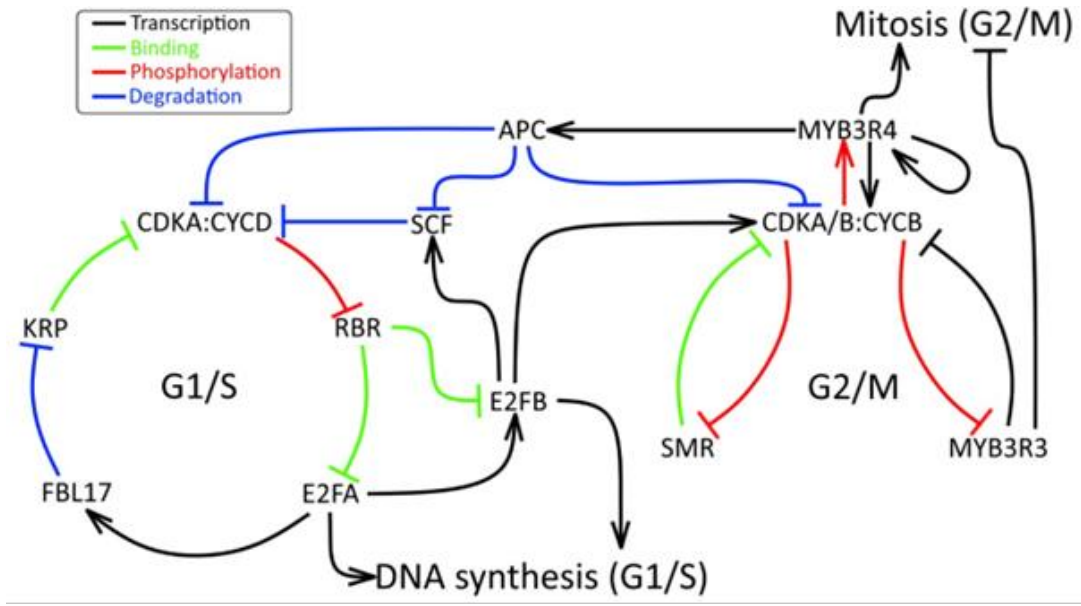
control at G1/S only was insufficient to control for the asymmetric divisions in meristematic tissues (Figure 1.4 B and C Williamson et al., 2023). Here, it was shown theoretically that when cell size control operates at both the G1/S and G2/M transitions, a population with variation in cell sizes during the G1/S transition achieve size equilibrium upon mitosis, over a period of time (Figure 1.4B; Williamson et al., 2023). However, when size control at the G2/M transition is removed, variation is observed in cell sizes, at both G1/S and M (Figure 1.4C; Williamson et al., 2023). This is consistent with previous observations that both the length of the G1 and G2 phases of the cell cycle are flexible in plants (Jones et al., 2017) and suggests that one or more regulator at the G2/M transition (Figure 1.3C) may perform a size function.

Given the important role of inhibitory proteins for cell size control at the G1/S transition in *Arabidopsis* (D'Ario et al., 2021), it is possible that cell size information might also be integrated via inhibitory regulators at the G2/M transition. Therefore, size candidates with negative roles at this checkpoint were considered (Figure 1.2A; Figure 1.3C). MYB3R3 has been shown to inhibit the cell cycle, to decrease cell proliferation and organ size in a number of stress conditions including DNA damage (Chen et al., 2017), salt stress (Okumura et al., 2021), and heat stress (Takahashi et al., 2019). However, its role in the progression of non-stressed cell cycles has not been reported. Equally, SMR proteins are of interest. SMR proteins perform a function at the G2/M transition that is analogous to the function of KRP at the G1/S (Yamada et al., 2022). Furthermore, depletion of SMRs in the root meristem produces smaller cells (Nomoto et al., 2022). However, how the concentration of SMR changes during the cell cycle has not yet been demonstrated. Interestingly, outputs from the computational model of the network (Figure 1.4B; Figure 1.4C; Williamson et al., 2023) hypothesise that SMR, but not MYB3R3 is able to coordinate cell size control, based on both D'Ario's model of equal inheritance theory (D'Ario et al., 2021) and inhibitor dilution (Williamson et al., 2023). However, these theoretical hypotheses are yet to be tested experimentally.

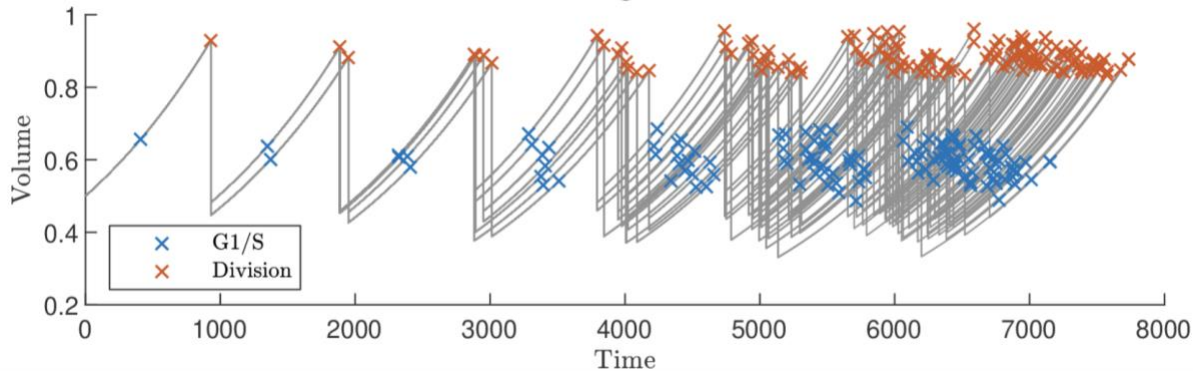
While inhibitor dilutors are hypothesised to play a size role at the G2/M transition, activator accumulators could also contribute to cell size control. MYB3R4, with an opposing role to MYB3R3, has been demonstrated to play a role in growth and

development; its reduction in function resulted in shorter plants, upon bolting, and rosette leaves shorter in length (Haga et al., 2011). Therefore, it is important to also consider this mode of size regulation, when elucidating size control at the G2/M transition.

A



B



C

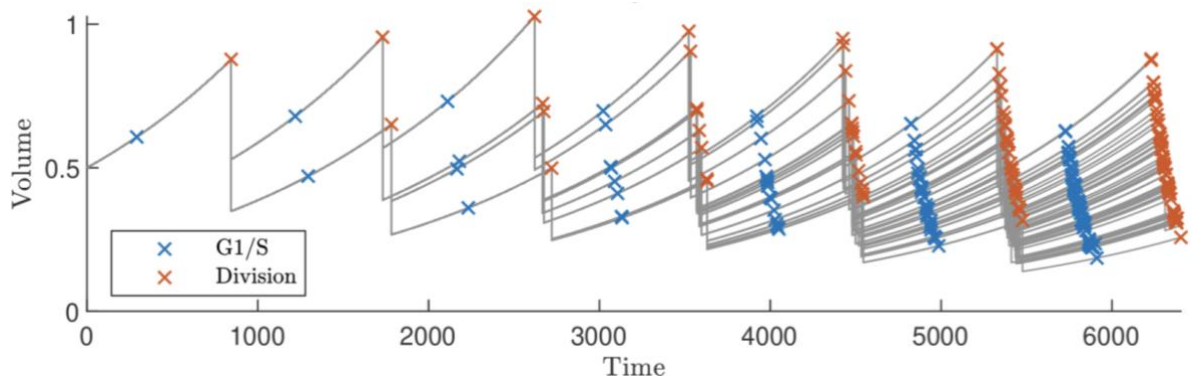


Figure 1.4: Modelling conducted to test for size control at both the G1/S and G2/M transitions, using a regulatory network (Williamson et al., 2023). A: Schematic of the regulatory network underpinning a computational model of the cell cycle. G1/S and G2/M transitions are emergent properties of the network. G2/M control involves the action of two inhibitors, MYB3R3 and SMR. The relationships between MYB3R3 and SMR concentration and cell size are not yet known. APC refers to Anaphase Promoting Complex which has roles in the degradation of cell cycle components at G1/S and G2/M. SCF represents ubiquitin ligase complexes which target CDKA/CYCD complexes at the G1/S transition for degradation. Other components are described (Figure 1.2A). B) Modelling to show a time course of a population of cells where all proteins are size-dependent, except for the negative regulators KRP (at G1/S) and SMR (at G2/M) which are size independent (sizers). Blue crosses show the cell volumes at G1/S, and orange crosses show the cell volumes at which they divide. Cell size is stable across generations. C) Modelling to show a time course of a population of cells where all proteins are size dependent except for KRP, hypothesised to only act as a sizer at the G1/S transition. Cell size is not stable across generations.

1.5 The use of a GR inducible system to translocate hypothetical “sizer” proteins from the cytoplasm into the nucleus, to break their dependency on cell size

This study aims to test the roles of potential sizer candidates, including MYB3R3, MYB3R4 and SMR, at the G2/M transition experimentally. It has long been established that as a cell increases in size, its biosynthetic capacity to produce RNA and proteins also increases (Elliott & McLaughlin 1979; Creanor & Mitchison, 1982; Merhar et al., 2015). Therefore, to study the proteins independently of their normal relationship to cell size, an approach was chosen with a goal of mis-expressing proteins to alter their dependency on cellular volume (Figure 1.5). Here, candidate sizer proteins were expressed under the control of a constitutive promoter to drive ubiquitous expression throughout the cell, then later translocated from the cytoplasm to the nucleus.

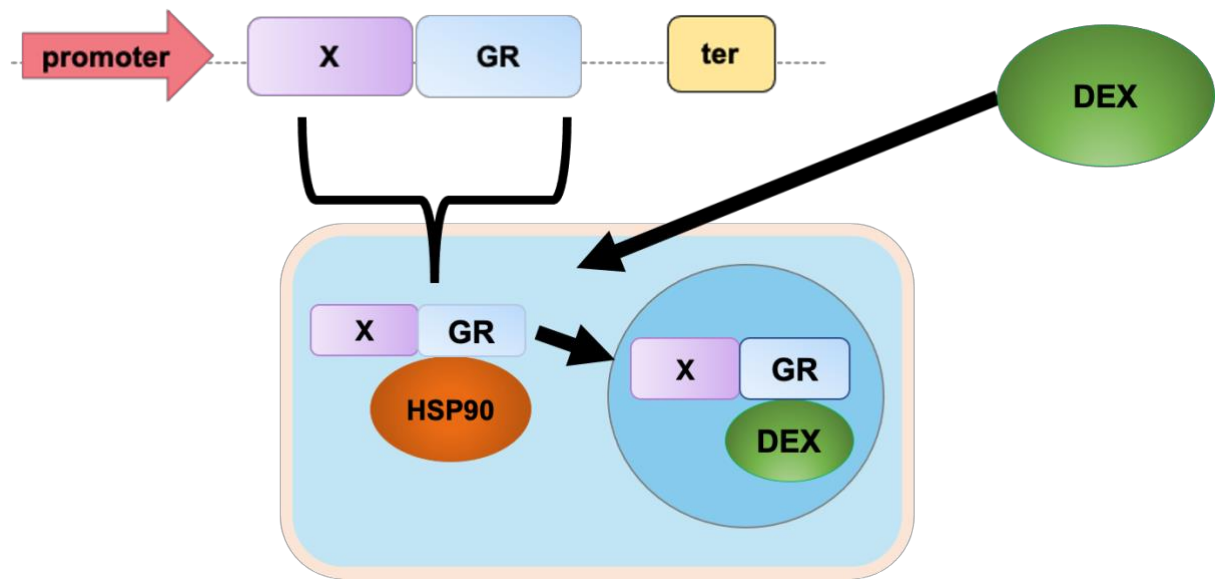
Inducible systems have been widely documented in plants (Aoyoma and Chau, 1997; Zuo and Chau, 2000; Schlücking et al., 2013). Canonical induction systems, including the Glucocorticoid Domain (GR) dexamethasone induced system (Aoyoma and Chau, 1997), the Estrogen Receptor (ER), induced by estradiol (Bruce et al., 2000) and the AlcA system, induced by ethanol (Caddick et al., 1998; Roslan et al., 2001), require the use of a chimeric protein comprised of a DNA binding domain, an activation domain and a domain highly specific to a chemical inducer (Schlücking et al., 2013). Traditionally, these have been used to activate genes in order to study the downstream effects of specific transcription factors (Wildwater et al., 2005; Craft et al., 2005). Therefore, systems are usually required to have low basal expression prior to induction (Schlücking et al., 2013). Further, there must be no toxicity of the inducer on the target organism (Yamaguchi et al., 2015) and must elicit strong, consistent activation.

One such system in plants, uses the dexamethasone (DEX) induced glucocorticoid receptor (GR) from rat (Aoyoma and Chau, 1997). This system has been widely used to study transcription factor function in plants, both via simple fusions to the GR domain (Wildwater et al., 2005) and as key part of transactivation systems (Craft et al., 2005). The system works by fusing a gene of interest (GOI) to the GR domain, driven by a promoter of choice and transforming this into *Arabidopsis* (Figure 1.5A).

Here, the GR domain associates with an endogenous protein, Heat Shock Protein 90 (HSP90) (Cadepond et al., 1991) that is confined to the cytoplasm. Upon application of the steroid hormone DEX, the GR domain dimerises and translocates to the nucleus, co-transporting the attached protein of interest (POI) (Zuo and Chau, 2000). This system has been useful in the characterisation of the downstream targets of transcription factors (Yamaguchi et al., 2015), as the nuclear localisation rapidly increases opportunity for the transcription factor proteins to bind to target genes.

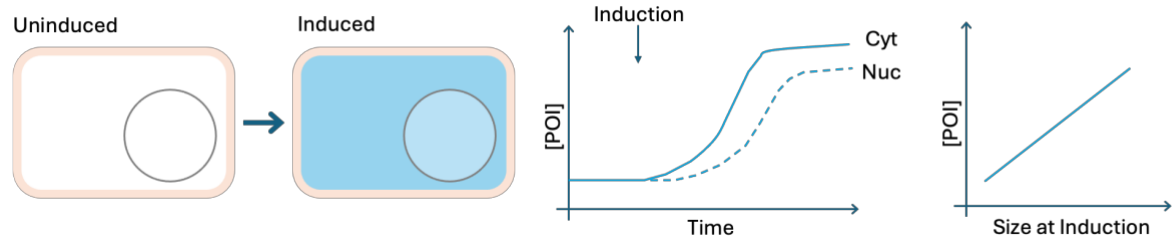
While other systems can be applied such as the highly inducible β -Estradiol-Inducible system (Zuo et al., 2000); Yamada et al., 2022) and the ethanol induced *alc* gene system from *Aspergillus nidulans* (Roslan et al., 2001), here, the GR system was selected. Here, we use the DEX system in a novel way, for translational induction (Figure 1.5A). The rationale of this is to apply DEX after several cell cycles, allowing the concentration of a potential sizer protein to accumulate and stabilise prior to induction. Addition of the GR tag means that newly synthesized protein of interest will be exported from the nucleus and sequestered in the cytoplasm where they are inactive (Yang et al., 2021). Sequestration over a number of cell cycles should allow protein levels of the GOI to reach a steady state. Quick induction using DEX would then translocate the sequestered proteins back into the nucleus at a high concentration, that is independent of the size of the cell and its current biosynthetic capacity (Figure 1.5B; Proulx-Giraldeau et al., 2022). In the nucleus, the proteins of interest in this study (MYB3R3, MYB3R4 and SMR2) would be hypothesised to actively perform their native functions. MYB3R3 and MYB3R4 are transcription factors that bind to genomic DNA (Kobayashi et al., 2015), and MYB3R4 is actively shuttled from the cytoplasm to the nucleus at two distinct points, during the G2/M transition to facilitate cell division (Yang et al., 2021). SMRs are not transcription factors, but their expression has been demonstrated to be nuclear (Yamada et al., 2022). Successful application of the DEX system to control SMR activity could therefore provide a novel and useful tool for future studies.

A



B

1) Transcriptional Induction



2) Translocational Induction

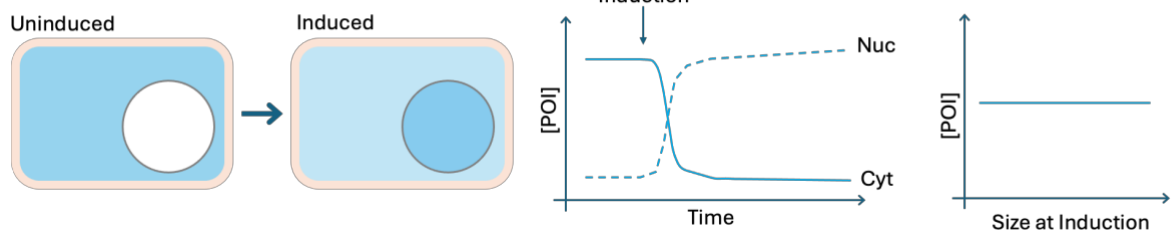


Figure 1.5: A: A schematic shown in animal cells of the DEX inducible system. A construct is assembled with a GOI (X), fused to the GR domain. It is transformed into plants and is translated and bound in the cytoplasm to heat shock protein 90 (HSP90). Upon DEX application, this interaction is displaced, and the protein is translocated into the nucleus, manipulating the subcellular localisation (Aoyama and Chau, 1997).

B: Schematic comparing hypothesized relationship between cell size and accumulation of protein of interest (POI) under different inducible expression systems. A) Under the control of a transcriptional induction system POI synthesis is triggered by application of the inducer molecule. Protein is expected to accumulate first in the cytoplasm and then in the nucleus after a lag period of a number of hours. The maximum concentration of POI is likely to be linked to cell size as small cells are likely to have a lower protein synthetic capacity than large cells. B) Under the control of a translocational induction system the POI is constitutively produced and sequestered inactive in the cytoplasm. Upon application of the inducer molecule, protein is rapidly translocated to the nucleus. Since protein production is constitutive, it is hypothesised that the concentration of POI in the cytoplasm will have reached equilibrium over a number of cell cycles prior to inducer application and as a result, differences in POI production due to cell size will be minimised. Translocational induction therefore offers a better opportunity to break underlying relationships between cell size and protein production.

1.6 Aim and objectives of the study

The overall aim of the study is to develop a translational induction system to test the functionality of potential sizers, in terms of their relationship to cell size. Our hypothesis is that the normal relationship between cell size and sizer concentration can be broken if the synthesis of a sizer protein and its translocation to its site of action in the nucleus are temporally separated events. To do this, the following objectives were identified:

Objective 1: Design a reusable, modular cloning strategy for generating N and C terminal GR fusions to Genes of Interest (GOIs) using the Golden Gate system.

Objective 2: Produce GFP-GR fusion proteins to test the system, quantify cytoplasmic and nuclear GFP pools with and without DEX and produce an optimised induction protocol.

Objective 3: Construct one or more GOI-GR fusions, transform *Arabidopsis* and compare root growth with and without DEX.

2. Materials and Methods

2.1 Gel electrophoresis

Agarose gel electrophoresis was carried out in accordance to standard procedures (Green and Sambrook, 2012). Gels were made by dissolving the following reagents to a final concentration (all concentrations here are final) of 1% Molecular Grade Agarose (Bioline, UK) in 1 x Tris-acetate EDTA (TAE) buffer (40 mM Tris (ThermoFisher, USA), pH 8.0, 20 mM acetic acid (Sigma, UK), and 1 mM ethylenediaminetetraacetic acid (EDTA) (ThermoFisher, USA)). To view DNA 0.00005 % (v/v) SafeView Nucleic Acid Stain (NBS Biologicals, UK) was added to the solution, when cooled. 5 µL of SmartLadder, 200bp-10kb (Eurogentec, Belgium) was used as a size ladder. 10 X loading dye consisting of 0.2 g Bromophenol Blue (Sigma, UK) dissolved in 3 :7 glycerol (Sigma, UK) to distilled ELIX water (Merck, Germany) was added to DNA prior to loading on the gel. Gels were run at 100 V for approximately 30 minutes and visualised on a UV transilluminator (Syngene, UK).

2.2 Polymerase chain reaction (PCR) of DNA using Phusion

DNA was amplified using Phusion® High-Fidelity DNA Polymerase (New England Biolabs, USA). Polymerase chain reactions (PCRs) were carried out according to the manufacturer's instructions in a total volume of 100 μ L to give the following final concentrations: 1 X Phusion HF buffer (New England Biolabs, USA), 0.3 μ M of each forward and reverse primer, 200 μ M dNTPs (ThermoFisher, USA), 1 unit of Phusion DNA Polymerase per 100 μ L, between 50-250 ng genomic DNA, 3% dimethylsulfoxide (DMSO) (Sigma, UK). Reactions were made up to volume using nuclease-free "Milli-Q" water (Merck, Germany). Thermocycling conditions began with an initial denaturation at 98°C for 30 seconds followed by 35 three-step cycles of: denaturation at 98°C for 30 seconds ; annealing for 30 seconds between 45-72°C at a temperature determined by gradient PCR, and extension at 72°C. Duration of the extension step was dependent on amplicon length, where 15-30 seconds corresponded to the time needed for amplification of 1 kb. Gradients were performed to determine optimum annealing temperatures up to the primer T_m . The final extension at 72°C lasted for 5 minutes, before the reaction was held at 4°C.

2.3 Purification of DNA from PCR and agarose gels

In order to extract fragments of DNA for downstream cloning applications, specific bands were cut out from gels on a blue-light E-box transilluminator (Vilber, France), using a razor. Purification was performed using Zymoclean Gel DNA Recovery Kit (Zymo Research, USA). Subsequent steps were followed in accordance with the manufacturer's instructions. As additional steps, an equal volume of nuclease-free water was heated to 55°C was added once the gel was melted and flowthrough was always reapplied a second time, to assist with DNA recovery. The final elution was performed in 15 μ L of nuclease free water heated to 55°C. DNA was checked for downstream cloning applications by measuring the concentration on a NanoDrop-1000 Spectrophotometer (ThermoFisher Scientific, USA), and examining a 1 μ L sample by gel electrophoresis.

2.4 *Escherichia coli* transformation

Transformation protocols using competent DH5 α cells were adapted from standard molecular biology protocols (Green and Sambrook, 2012) and manufacturer's instructions (New England Biolabs, UK). To transform plasmids into *Escherichia coli* (*E. Coli*), 1 μ L of pure plasmid DNA, or 5 μ L of ligation mix was added to 50 μ L of defrosted DH5 α cells (New England Biolabs, UK) and left on ice for 10 minutes. 125 μ L of SOC media (New England Biolabs, UK) was added, and samples were put into a shaking incubator at 37°C for 1 hour. 50 μ L and 100 μ L of the mix was streaked onto separate plates comprised of Luria-Bertani (LB) agar with an antibiotic specific to the resistance of the plasmid. LB broth (Melford, UK) was prepared in ELIX water in accordance with the manufacturer's instructions, with the pH adjusted to 7.2 with sodium hydroxide (NaOH, Sigma, UK). LB agar was prepared from LB broth supplemented with 1.2 % microagar (Duchefa, Netherlands). The final concentrations of antibiotics used in this study included 50 μ g/mL kanamycin, 100 μ g/mL spectinomycin and 100 μ g/mL ampicillin (All supplied by Sigma, UK). For MoClo reactions (Weber et al., 2011; Engler et al., 2014), 5-bromo-4-chloro-3-indolyl- β -D-galactopyranoside (X-gal, 20 μ g/mL, Sigma UK) and isopropylthio- β -galactoside (IPTG, 0.1 mM, Sigma, UK) were added to enable blue-white screening of colonies.

2.5 Colony PCR

Under aseptic conditions, colonies were selected using 10 μ L tips, streaked onto a master plate containing LB agar and the antibiotic specific to the plasmid, and then dipped into 10 μ L of nuclease free water. The resulting solution was used as a template for PCR. PCRs were prepared in a volume of 10 μ L using 2x Taq PCR Master Mix (Qiagen, Netherlands), 0.3 mM of each forward and reverse primer, 1 μ L of template DNA and the remaining volume, nuclease free water. Thermocycling conditions included an initial denaturation for 3 minutes at 95°C, followed by 35 cycles of: denaturation at 94°C for 30 seconds, annealing at a temperature specific to primer T_m for 30 seconds and extension at 72°C for one minute per kb of amplicon length. The final extension was performed at 72°C for ten minutes and the reaction was held at 4°C.

2.6 Plasmid purification

To obtain a purified plasmid, *E. coli* cultures were prepared by inoculating a desired colony in 3 mL of LB broth, and incubating it overnight at 37°C, shaking at 225 rpm. Subsequently, a modified protocol based on the QIAprep Spin Miniprep Kit (Qiagen, Netherlands) was employed. Cells were initially pelleted in a benchtop microcentrifuge (E5417R, F45-30-11 rotor, Eppendorf, Germany) at 20817 g for three minutes prior to resuspension in a homemade buffer (P1: 50 mM Tris-hydrochloride (HCl) (Sigma, UK) pH 8.0, 100 μ g/mL RNaseA (Sigma, UK)). After being left to dry for five minutes, pellets were treated with Buffer P2: 200 mM NaOH, 1% (w/v) sodium dodecyl sulfate (SDS, Sigma, UK) to lyse the cells. Neutralisation was carried out using P3: 4.2 M guanidine hydrochloride (Sigma UK), 0.9 M potassium acetate (Sigma, UK), pH 4.8. Solutions were centrifuged for ten minutes at 20817 g to remove precipitates and the supernatant was applied to an Econospin RNA/DNA Micro Spin Column (Epoch Life Science, USA). The flowthrough was always reapplied to the spin column after centrifugation to optimize DNA binding. The wash step was carried out using a buffer made of 10 mM Tris-HCL pH 7.5, 80% ethanol (Sigma, UK). DNA was eluted in 50 μ L of nuclease free water (Millipore, Germany) and heated to 55°C. Plasmid DNA was stored at -20°C.

2.7 Design of inducible GFP GR reporter fusion protein cassette in both positions

Initial design of expression cassettes addressed the aim to build a reusable inducible GR cassette to study genes of interest. In order to test the system, reporters were firstly considered. Here, the fluorescent protein GFP was chosen to visualise expression and test the system, prior to incorporating in a gene of interest (GOI). Two cassettes were designed where the GR domain was fused to the GFP domain both N and C terminally to determine which position was more efficient. A linker region consisting of the amino acids proline, valine, alanine and threonine (PVAT) was incorporated to either the C or N terminal end of GR via PCR with regards to where it joined to GFP (Figure 2.1). A final positive control expressing our chosen GFP with no GR or linker was included, to confirm GFP functionality in the absence of a fusion protein and serve as a positive control while screening transgenic fusions. The cauliflower mosaic virus (CaMV) 35S promoter (Weber et al., 2011) was chosen to drive ubiquitous expression and the Nos terminator (Tnos) (Weber et al., 2011) was used to end transcription.

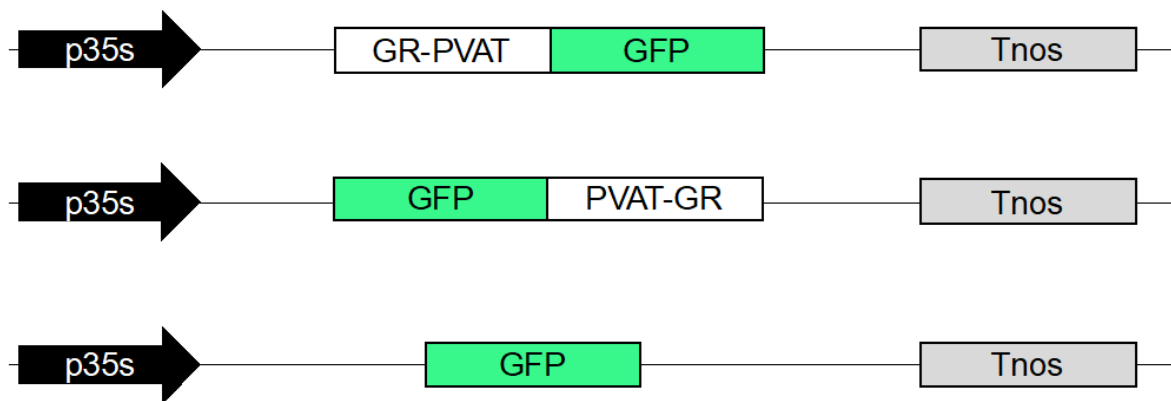


Figure 2.1: Overview of strategy for generating inducible reporter fusion proteins. p35s (cauliflower mosaic 35s promoter), PVAT is a linker region consisting of proline, valine, alanine and threonine and Tnos (nos terminator). p35s::GR-PVAT-GFP; the position of the fusion protein where the GR domain is in the N terminal position, with a C terminal linker (PVAT). p35s::GFP-PVAT-GR; the position of the fusion protein where the GR domain is in the C terminal position, with an N terminal PVAT linker region. p35s::GFP; a ubiquitously expressed GFP construct, as a positive control for both positions of the fusion protein.

2.8 Reporter and control plasmid constructions using Golden Gate Modular Cloning (MoClo)

To build the reusable inducible GR system to study GOIs, Golden Gate, a modular cloning strategy was employed (Figure 2.5; Weber et al., 2011; Engler et al., 2014). Constructs were designed using parts from the MoClo kit (Table 2.2; Weber et al., 2011), in order to express the devised cassettes (Figure 2.1). This modular cloning system works by the use stepwise assembly into three vectors, termed Level 0, Level 1 and Level 2 (Figure 2.2). Each plasmid is flanked by Type IIS restriction endonucleases, (*Bpil* and *Bsal*) to allow for a one-step reaction, consisting of digestion and ligation, to subsequently assemble a plasmid which can be transformed into *Arabidopsis thaliana* (Figure 2.2). The plasmids contain a resistance gene, specific for a different antibiotic for each level (Table 2.3). Empty Level 0 and Level 1 plasmids without an insert, and assembled Level 2 plasmids containing the end link fragment from pICH49266 (Table 2.3) contain the LacZ acceptor site, which produces blue colonies by metabolising X-Gal (Section 2.4). This assisted in screening procedures.

To prepare the GR domain for the Level 0 plasmids from the kit, GR was amplified by PCR from a pGreen vector containing a *p35s::GENE-GR* construct, built for the TGV system (Böhner et al., 2002) using primers in Table 2.1. These primers (Table 2.1) incorporated the PVAT linker, along with four specific bases, corresponding to *Bpil* cleavage sites, for insertion into pAGM1276 (NT1) for the N terminal position and pICH41308 (CDS1) for the C terminal position (Figure 2.2). These primers also added *Bpil* sites at the far 5' and 3' ends, followed by two nucleotides, as the enzymes cut two nucleotides (NN) downstream of their recognition sites. (Figure 2.2). Primers were also designed to amplify GFP from pICH41531, incorporating in bases to enable its assembly into pAGM1276 (NT1), the plasmid corresponding to an N terminally positioned protein (Table 2.1). This was done to ensure comparability between the fusion proteins, in terms of the GFP used.

Prepared fragments were ligated with their respective Level 0 Acceptor plasmids, in a one-step reaction using T4 ligase (New England Biolabs, UK) and *Bpil* (ThermoFisher Scientific, USA) (Table 2.4). Transcriptional units were then and

digested with *Bsal* (ThermoFisher Scientific, UK) and ligated into a Level 1 Acceptor (pICH47732, B3) using p35s + 5'UTR (pICSL13001; pICH51266) GFP (pICH41531; pICSL30006) and Tnos + 3'UTR (pICH41421) found Level 0s in the kit (Table 2.2), as these vectors contained complementary cleavage sites ensuring assembly in the correct order (Figure 2.2). Subsequently, Level 1 constructs were ligated and digested with *Bsal* with a Kanamycin resistance gene (KN02 - L1:P2F) and an end linker with a LacZ gene (pICH49266) into the Level 2 Acceptor (pAGM4673, H2) (Figure 2.2). These steps resulted in the assembly of three Level 2 plasmids (Figure 2.3) each separately containing the three individual reporter cassettes designed in this study (Figure 2.1). Here, each cassette resided in the pAGM4673 (H2) Level 2 vector, which enabled transformation and subsequent expression in *Arabidopsis thaliana* (Figure 2.3).

Table 2.1: Primers used to construct inducible GFP-GR reporters, with GFP in both N and C positions. Upper case letters indicate bases incorporated by the primers, lower case letters are bases endogenous to template DNA. The bases encoding the PVAT linker are CCTGTTGCTACT (5'-3'). The bases GAAGAC correspond to the BpiI recognition sites, required for assembly into a Level 0 Golden Gate plasmid (Table 2.2; Weber et al., 2011).

Name	Template	Sequence	Construct
GR N term link BPI FOR	GR	GAAGACTCAATGCCCGGGCCTGT TGCTACTaaaaaatcaaaggattcagcaag	p35s::GFP-GR
GR stop codon BPI REV	GR	GAAGACTCAAGCTCAttttgatgaaacag aagc	p35s::GFP-GR
GFP for NT1 BPI CCAT FOR	GFP	GAAGACCTCCatggtgagcaaggcgagga g	p35s::GFP-GR
GFP for NT1 BPI REV	GFP	GAAGACCTCATTgatctaataagccgcgtttt gtac	p35s::GFP-GR
GR_BpiI_FR_CCAT	GR	GAAGACCTCCATGaaaaaatcaaagggat tc	p35s::GR-GFP
GR C term linker BPI G REV	GR	GAAGACCTCATTCCAGTAGCAAC AGGCCCGGGttttgatgaaacagaagc	p35s::GR-GFP

Table 2.2: MoClo plasmids used in this study. Plasmid names, descriptions of their roles in the constructs and their “Level” respective to the three plasmid levels found in the MoClo kit (Engler et al., 2014). Level 0 parts are combined to assemble a transcriptional unit into a Level 1 Acceptor plasmid (pICH47732). Constructs were subsequently ligated into a Level 2 Acceptor (pAGM4673) with a Level 1 unit conferring Kanamycin resistance in transformed plants (KN02 - L1:P2F) and a Level 1 end linker (pICH49266) to provide a lacZ acceptance site to allow for screening of positive colonies.

Plasmid	Description	Level
pAGM1276	Level 0 acceptor for N terminal modules (NT1)	0
pICH41308	Level 0 acceptor for C terminal modules (CDS1)	0
pICSL13001	CaMV 35s Promoter (Long)+ 5'UTR for fusion proteins	0
pICH51266	CaMV 35s Promoter (Long)+ 5'UTR for single proteins	0
pICH41531	GFP for single reporter C terminal fusion protein (GR is N terminal)	0
pICH41421	NOS terminator + 3'UTR	0
pICH47732	Level 1 Acceptor position 1, forward position	1
KN02 - L1:P2F	Kanamycin resistance gene driven by the Nos promoter and OCS terminator, position 2	1
pICH49266	End-link 2 for assembling 2 level one part into a level 2 acceptor. With lacZ acceptor site	1
pAGM4673	Level 2 Acceptor	2

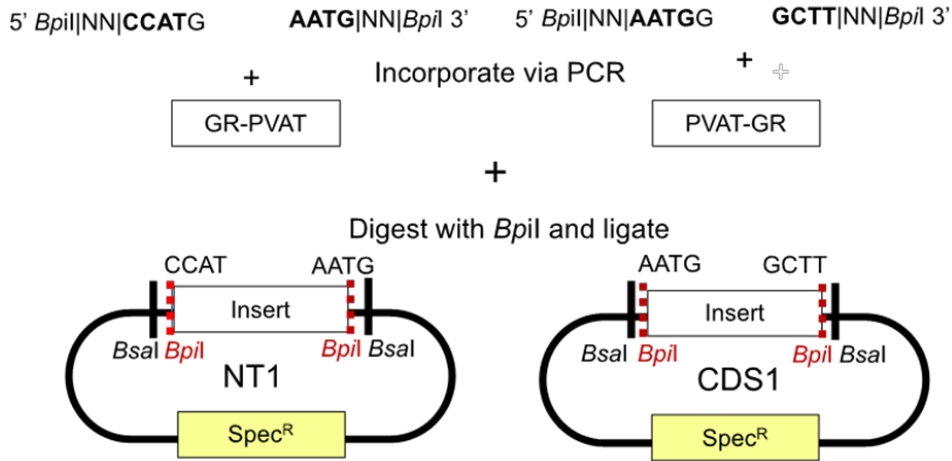
Table 2.3: Table summarising features of Golden Gate acceptor plasmids by reaction level (Weber et al., 2011; Engler et al., 2014). Reaction level of plasmid determines the Type IIS restriction endonucleases required, the antibiotic selection that should be used to select for the plasmid and the colour of colony to select under presence of IPTG and XGAL to indicate correct uptake of the insert. Level 2 is the only reaction level which when assembled with the insert will produce positive blue colonies due to the presence the lacZ acceptor site.

Reaction Level	Type IIS Endonuclease Cut sites	Resistance	Selection
0	<i>BpiI</i>	Spectinomycin	White
1	<i>BsaI</i>	Carbenicillin	White
2	<i>BsaI</i>	Kanamycin	Blue

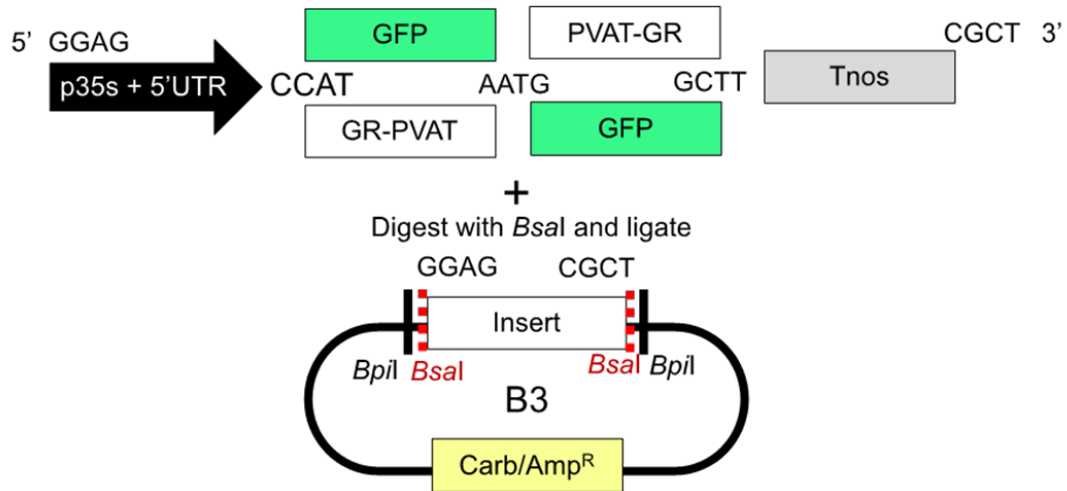
2.4: Table of preparation for one-step digestion and ligation of parts at each level. Insert(s) were ligated with the vector in a 2:1 ratio. One reaction had a volume of 20 μ L.

Reagent	Volume (μ L)
Insert(s)	X to provide 2x Vector concentration
Vector	X to provide 150 ng
<i>BpiI</i> or <i>BsaI</i>	1
T4 Ligase 400,000 units/ml	1
10X T4 ligase buffer	2
BSA 10X	2
Nuclease free H ₂ O	X up to 20

Level 0 Construction



Level 1 Construction



Level 2 Construction

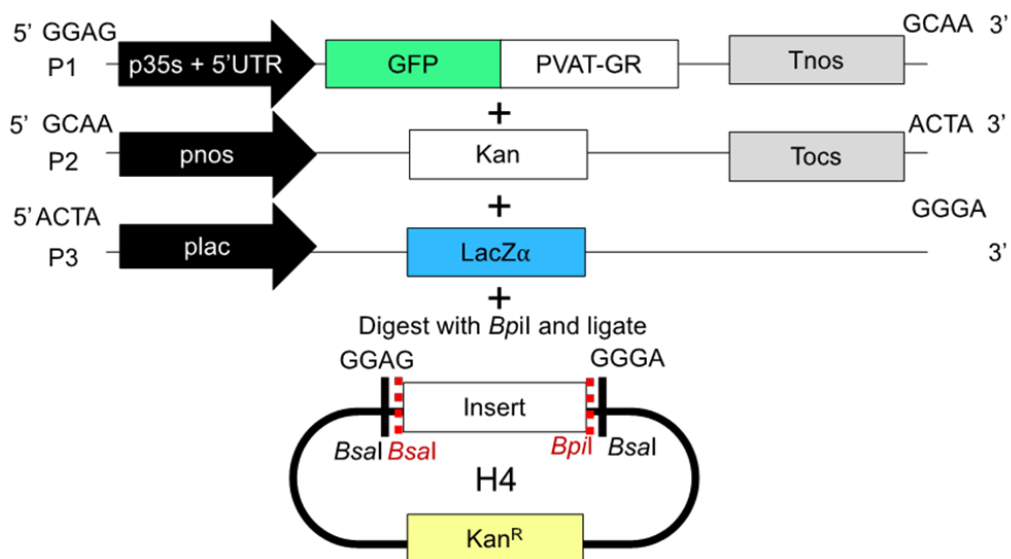
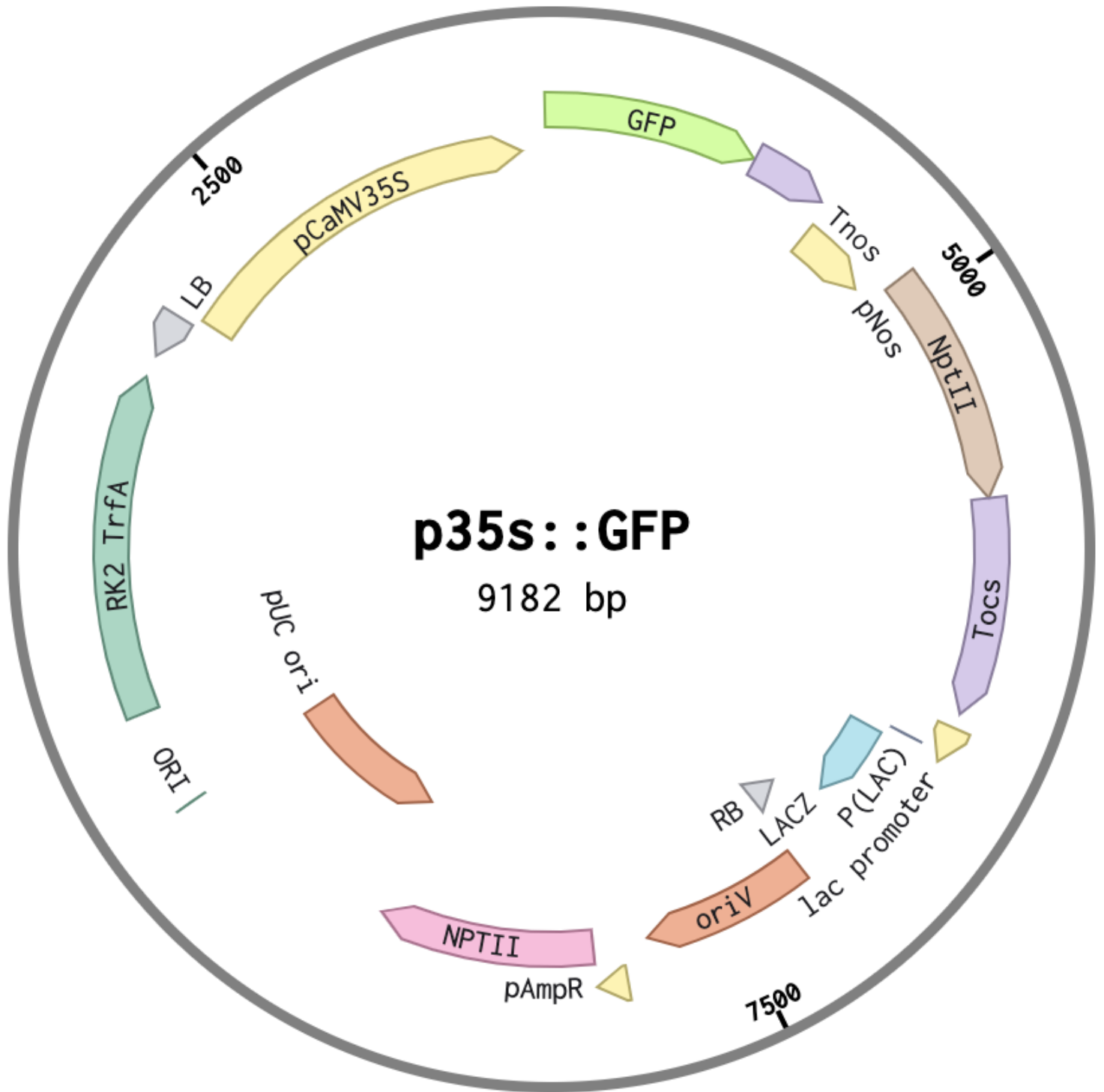
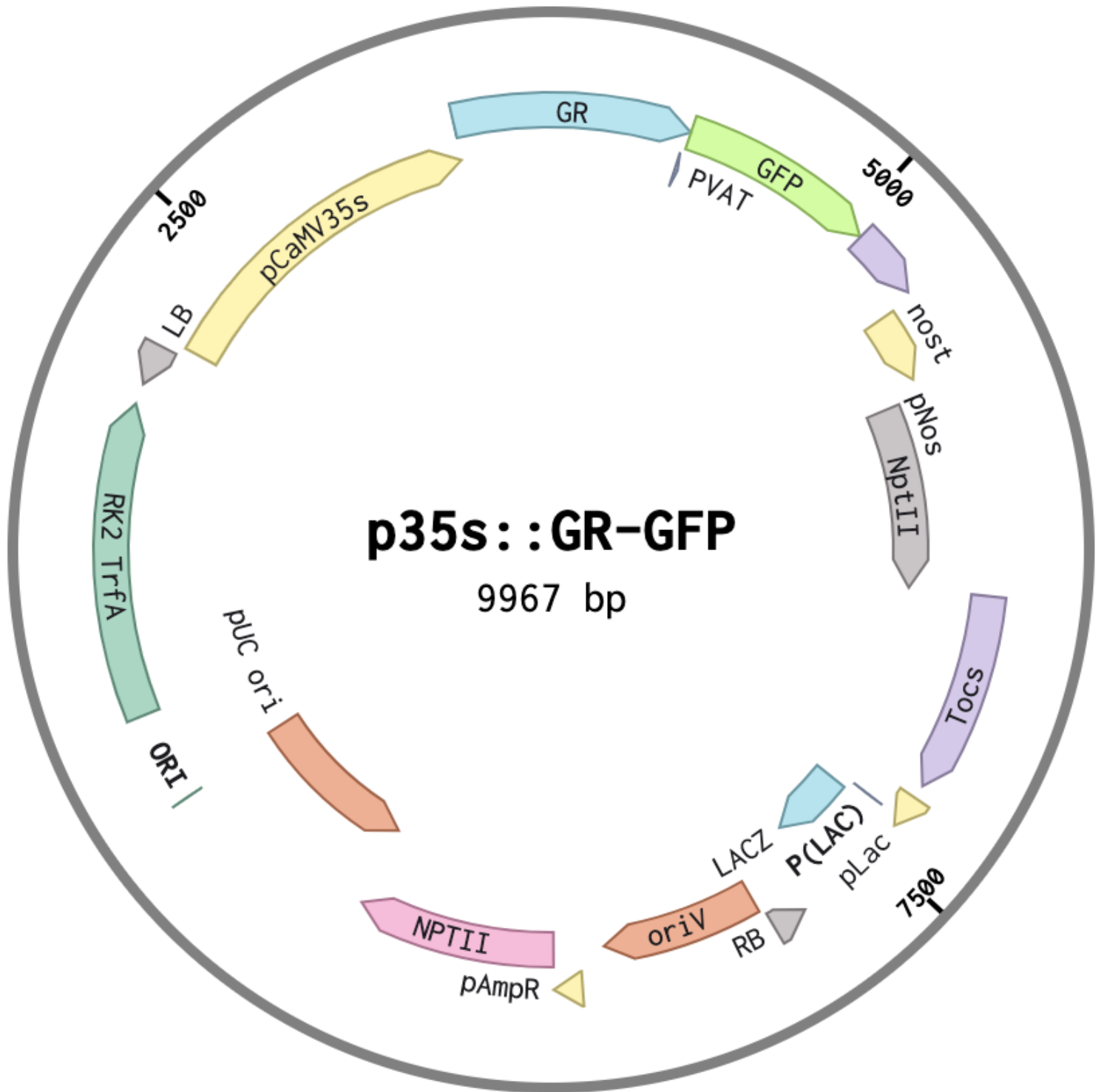


Figure 2.2: Schematic of consecutive stages of plasmid construction using MoClo parts (Engler et al., 2014), for Level 0, 1 and 2. Initially, primers were designed (Table 2.4) to incorporate the PVAT linker onto either end of the GR domain (nucleotides not shown here). Also incorporated were the complementary overhangs from the cleavage site of Bpil in the Level 0 plasmid, followed by two random nucleotides and at the far 5' and 3' end, bases corresponding to the recognition sites for Bpil (GGTCTC). The digestion and ligation of these fragments with either Level 0 Acceptor, NT1 (pAGM1276) or CDS1 (pICH41308) digested the vector at the two Bpil sites (shown in red dotted lines), allowing subsequent insertion. Stable fragments are then flanked by Bsal, enabling for assembly into a Level 1 Assembly Vector (B3, pICH47732) with p35s, GFP and Tnos to form a transcriptional unit. Level 2 construction involved the combinational of three transcriptional units including the construct, kanamycin resistance gene and the LacZa operon. This step is facilitated by the digestion of all parts and vector (H4, pAGM4673) with Bpil, leaving the insert flanked by Bsal.

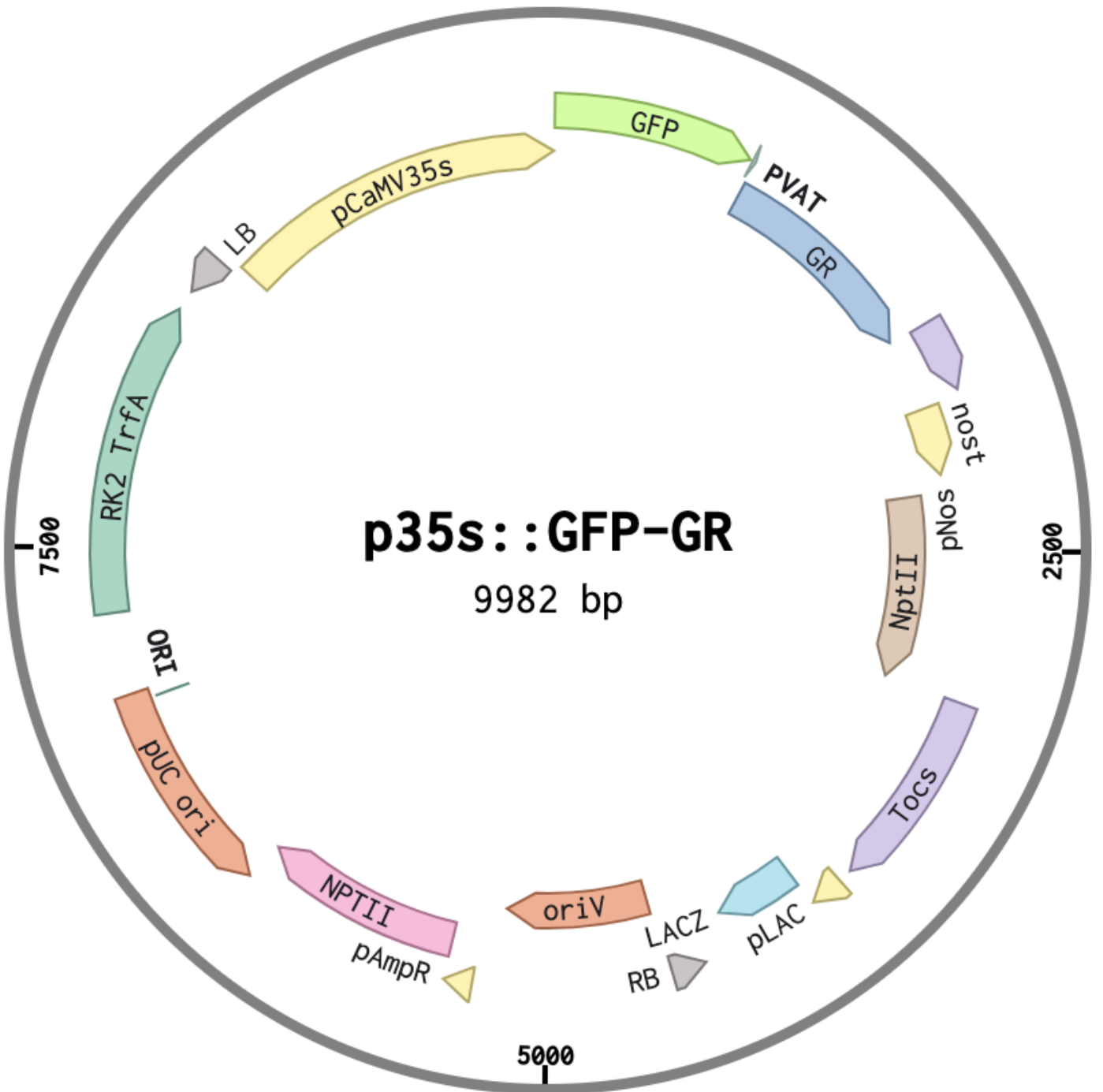
A



B



C



D

Feature	Description
pCaMV35s	CaMV 35s promoter
GFP	GFP gene
GR	GR gene
Tnos	NOS terminator
pNos	NOS promoter
NptII	Kanamycin resistance gene
Tocs	ocs terminator
pLAC	LAC promoter
LACZ	LACZ gene
pAMPr	AMPr promoter
pUC ori	Origin of replication from pUC plasmid
ORI	Origin of replication
oriV	Origin of replication
RK2 TrfA	Gene for TrfA system
LB	Left border
RB	Right border

Figure 2.3: Final assembly of reporter cassettes into the destination plant vector pAGM4673 (Weber et al., 2011). pCaMV35s, GFP, GR and Tnos are components in the expression cassette (Figure 2.1). Between the left (LB) and right (RB) borders, all constructs share the same backbone sequence, to allow for transformation and expression in Arabidopsis. Annotations are written on or clockwise to the coloured label. Primers are shown as small triangles. A: Plasmid map of p35s::GFP, 9182 bp. All primers shown are used for all reporter plasmids B) Plasmid map of p35s::GR-GFP, 9967 bp. The GR BPI FP primer is used for all plasmids containing the GR domain. C) Plasmid map of p35s::GFP-GR, 9982 bp. D: Table showing annotations of plasmid maps in A-C. NptII driven by pNOS confers kanamycin resistance in E. coli. NptII driven by pAMP^r confers kanamycin resistance in A. tumefaciens. pUC ori results in a high copy number in E. coli, to increase the return of positive colonies during cloning. oriV is the origin of replication for the RK2 TrfA gene which enhances gene expression. The LACZ gene is driven by pLAC, the gene required to produce blue colonies for blue/white screening procedures

2.9 NEB HiFi DNA Assembly Strategy

After testing both positions of the fusion protein at T1 and T2 level post transformation, *p35s::GFP-GR* was selected as the basic inducible expression construct. A further cloning strategy was designed to enable an insertion of a GOI into this cassette, in a one-step reaction. NEBuilder (<https://nebuilder.neb.com/>) was used to design primers to incorporate one cut site between the CaMV 35s promoter and GFP, for future GOI insertion.

To prepare the reporter backbone, a digestion was carried out with 34 μL of vector DNA was mixed with 4 μL 10X CutSmart® Buffer (New England Biolabs, USA) and 1 μL of *StuI* and *SrfI* (New England Biolabs, USA), enzymes with cut sites in the middle of the CaMV 35s promoter and between GFP and GR, respectively (Figure 2.8B). Nuclease free water was added to a final volume of 40 μL . This yielded a fragment of 8453 bp which was gel purified (Section 2.3).

For the insert, primers were designed (Figure 2.5A) which divided the remaining fragment of *p35s::GFP-GR* into two parts. The first consisted of the *StuI* cut site to 2 bp after the end of the *p35s* and the latter. For the second part, the reverse primer finished at the *SrfI* cut site and the forward primer incorporated a cut site for the enzyme *PacI*; a site which could be cut to allow a ligation of the reporter backbone with a GOI. Subsequently, the purified parts were ligated at 50°C for 60 minutes with the empty backbone in a 2:1 ratio using NEBuilder HiFi DNA Assembly Master Mix (New England Biolabs, USA), in a final volume of 20 μL .

A

Name	Sequence	Cut site
FP1 HIFI gfp-pvatgr	GACCCACAGATGGTTAGAGAGGC	<i>StuI</i>
RP1 HIFI gfp-pvatgr	GATGAGACTTGCTGCGTAGGcctctetaac	<i>StuI</i>
PacI PVAT GFP FP	ttaattaaCCTGTTGCTACTATGGTGAGCAAGGGCGAG	<i>SrfI</i>
Insert P2		
RP2 HIFI gfp-pvatgr	GTAGCAACAGGCCCGGGCATTGATCTAATAG	<i>SrfI</i>

B

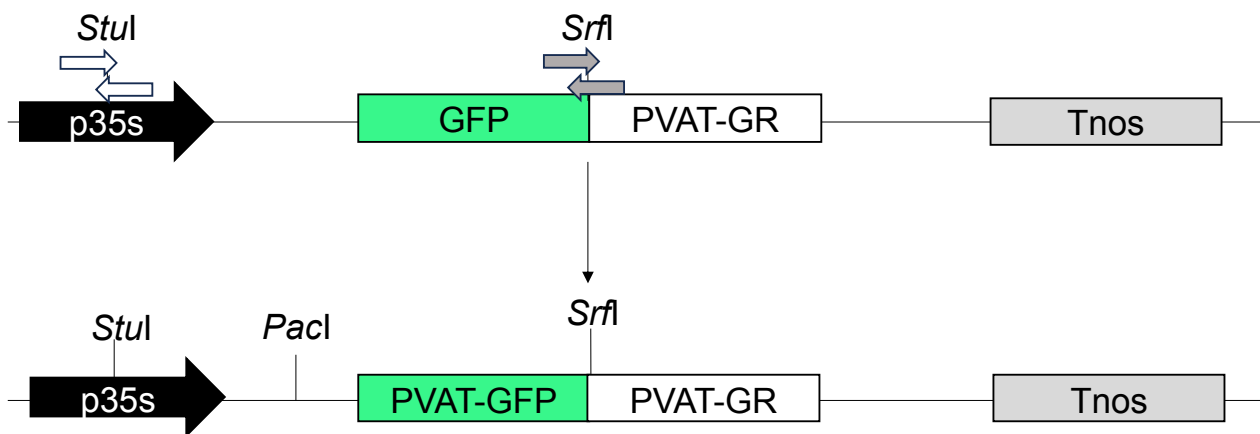


Figure 2.4: Preparation of p35s::GFP-GR as a destination vector for sizes. A: Table depicting primers used to prepare the fragments located between the cut sites. Lower case letters correspond to additional bases, for a PacI site used for HiFi cloning and to prevent a frame shift. B: Schematic of the reporter construct p35s::GFP-GR with the restriction sites used to incorporate in a single PacI cut site (ttaattaa) to allow for a one-step ligation with future genes of interest. White arrows show the overlapping primers used at the StuI cut site and grey arrows show the overlapping primers at the SrfI cut site C: Final HiFi Assembly Vector, showing binding sites for the primers listed in Table A. Plasmid shares common features with the reporter plasmids (Figure 2.3).

2.10 DNA extraction

Genomic DNA was extracted from wildtype *Col-0* plants for downstream cloning applications. DNA isolated from circular leaf discs using a modified cetyltrimethylammonium bromide (CTAB) protocol (Allen et al., 2006). Samples were incubated with the extraction buffer at 60°C for 30 minutes. Centrifugation steps were carried out at maximum speed, 20817 x g (E5417R, F45-30-11 rotor, Eppendorf, Germany). The pellet was resuspended in 50 µL of nuclease free water and stored at -20°C.

2.11 Genomic DNA Extraction and primer design for GOIs

To obtain DNA encoding potential sizer proteins, genomic DNA was firstly extracted from *Col-0* plants (Section 2.10). The sequences for GOIs were obtained from Tair and NCBI (Table 2.5) and primers were designed which included all genomic DNA, minus the 5' and 3' UTRs (Figure 2.5A), and overlapping regions of the HiFI Assembly Vector, adjacent to the *PacI* site in both the 5' and the 3' direction (Figure 2.4C). They also eliminated the *PacI* site upon correct assembly (Figure 2.5). PCR was performed using Phusion polymerase (New England Biolabs, United Kingdom), in accordance to the manufacturer's instructions (Section 2.2) with annealing temperatures optimised by gradient PCRs and extension times respective to the length of DNA (Table 2.5). Fragments were purified by gel extraction (Section 2.3). HIFI assembly was then conducted (Section 2.9) to produce inducible sizer constructs (Figure 2.6).

Table 2.5 Table showing accession numbers correspond to the Tair database and length of total genomic DNA, genomic DNA without the UTRs used in the study and coding DNA (cds). Primers were designed to extract genomic DNA, minus the 5' and 3'UTRs and the stop codon, enabling any of possible splice variants to be translated.

Gene	Tair Accession Number	Total genomic length (bp)	Length without UTRs and stop codon (bp)	cds length (bp)
MYB3R3	AT3G09370	3003	2592	1557
MYB3R4	AT5G11510	5137	4230	2886
SMR2	AT1G08180	958	333	336

A

Name	Template Sequence	Construct
MYB3R3 HIFI FP PACI Eliminate FP	MYB3R3 CATTGGAGAGGACACGCCCATGAGCTCCACTTTTAATC	p35s::MYB3R3- GFP-GR
MYB3R3 PACI DELETE RP	MYB3R3 CTCACCATAGTAGCAACAGGGCCTAGGAGTTGAGAATC	p35s::MYB3R3- GFP-GR
MYB3R4 HIFI Eliminate FP	MYB3R4 CATTGGAGAGGACACGCCCATGGAAGCTGAGTCTTCAAC	p35s::MYB3R4- GFP-GR
MYB3R4 HIFI Eliminate RP	MYB3R4 CTCACCATAGTAGCAACAGGCCTACATCCCTTCAAGAG	p35s::MYB3R4- GFP-GR
SMR2 GFP GR HIFI FP	SMR2 CATTGGAGAGGACACGCCCATGTCTAAGCTTCTCGAG	p35s::SMR2- GFP-GR
SMR2 GFP GR HIFI RP	SMR2 CTCACCATAGTAGCAACAGGGGCACTATTACTCCTTCG	p35s::SMR2- GFP-GR

B

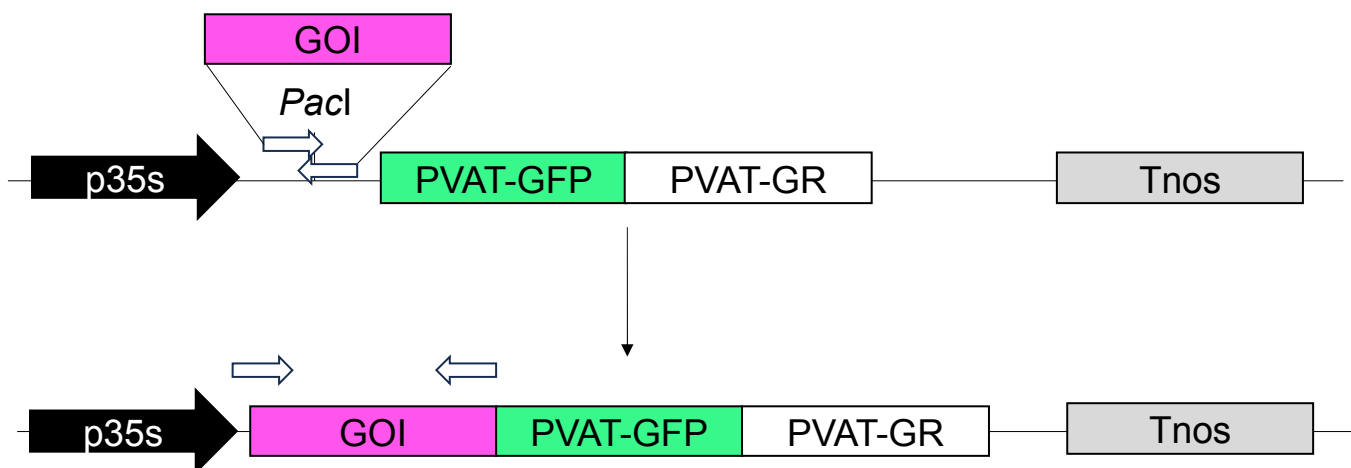
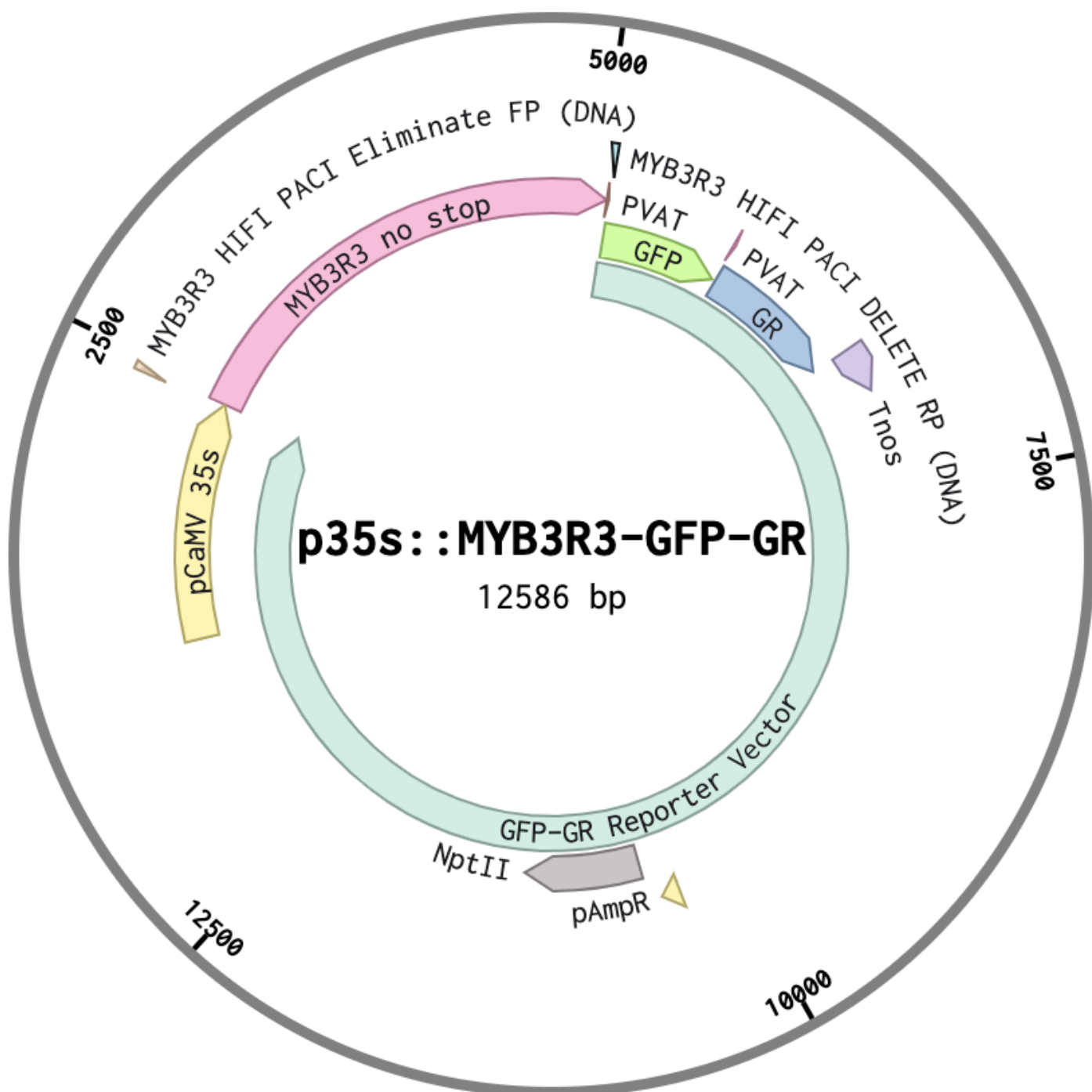
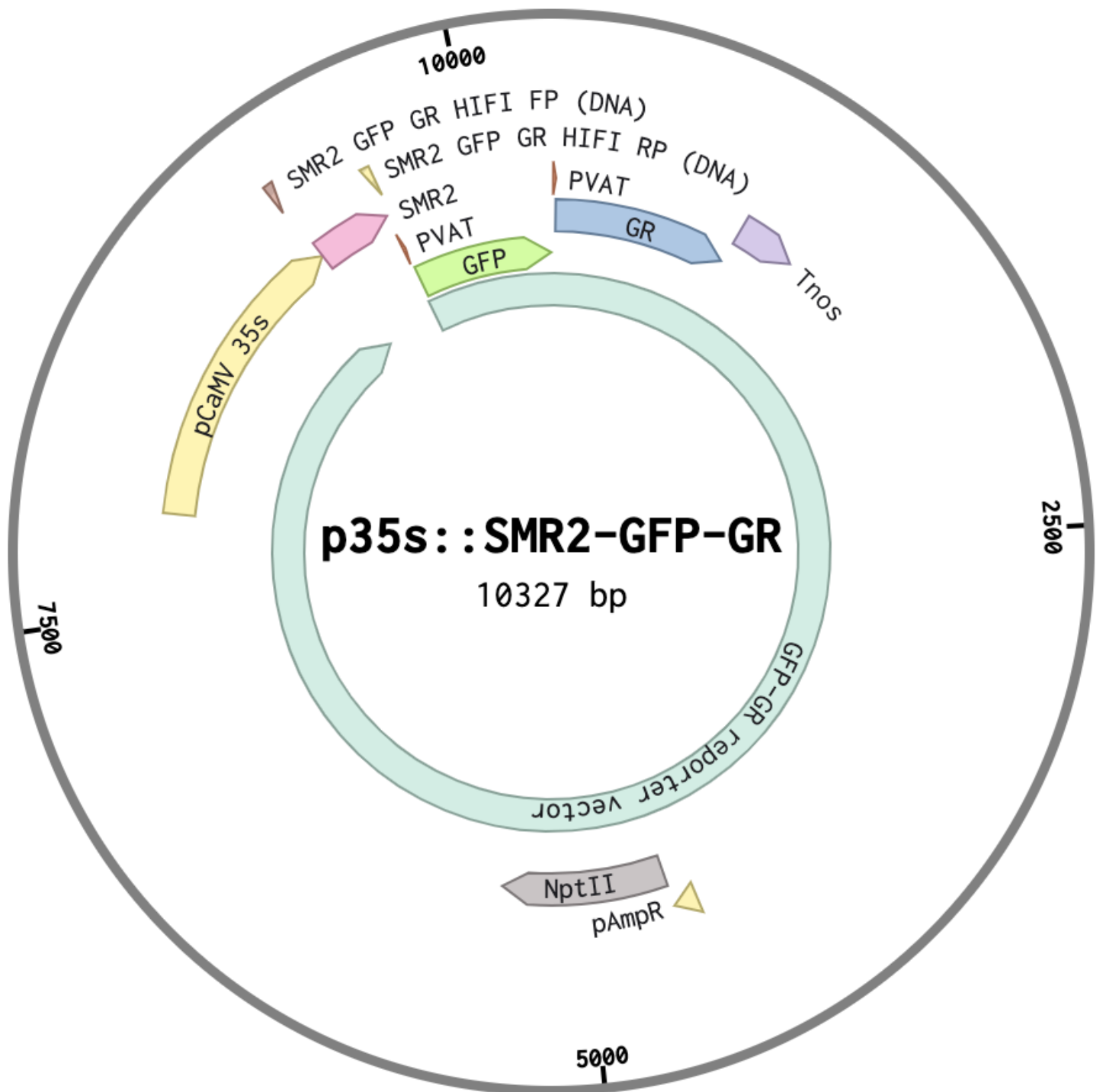


Figure 2.5: Polymerase chain reaction to facilitate the incorporation of a sizer into the HIFI DNA Assembly Vector (Figure 2.4). A: Primers used to clone in genes of interest (GOIs) and remove the PacI site, using HiFi DNA Assembly. B: Schematic of the inducible fusion cassette, including an interchangeable gene of interest (GOI) detailed in the table, joined at the C terminal end by GFP with an N terminal PVAT linker, attached C terminally to GR with an N terminal PVAT linker. White arrows indicate the overlapping forward and reverse primers (A) spanning the PacI site, which incorporate in the gene of interest (Table 2.5). These primers also remove the PacI site from the final, assembled construct, to negate the incorporation of a stop codon.

A



B



C

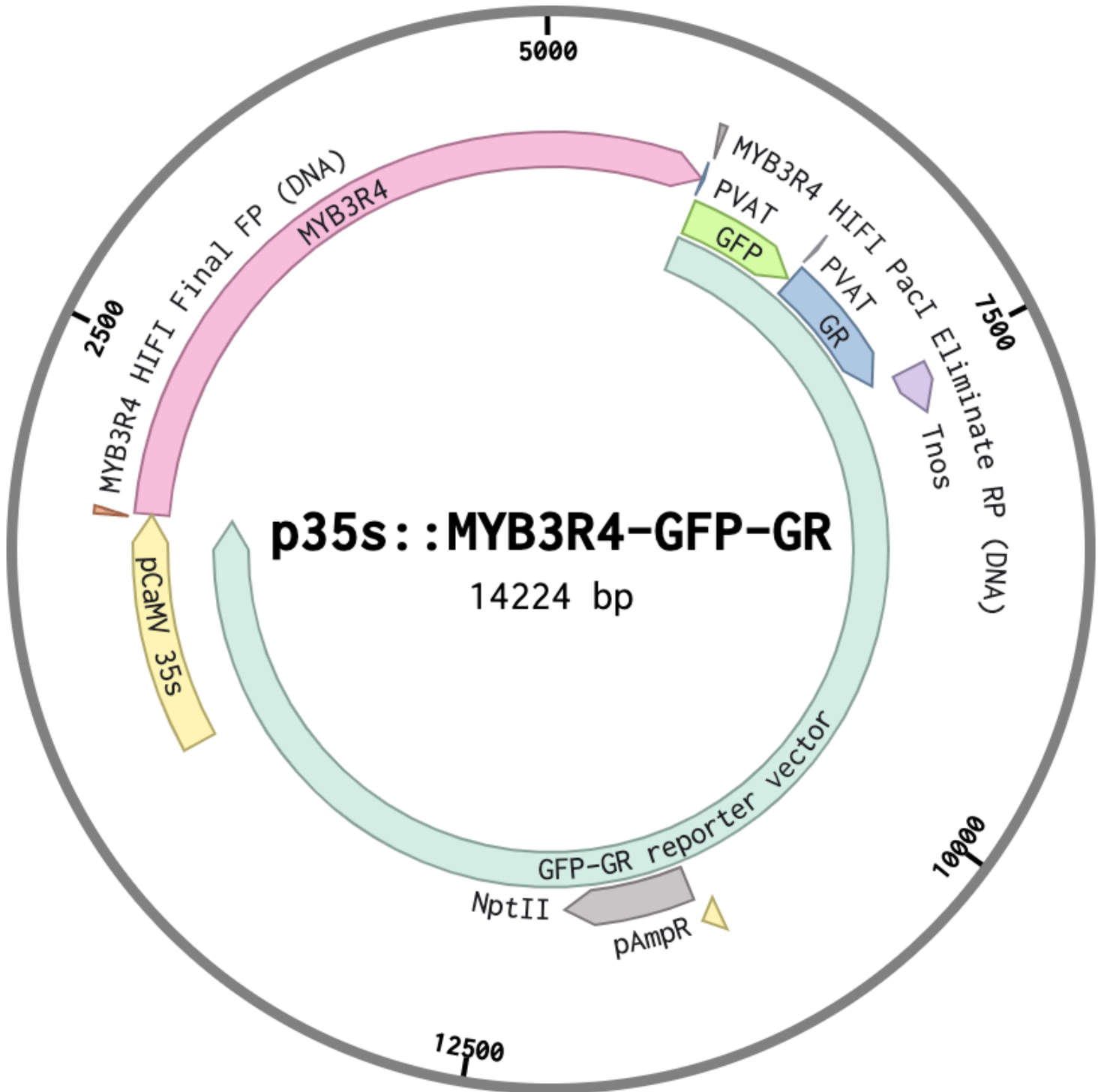


Figure 2.6: Plasmid maps of inducible sizer constructs, assembled from the PacI digested p35s::GFP-GR HiFi Assembly Vector (Figure 2.4C), using HiFi DNA Assembly (Figure 2.5). Maps show the expression cassette driven by the CaMV 35s promoter and the kanamycin plant resistance gene, driven by pAmpR. Marked primers correspond to Figure 2.5A, which were used to clone sizer genomic DNA (Table 2.5) into the prepared vector. GFP-GR reporter vector is shared commonly between the plasmids, corresponding to the PacI digested p35s::GFP-GR HiFi Assembly plasmid (Figure 2.4). A: p35s::MYB3R3-GFP-GR, 12586 bp. B: p35s::SMR2-GFP-GR, 10327 bp. C: p35s::MYB3R4-GFP-GR, 14224 bp.

2.12 Sequencing

For all constructs, 15 μL of 50 $\text{ng}/\mu\text{L}$ plasmid DNA were sent off with appropriate sequencing primers (Table 2.6) at a final concentration of 10 μM , to span the entire length of the insert and partway into the left and right borders (LB and RB) of each specific MoClo plasmid (Table 2.1), to be verified by Sanger sequencing (Eurofins Scientific, Luxembourg). Resulting sequence data was aligned against the expected sequence using the Benchling cloud-based platform (<https://www.benchling.com/>).

Table 2.6: Sequencing primers used for all constructs. Template indicates the part of the transcriptional unit, or which vector the primer bound to. From this point, sequencing reads for approximately 600 bp were obtained downstream.

Name	Template	Sequence
Level 0 Check FP	NT1 and CDS1	CGTTATCCCCTGATTCTGTGGATAAC
Level 0 Check RP	NT1 and CDS1	GTCTCATGAGCGGATACATATTTGAATG
Level 1 Check FP	B3	CTGGTGGCAGGATATATTGTGGTG
Level 1 Check RP	B3	CTGGTGGCAGGATATATTGTGGTG
Level 2 Check FP	H4	GTGGTGTAAACAAATTGACGC
Level 2 Check RP	H4	GGATAAACCTTTTCACGCC
CaMV pro seq 1 FP	p35s	TCCATTGCCAGCTATCTGTC
CaMV pro seq 2 FP	p35s	GGACTAATTGCATCAAGAACACAG
GFP FP	GFP	ATCATGGCCGACAAGCAGAA
GFP RP	GFP	TCGTTGGGGTCTTTGCTCAG
GR BPI FOR	GR	GAAGACCTCCATGAAAAAATCAAAGGGATTC
Tnos For	Tnos	GAATCCTGTTGCCGGTCTTGCG
Tnos Rev	Tnos	CGATCTAGTAACATAGATGACACCG
MYB3R3 Seq 1 FP	MYB3R3	GCAGCACTCGTTTGC GAATTTGC
MYB3R3 Seq 2 FP	MYB3R3	TGCATCGGTGGCAGAAAGTTC
MYB3R3 Seq 3 RP	MYB3R3	CGTTACTGTGCACATTCCTACACGG
MYB3R4 Seq 1 FP	MYB3R4	TCGAACTGATGTCCAGTGCC
MYB3R4 Seq 2 FP	MYB3R4	GCTATGTTATCAACAGGTCGG
MYB3R4 Seq 3 FP	MYB3R4	GACACCTGAAACGGAATGTTGCAG
MYB3R4 Seq 4 RP	MYB3R4	GAGATTCAAGACCTCTCCTG

2.13 *Agrobacterium tumefaciens* transformation

1 μL volumes of plasmids verified by Sanger sequencing were mixed with 50 μL electrocompetent GV301 prepared *Agrobacterium tumefaciens* cells (Kámán-Tóth et al., 2018), and transferred to an electroporation cuvette. Cells were pulsed in a Micro-Pulser machine at 2.5 V, supplemented with 1 mL of LB broth, then shaken at 28°C for 2-3 hours at 225 rpm. 100 μL and 200 μL of the mix was plated onto LB agar with the antibiotics rifampicin and gentamycin (Sigma, UK), both at a final concentration of 20 $\mu\text{g}/\text{mL}$, and 50 $\mu\text{g}/\text{mL}$ kanamycin, the antibiotic specific to the Level 2 plasmid. Plates were incubated at 28°C for 2-3 hours for 3 days. Colony PCR was performed for verification (section 2.5).

2.14 Floral dipping

For all plant transformations the “Direct Dipping” modifications (Davis et al., 2009) of the standard floral dipping procedures (Clough and Brent, 1998) were followed (Clough and Brent, 1998). YEBS Media for this was prepared in accordance to Konagaya et al., 2020), replacing the beef extract with yeast extract (Melford, UK).

T1 seeds were harvested and plated onto GM with 200 $\mu\text{g}/\text{mL}$ cefotaxime (Sigma, UK) and screened on kanamycin (50 $\mu\text{g}/\text{mL}$). Antibiotic screening was used for subsequent generations of seeds. Segregation analysis was performed on T2 seedlings using Chi-squared analysis to find lines segregating 3:1, with one copy of the transgene.

2.15 Plant growth conditions

For all experiments, seeds were sterilised with 10% (v/v) W! Thin Bleach (Mirius, UK), 0.1% (v/v) Triton x 100 (Sigma, UK) in water then sown onto GM medium (4.4 g L⁻¹ Murashige Skoog (Duchefa, Netherlands), 1.5 % sucrose, 0.5 g L⁻¹ 2-(N-Morpholino) ethanesulfonic acid sodium salt (MES) (Sigma, UK) and 1 % microagar (Duchefa, Netherlands), to pH 5.8 with potassium hydroxide (KOH, Sigma, UK), in 90 mm round plates. Subsequently, seeds were stratified at 4°C in the dark for 72 h then grown vertically under standard long day conditions (16 h light at 150 µmol m⁻² s⁻¹, 8 h dark, 21 °C) at 22°C, where they germinated. Once over 7 days old, plants were transferred to soil in a 3:1 compost to sand ratio and grown under a 16-hour photoperiod at 21°C. Plants were watered every 2-3 days.

2.16 Fluorescence microscopy

Seedlings were screened for GFP using a Zeiss AxioCam MRc5 microscope with a GFP filter, between 5 and 8 days after germination. Roots were viewed for GFP, using Col-0 as a negative control.

2.17 Confocal microscopy

Imaging was performed on a Zeiss LSM 710 Meta. Roots were stained with 100 µg/mL of propidium iodide (Sigma, UK) and imaged at 20 X magnification. Laser power was 4500. GFP gain was variable, but was kept the same within an experiment to permit comparisons between samples.

2.18 DEX Induction

For induction screening and experiments, seedlings were moved to plates with a specified concentration of dexamethasone (DEX) (Sigma, UK) dissolved in DMSO. Concentrations were prepared so that the same amount of DMSO (0.00033 % DMSO v/v) was added to GM medium for each DEX concentration used. Alongside as a control, some seedlings were moved to DMSO only plates containing 0 μ M DEX. For screening, 90 mm plates were used. For DEX induction experiments, 5 x 5 inch square plates (120 mm) were used.

2.19 Root Length Analysis

Upon transfer to DEX, the position of the root was marked. After three days, plates were scanned at 600 dpi using an Epson Perfection V500 scanner. A segmented line on Fiji (<https://imagej.net/imagej-wiki-static/Fiji>) was drawn from the position of the dot (which marked position of root on transfer) to the end of the root tip and measured for each seedling. The mean uninduced root length was calculated for each genotype. Relative Root Growth (RRG) was calculated by subtracting the relevant mean uninduced root length from each measurement of induced root length. (Appendices 1.8). Standard error for the RRGs of *Col-0* and *p35s::GFP-GR* 7.2.3.1 were calculated using the Rmisc and plyr packages (Appendices 1.9).

2.20 Cortex Cell length Analysis

Cortex cells lengths (CCL) were analysed from confocal microscopy snaps. A segmented line was drawn from the first cell of the QC, spanning all cortex cells shown in the image. This line was processed using cell-o-tape (French et al., 2012). Measurements included the apical and basal meristem and stopped once cells began to elongate. Lengths were transformed by the natural logarithm for plotting and analysis.

2.21 Graphs and statistical analysis

Graphs were made and statistical analysis was performed using Rstudio (Version 4.0.3). Boxplots and the RRG line graph were made using the ggplot2, tidyverse, hrbthemes and viridis packages (Appendices 1.1; 1.2; 1.3; 1.13; 1.10). To test the effect of DEX concentration on RRG and CCL, linear regression models, using an interaction term between Dex concentration and Genotype (Appendices 1.5; 1.11). The overall p value of the models were reported. For RRG, *Col-0* and *p35s::GFP-GR 7.2.3.1* were compared, whereas for CCL *p35s::MYB3R3-GFP-GR* was also included.

To test the effect of increasing DEX induction on the CCL length of each genotype, subsets were created (Appendices 1.7). A simple linear regression was performed using the lme4 and lmerTest packages, and subsequently Tukey's Post-Hoc HSD tests were conducted using the multcomp packages (Appendices 1.4). This was repeated to perform pairwise comparisons of CCL for genotypes at the non-induced condition (0 μ M DEX) and the selected optimum concentration (100 μ M DEX) (Appendices 1.6).

Linear regressions were performed in the same way for genotypic subsets created from RRG data (Appendices 1.12). Tukey's Post-Hoc HSD tests were performed.

2.22 Fluorescence Intensity Measurements

To get an approximate quantification of the brightness visualised in the images of induced *p35s::MYB3R3-GFP-GR* and *p35s::GFP-GR* roots, images were analysed for fluorescence. Snaps were taken by confocal microscopy, in the plane where the QC and cortex cells were visible, of which there were five replicates for each line. Fiji was used to conduct analysis. Segmented lines were used to draw around the roots, and using set measurements on Fiji: the root area and integrated density (correlating to the GFP fluorescence intensity of the pixels in the image). This was calculated for both the induced and non-induced roots, for each genotype.

A region of the image containing no root tissue and therefore no fluorescence was then selected and measured as background. Corrected Total Cell Fluorescence (CTCF) values were subsequently generated by multiplying the area of the root by the background fluorescence, and subtracting that value from the Integrated Density output for the root. The mean of each value for each genotype, under each condition was recorded. Subsequently, the mean CTCF value for each genotype under the non-induced condition was subtracted from the mean CTCF value for each genotype under the induced condition, separately.

One three-dimensional Z stacks under the same settings for each genotype induced at 100 μ M DEX was also obtained. From these images, maximum intensity projections were created using the software on the confocal microscope (Section 2.17), for qualitative comparison.

3. Results

3.1 The position of GR within the fusion protein affects functionality in *Arabidopsis thaliana*

To validate the GR induction system and determine the most effective position for the GR domain, two p35s GFP reporter constructs were designed; one with GR at the N-terminal and one with GR at the C-terminal. To prevent steric hindrance and ensure functional protein folding, a linker region (proline, valine, alanine and threonine, PVAT) was incorporated onto the GR domain at either N or C-terminal, with respect to where the protein fused with GFP. As both N and C positions were to be experimentally tested side by side, *in silico* modelling was not carried out. These constructs were defined as *p35s::GR-GFP* and *p35s::GFP-GR*, respectively. To serve as a positive control and confirm that the GFP sequence supplied in the MoClo kit (Engler et al., 2014) functioned well in *Arabidopsis*, *p35s::GFP* was also created. All cassettes were assembled in the same binary vector (pAGM4673; Figure 2.2; Figure 2.3), carrying a kanamycin selectable marker for plant transformation. The constructs were assembled into *E. coli* using the Golden Gate method (Figure 2.2; Weber et al., 2011; Engler et al., 2014) checked first by colony PCR (Section 2.5), and then via Sanger sequencing (Section 2.12) to obtain the complete sequence of the construct. Plasmids with the verified sequences were subsequently transformed into *Agrobacterium tumefaciens* (Section 2.13) and verified by colony PCR (Figure 3.1). Selected colonies were used to transform *Arabidopsis* via floral dipping (Section 2.14) and resulting T1 seeds were harvested and screened with kanamycin. All three constructs produced resistant seedlings.

The roots of these seedlings were subsequently viewed by fluorescence microscopy. *p35s::GFP* showed strong ubiquitous expression across all resistant seedlings (Figure 3.2 shows one example seedling), confirming that the GFP in the MoClo kit in combination with the 35s promoter expresses strongly and consistently in *Arabidopsis thaliana* roots. However, GFP was not detectable in any seedlings belonging to *p35s::GRP-GFP* (not shown) suggesting that this orientation of the fusion protein is unable to correctly fold and express in *Arabidopsis*, failing to serve

as a reporter. Contrastingly, *p35s::GFP-GR* seedlings were GFP positive 1 in 10 times (Figure 3.1B). Therefore, this orientation of the fusion protein was selected to optimise DEX induction and incorporate genes of interest (GOIs) into the inducible system. For use as controls in later experiments, 24 GFP positive *p35s::GFP-GR* T1 seedlings were put onto soil and grown to the next generation.

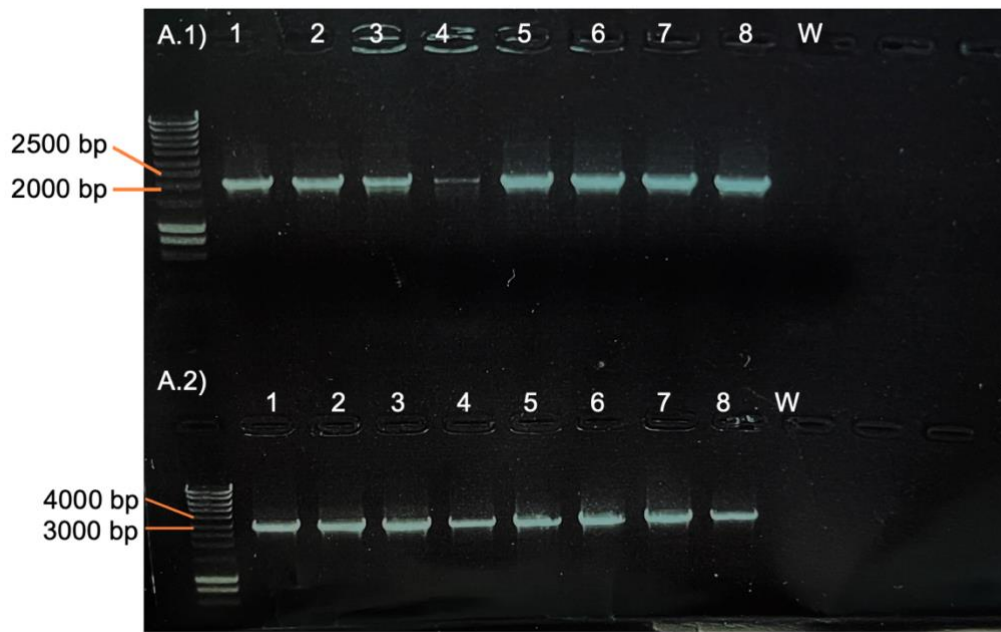
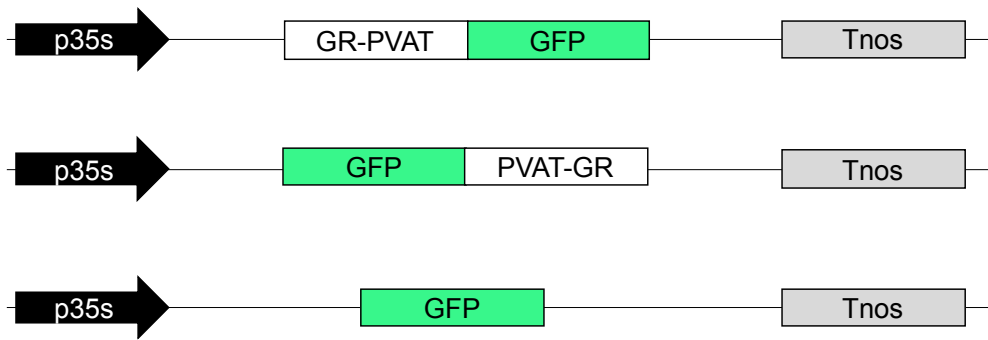


Figure 3.1: Gel electrophoresis images of colony PCRs of Agrobacterium tumefaciens transformations. The ladder is SmartLadder, 200bp-10kb, (Eurogentec). 1-8 corresponds to the colony number on a labelled master plate. The lane labelled P contains a 1 in 100 dilution of the sequenced E. coli plasmid used for the transformations, as a positive control. The W lane consists of water as a negative control. A) p35s::GFP. A.1) The first half using the primers Level 2 FP and GFP RP, amplicon size 2165 bp. Colony 1 was taken forward. A.2) The second half of the construct, where the primers GFP FP and Level 2 RP are used to create an amplicon of 3145bp. Annealing temperature 57°C, extension time 3 minutes 30 seconds. B) p35s::GFP-GR and C) p35s::GR-GFP. Primer Set 1: Level 2 FP and Tnos RP, amplicon size of 3310 bp for B and 3295 bp for C. Primer Set 2: GR Bpi FP and Level 2 RP to create an amplicon size of 3730 bp for B and 4471 for C. Annealing temperature 57°C, extension time 4 minutes 30 seconds.

A**B**

Construct	Purpose	Fluorescence observed?
<i>p35s::GFP</i>	Positive GFP control	Yes – always
<i>p35s::GR-GFP</i>	Reporter fusion protein	No
<i>p35s::GFP-GR</i>	Reporter fusion protein	Yes – in 1/10 seedlings

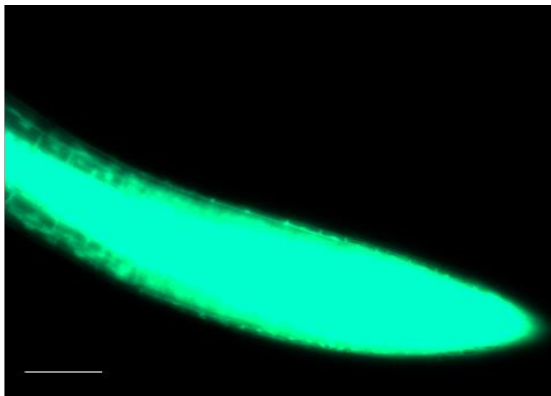
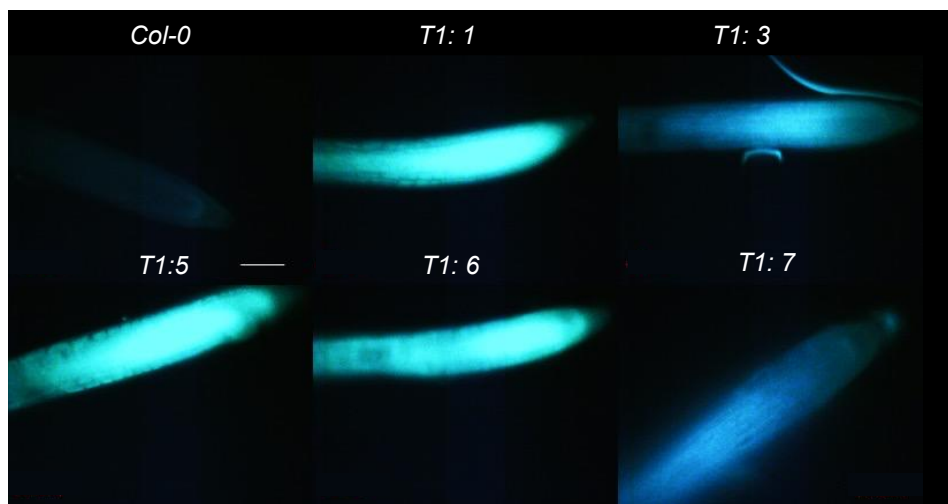
C**D**

Figure 3.2: Initial design and screening of transgenic constructs. A: Schematics of expression cassettes built by MoClo modular cloning. All expression cassettes were inserted into the pAGM4673 (H2) Level 2 Acceptor (Table 2.2) via Golden Gate cloning (Figure 2.2; Weber et al., 2011). Cassettes are comprised of the Cauliflower Mosaic promoter from the Golden Gate kit (Table 2.2; Engler et al., 2014), GFP and Nos terminator from the kit and the GR domain amplified from a pGreen vector containing a p35s::GENE-GR construct, built for the TGV system (Böhner et al., 2002). PVAT stands for the linker comprised of Proline, Valine, Alanine and Threonine. B: Table of constructs including their purpose and GFP expression, qualitatively determined by fluorescence microscopy. C: A T1 seedling selected from the ubiquitously expressed p35s::GFP transgenic line. Roots of T1 seedlings grown on GM microagar without DEX and imaged screened by fluorescence microscopy (20 X). Scale bar = 200 μ m. D: Five independent T1 seedlings transformed with the construct p35s::GFP-GR, with Col-0 as a negative control, grown on GM microagar without DEX and all imaged under the same settings, 20x magnification. Scale bar = 200 μ M. All images grouped on PowerPoint and adjusted for visibility (Brightness -4%, Contrast 61%).

3.2 Segregating *p35s::GFP-GR* transgenics displayed a range of expression, with and without DEX

In order to test the GR reporter protein further, a screening pipeline based on antibiotic resistance and GFP expression was implemented (Figure 3.3). Seeds were harvested from the GFP positive *p35s::GFP-GR* transgenics which had been put onto soil and allowed to self. Segregation analysis via Chi-squared testing found twelve T2 lines with the correct 3:1 ratio of positive to negative seedlings, with regards to antibiotic resistance, expected for a single insertion event. Of those, eight lines with the smallest Chi-squared values were selected for screening with and without DEX using confocal microscopy. In line with previous studies (Craft et al., 2005), and observations of the T1 generation (Figure 3.2), it was expected that prior to induction, seedlings would exhibit ubiquitous GFP expression, which would translocate from the cytoplasm into the nucleus upon DEX application. Interestingly, very minimal, if any GFP expression was visualised without DEX, inconsistent to the behaviour of the lines in their previous generation. However, once seedlings had been transferred to plates with 60 μ M DEX for 24-36 hours, GFP was seen in the root tip. Figure 3.4A shows the comparison of one line, *p35s::GFP-GR T2: 3.2* before and after DEX induction. After induction, GFP signal was visualised throughout as multiple circular manifestations, resembling nuclei. Therefore, it was concluded that DEX application enabled functional folding of both GR and GFP proteins in the fusion, firstly enabling dissociation of the GR domain from HSP90 in the cytoplasm, and subsequently enabling it to enter the nucleus while reporting GFP fluorescence. This was observed across all eight lines (four shown in Figure 3.4B). Interestingly, some lines, such as *p35s::GFP-GR 2.1*, while having signal with distinct nuclear appearance, also presented cytoplasmic GFP, whereas other lines seem to have less cytoplasmic GFP (Figure 3.4B). This could be indicative of differences in expression levels between the lines, and therefore different responses to DEX; it could take longer for all the protein to translocate into the nucleus depending on the amount of protein that has accumulated. This also could be due to different copy numbers of the transgene, as these populations are heterozygous. Overall, screening of the segregating *p35s::GFP-GR* T2 families provided a selection of lines which demonstrated the activation and translocation of the GFP reporter to express

in the nucleus. Lines from eight different families were selected and put onto soil, to obtain homozygous lines which would undergo a DEX optimisation protocol.

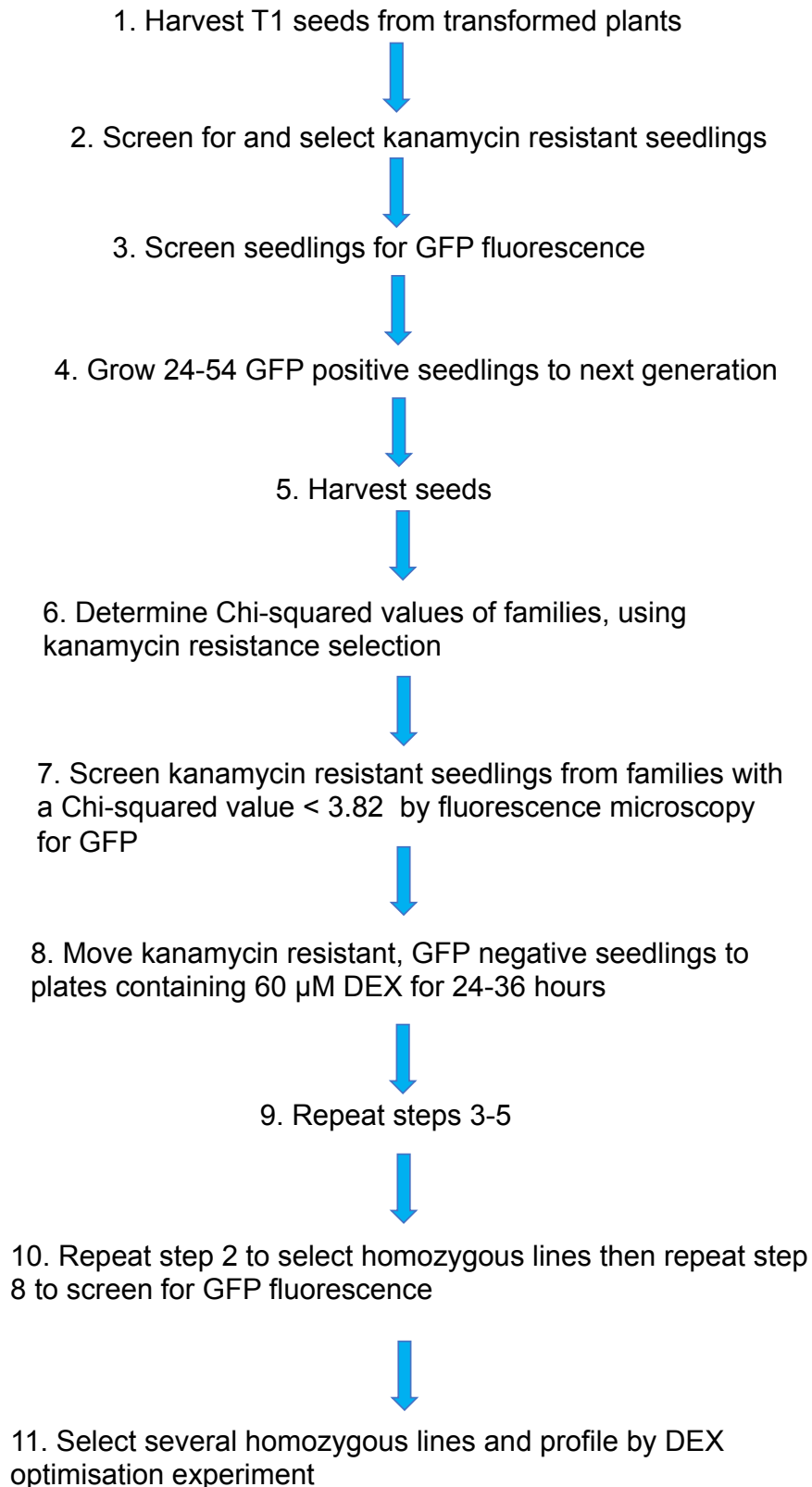
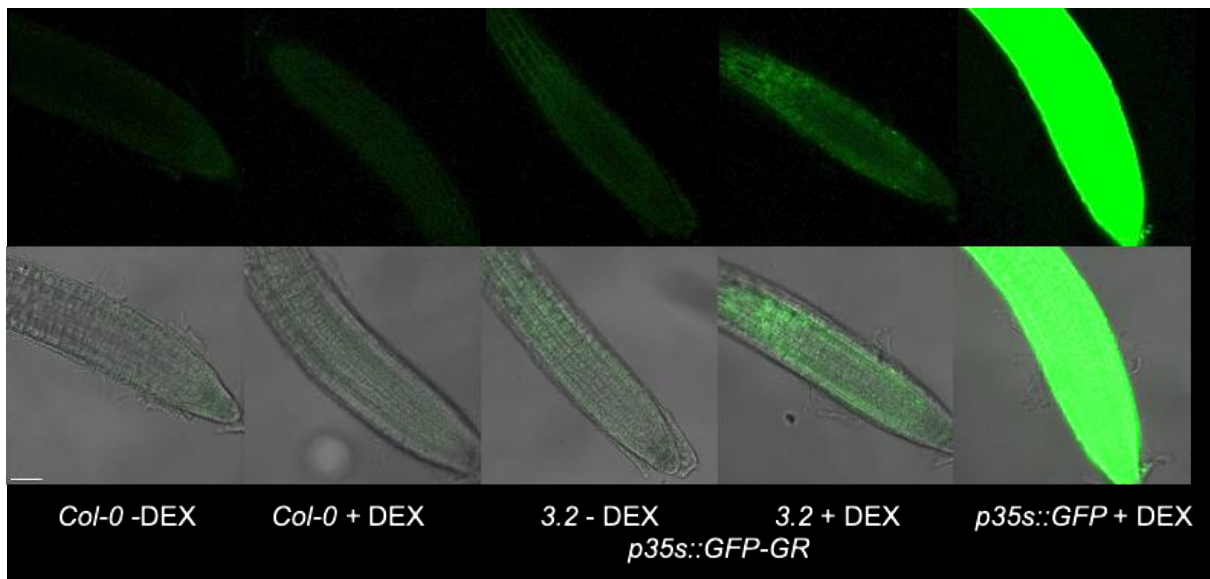


Figure 3.3: Initial screening pipeline for screening of p35s::GFP-GR reporter constructs. T1 seeds refer to the seeds collected from Col-0 plants which had been transformed with constructs via floral dipping procedures. Steps 3-5 were implemented for T2 and T3 seeds.

A



B

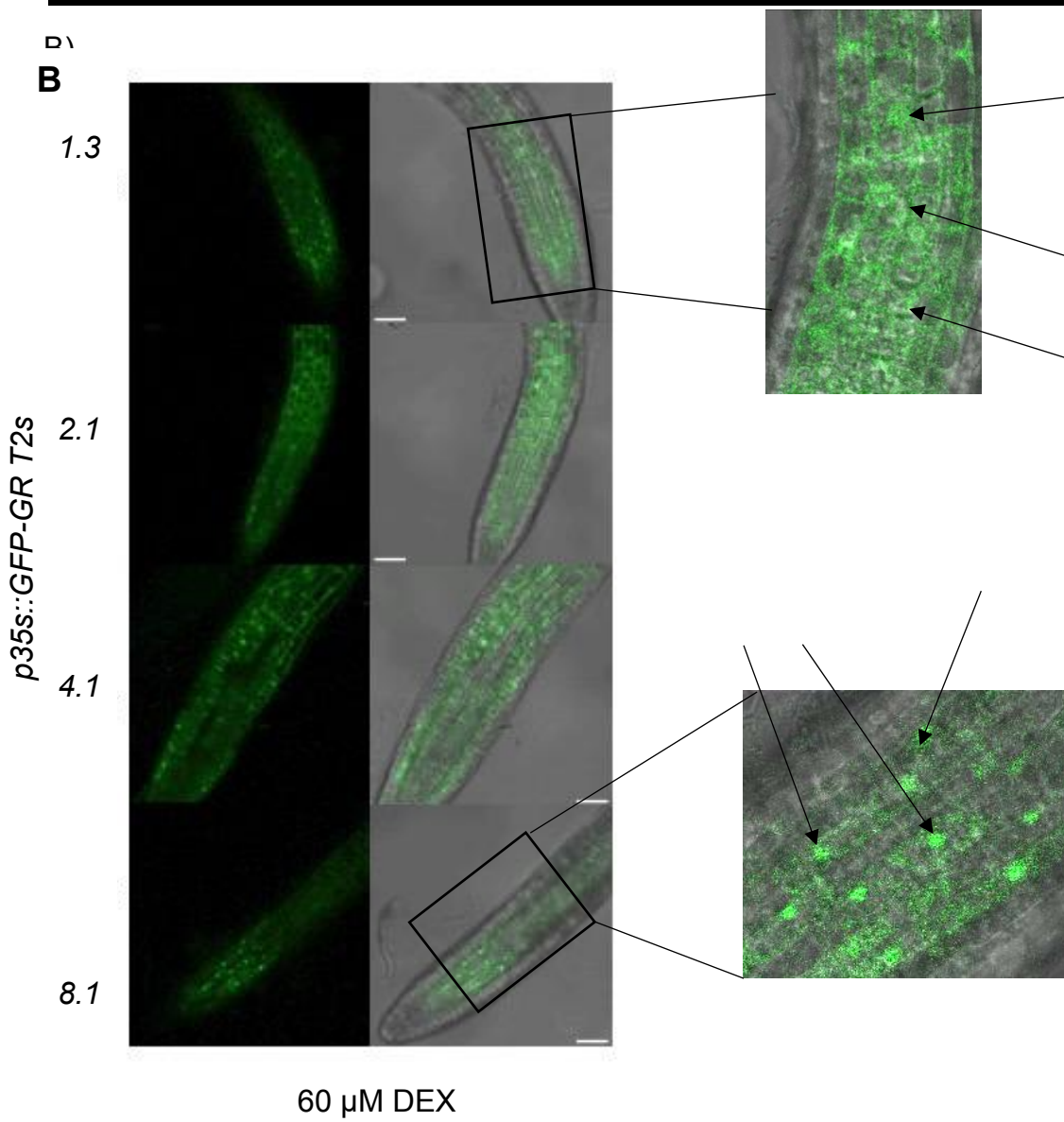


Figure 3.4: Confocal scans of p35s::GFP-GR T2 root tips at 20 X magnification. Top row shows the GFP channel (Gain 1016) and the bottom is the composite of the GFP channel together with a transmitted light image. Scale bar for both sets of images is 200 μm . A: p35s::GFP-GR T2: 3.2, before and after 24 hours on 60 μM (- DEX and + DEX, respectively). Col-0 is used as a negative control, with and without DEX treatment and a p35s::GFP T2 with a 3:1 segregation ratio determined by Chi-squared analysis on DEX is used as a positive GFP control. Scale bar = 50 μm . Image altered on PowerPoint, Brightness = 43%, contrast = 13%, then altered again to Brightness 60% on Word). B: Comparison of four p35s::GFP-GR lines from different T2 families with 3:1 segregation ratios, which had been grown on GM microagar and transferred to 60 μM DEX for 36 hours. Not all 3:1 segregating T2s are shown. Arrows point to GFP signal indicative of nuclei (not including all of them). Scale bar = 50 μm . Final composite Image altered on PowerPoint; Brightness = 63%.

3.3 Selection of reliable homozygous *p35s::GFP-GR* reporter lines for use as induction controls

To obtain homozygous *p35s::GFP-GR* reporter lines to test the DEX induction system, the nine plants from each of the previous eight T2 lines were grown, harvested and screened on kanamycin, in accordance to the screening pipeline (Figure 3.3). Seven homozygous plants were recovered which belonged to two different families; one from 8.1 and interestingly, six plants from 6.1, suggesting this line could have multiple insertions (Table 3.1). Interestingly, upon screening T3 families, lines which were segregating appeared to have brighter GFP signal, visible across a higher number of seedlings, than any of the homozygous lines. Of the homozygous lines identified, *p35s::GFP-GR T3: 8.1.4* was selected to test and optimise the DEX induction system, as out of the two families, 8.1 and 6.1, it seemed the most promising, given the latter family was suspected to contain multiple insertions.

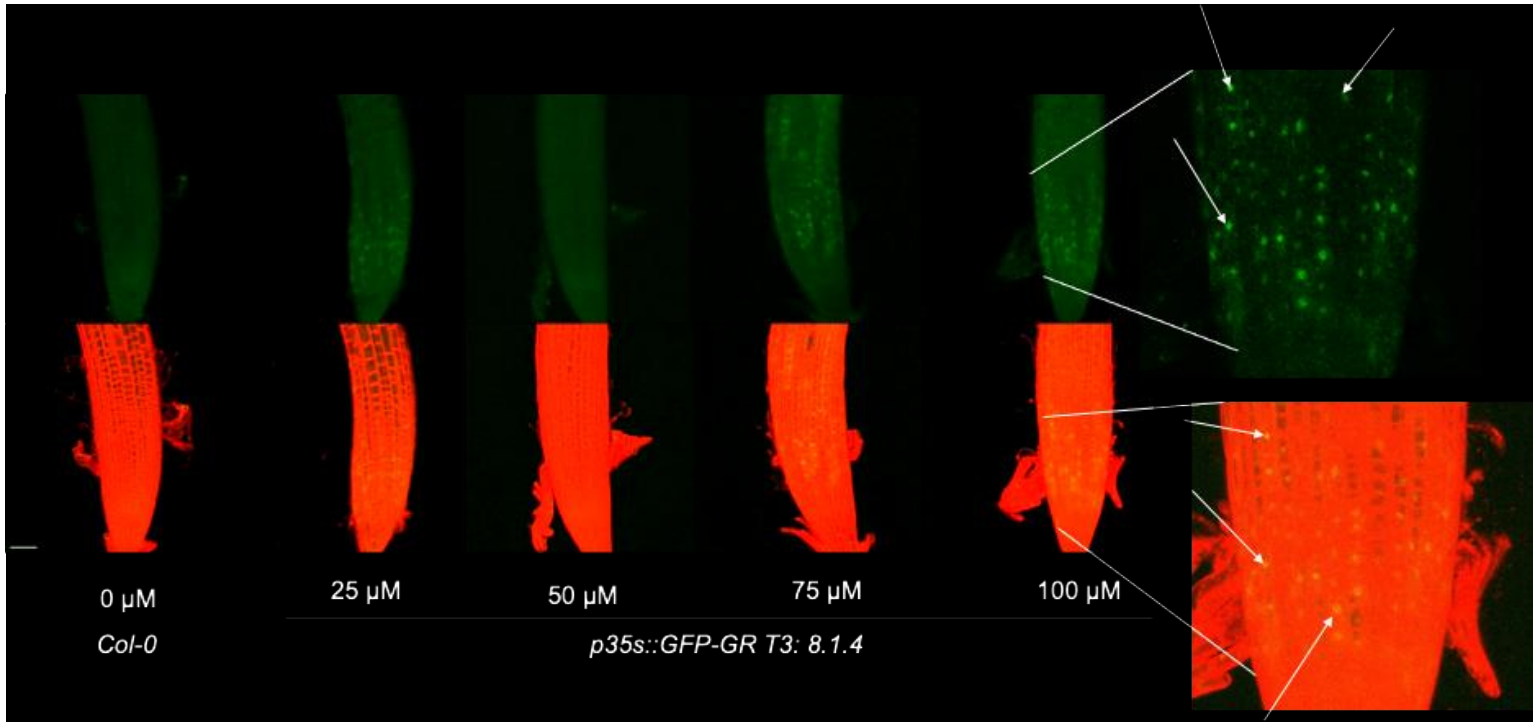
Four day old seedlings from this line were transferred to plates with 25 μ M, 50 μ M, 75 μ M and 100 μ M DEX for 24 hours, stained with 100 μ g/mL PI and visualised by collecting confocal microscopy Z stacks (Figure 3.5). GFP expression was observed in some seedlings following DEX treatment however GFP was not consistently seen (see Figure 3.5A, 50 μ M). Therefore, *p35s::GFP-GR T3: 8.1.4* was considered to be an unreliable reporter that would not provide a strong control for future experiments with a GOI. Consequently, steps 7-9 of the screening pipeline (Figure 3.3) were repeated. Families, where bright, consistent, punctate expression consistent with nuclear localisation had been detected post DEX induction, with the aim to find multiple homozygous lines in the T4 generation (Table 3.1).

Table 3.1: p35s::GFP-GR T2 families, segregating in a 3:1 ratio. Chi-squared values are indicated for each T2 family, all of which <3.82. No. of homozygous T3 indicates how many homozygous lines were found at the T3 generation, where nine plants of each T2 member had been harvested. Line taken forward for expression analysis indicates which line from the families at the T3 generation was selected for the DEX optimisation protocol. The last column indicates if the T3 family was selected for growth to the T4 generation, in order to find a homozygous line.

T2 Family	Chi-squared	No. Homozygous T3	Line selected for DEX optimisation	Grown to T4 generation?
1.3	1.018867925	0		Yes
2.1	0	0		Yes
3.1	1.92	0		Yes
3.2	2.245614035	0		Yes
4.1	0.049382716	0		Yes
6.1	0.216450216	6		No
7.2	0.011299435	0		Yes
8.1	0.681957187	1	8.1.4	No

Seeds belonging to the T4 *p35s::GFP-GR* families were harvested, generating six further homozygous lines. One line from each family was grown for four days then transferred to either 60 μ M DEX or to new GM plates four days after germination (DAG) and imaged after 24 hours by confocal microscopy. Interestingly, most of the lines across the families showed either very weak GFP signal, or no detectable expression at all, despite displaying strong, putatively nuclear signal at T2 and T3 generations. However, two lines, 2.4.1.16 and 7.2.3.1, showed consistent, putatively nuclear GFP expression in both the root apical meristem and higher up, in the transition zone (Figure 3.5B). Interestingly, unlike 7.2.3.1, 2.4.1.16 showed cytoplasmic GFP expression before DEX induction. Therefore, both lines were selected for further crossing and analysis, due to their reliability and relatively brighter GFP signal. Of the two, *p35s::GFP-GR T4: 7.2.3.1* was prioritised, as qualitatively it appeared to have a more concentrated GFP signal, with less uninduced, leaky expression the absence of DEX.

A



B

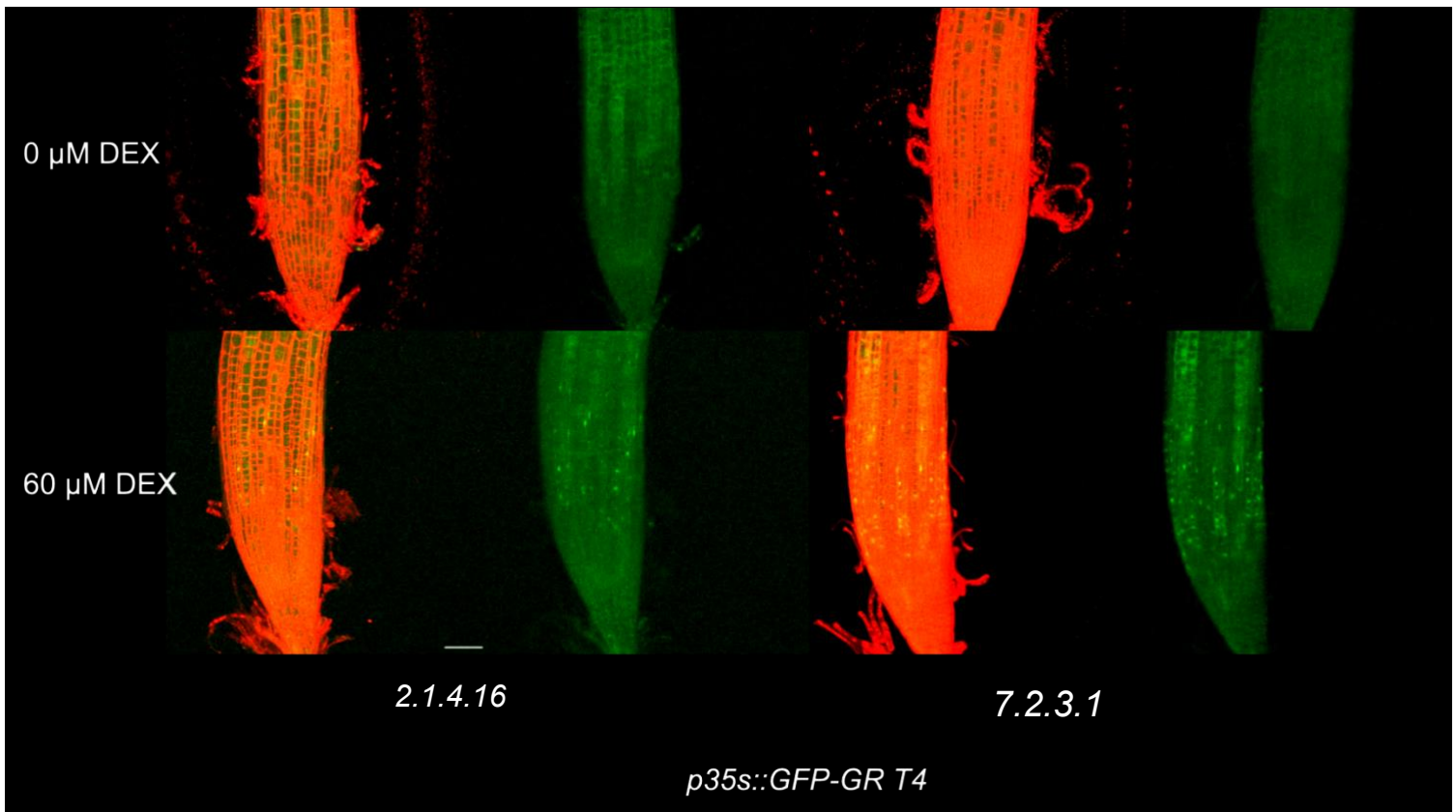


Figure 3.5: Root apical meristem confocal Z stacks, assessing homozygous p35s::GFP-GR reporter lines for GFP expression. Magnification = 20 X, scale bars = 50 μ m. A: DEX induction optimisation experiment for the line p35s::GFP-GR 8.1.4. Arrows point towards subcellular GFP structures with the approximate size and shape of nuclei. Top row shows the GFP channel, lower row shows a composite of the PI and GFP channels. GFP gain, 1061. Brightness: 21%, Contrast: 55%, altered on PowerPoint. B: Root apical meristems of p35s::GFP-GR T4: 2.1.4.16 and p35s::GFP-GR T4 7.2.3.1, 5 DAG, with Col-0 as a negative control. The images are from maximum intensity projections of z stacks, where for each line, the left image is a composite of GFP signal and propidium iodide and the right is GFP only. GFP gain, 1125. DEX refers to the seedlings which had been transferred at 4 DAG for 24 hours to plates with 60 μ M DEX, whereas for 0 μ M DEX, seedlings were transferred to GM microagar plates. Brightness: 20%, Contrast: 55%, altered on PowerPoint.

3.4 Functional expression of genes of interest in the GR inducible system is sequence dependent

Following the validation of *p35s::GFP-GR* as a functional inducible reporter construct, NEB HiFI assembly (New England Biolabs, USA) was used to incorporate genes of interest (GOIs) relating to proteins with roles at G2/M into the expression cassette (Section 2.11). Two MYB3R transcription factors (MYB3R3 and MYB3R4), which have hypothetical antagonistic size functions, were selected to test the system. The GOIs corresponding to these proteins were added at the N terminal of the fusion protein, upstream of GFP, as the lack of visual expression of the *p35s::GR-GFP* transgenics suggested that the addition of a protein to the C terminus of GR had hindered the ability of the fusion protein to fold and correctly function. The same linker used between GFP and GR, PVAT, was used again, between the GOI and GFP. *p35s::MYB3R3-GFP-GR* and *p35s::MYB3R4-GFP-GR* were correctly assembled (Figure 2.6 A and C), checked via Sanger sequencing (Section 2.12), transformed into *Arabidopsis* (Sections 2.13; 2.14) and verified by colony PCR (Section 2.5), (Figure 3.6B and 3.6C) .

As *p35s::GFP-GR* reporter T2s and T3s only yielded GFP signal when induced on media containing DEX, resistant inducible size T1s were transferred from antibiotic plates to GM microagar plates containing 60 μ M DEX and subsequently, screened for DEX via confocal microscopy (Figure 3.7). GFP positive seedlings were observed for *p35s::MYB3R3-GFP-GR* only; over 30 T1 *p35s::MYB3R4-GFP-GR* seedlings were all negative for GFP when screening on DEX induced media. Therefore, GFP positive *p35s::MYB3R3-GFP-GR* T1s were selected and carried forward to subsequent generations. T2 seedlings displayed level a range of expression across the seedlings, showing GFP signal characteristic of nuclear localisation (see Figure 3.8). Therefore, seedlings from ten different families with positive GFP signals were transferred to soil, to obtain homozygous lines for future experiments (Figure 3.7).

A)

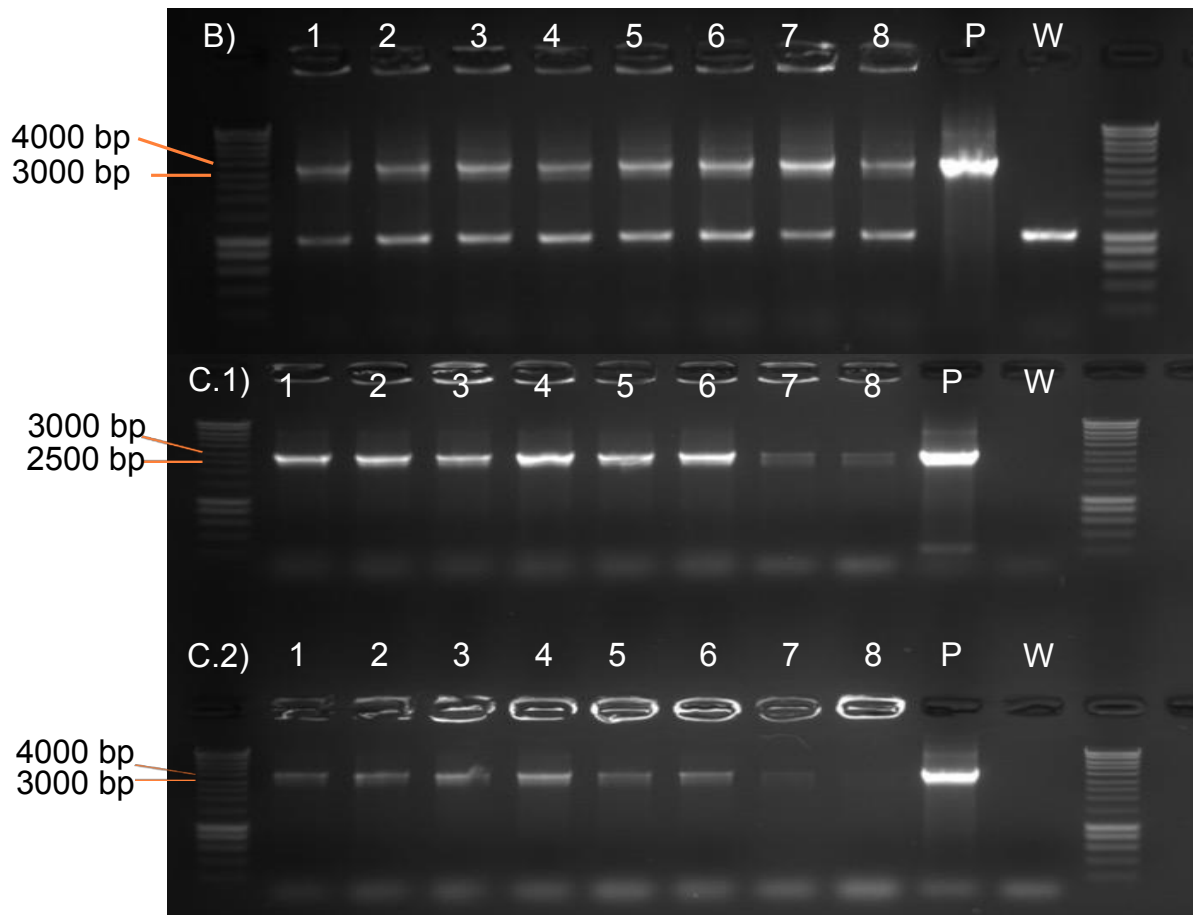
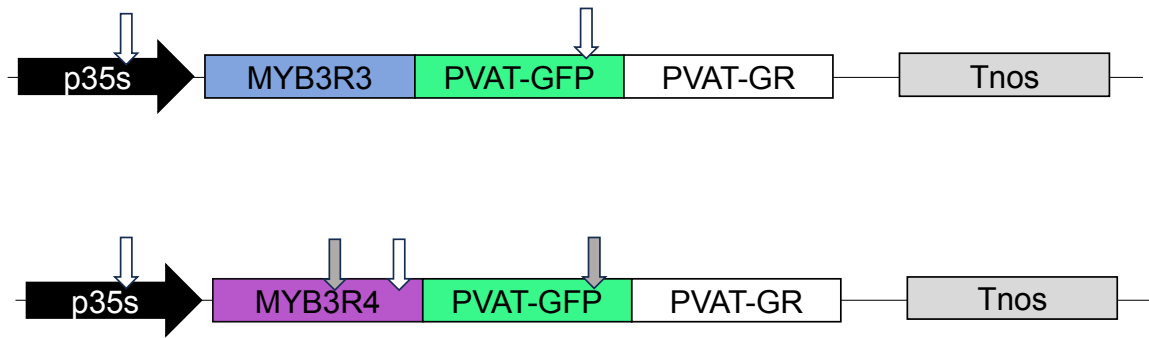


Figure 3.6: Schematic for two inducible sizer constructs from the MYB3R transcription family, p35s::MYB3R3-GFP-GR and p35s::MYB3R4-GFP-GR. A) Schematics of the cassettes created. These cassettes were inserted into the *PacI* digested HiFI Assembly Vector (Figure 2.4; Figure 2.6 A and C)) prepared from p35s::GFP-GR to facilitate a one step HiFI Assembly reaction. The linker sequence used is PVAT (proline, valine, alanine and threonine). Arrows show where the primers bind. For p35s::MYB3R3-GFP-GR, the primers are CaMV pro seq 1 FP and GFP FP. For p35s::MYB3R4-GFP-GR, white arrows correspond to CaMV pro seq 1 FP and MYB3R4 Seq 4 RP. Grey arrows indicate MYB3R4 FP 3 and GFP qPCR RP. B) and B) Gel electrophoresis images of colony PCRs testing *Agrobacterium tumefaciens* transformations. The ladder is SmartLadder, 200bp-10kb, (Eurogentec). Numbers 1-8 correspond to the colony number from a labelled master plate. The lane labelled P contains a 1 in 100 dilution of the sequenced *E. coli* plasmid used for the transformations, as a positive control. The W lane contains distilled (nuclease free) water as a negative control. This PCR was run at 57°C with an extension time of 4 minutes 30 seconds. A) p35s::MYB3R3-GFP-GR, using the primers CaMV pro seq 1 FP and GFP RP, with an amplicon size of 3552 bp. B) p35s::MYB3R4-GFP-GR divided into two parts, where B.1) is the second part, consisting of 2983 bp using the primers MYB3R4 FP 3 and GFP qPCR RP. B.2) is the first part, with an amplicon of 3927 bp using the primers CaMV pro seq 1 FP and MYB3R4 Seq 4 RP.

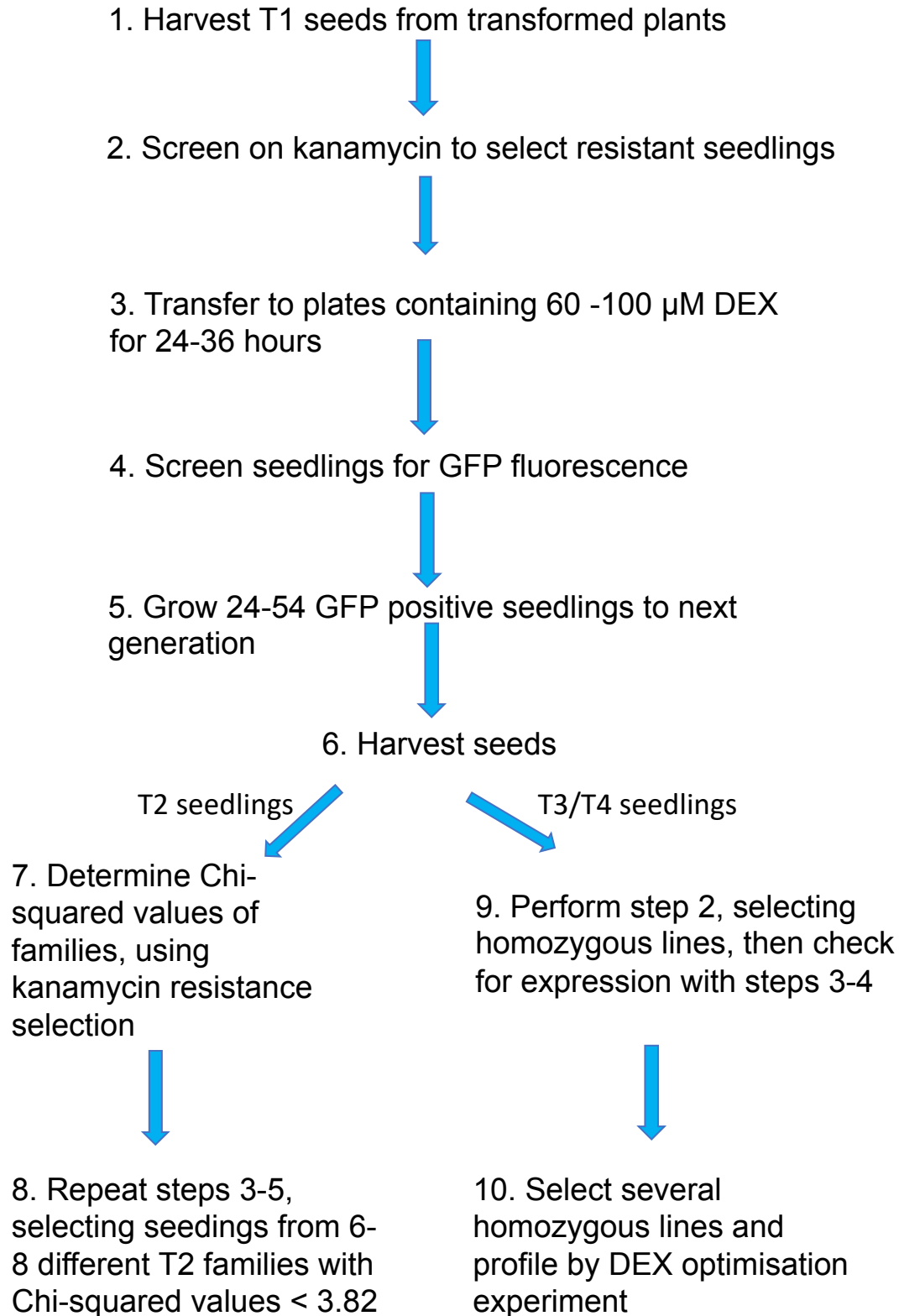


Figure 3.7: Updated screening pipeline for inducible GFP-GR constructs. Screening for fluorescence was conducted initially using DEX, unlike in the original pipeline for reporter constructs (Figure 3.3).

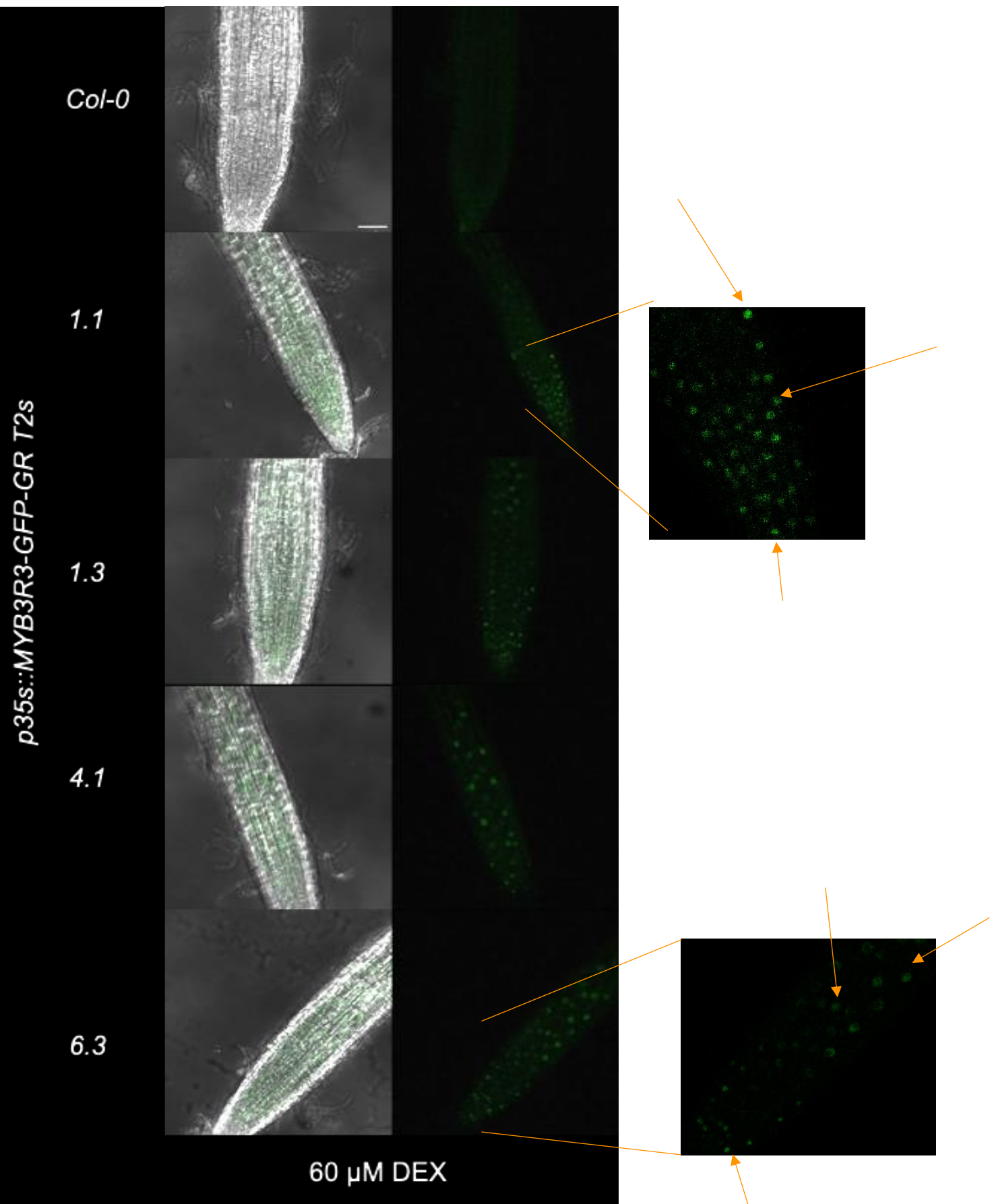


Figure 3.8: Roots of 6 day old p35s::MYB3R3-GFP-GR T2 seedlings with Col-0 as a negative control, transferred to 60 μ M DEX 24 hours prior. Magnification = 20 X, scale bar = 50 μ m. The left column shows the composite of the transmitted light channel and GFP, the right shows the GFP channel only. GFP gain = 1061. Orange arrows point towards putative nuclear signal. Not all 3:1 T2s screened are showed here. Brightness: 27%; Contrast: 40%, altered on PowerPoint.

3.5 Five *p35s::MYB3R3-GFP-GR* homozygous lines displayed consistent DEX induction

The T3 *p35s::MYB3R3-GFP-GR* seeds were harvested and screened for resistance on kanamycin, in accordance with the updated screening procedure (Figure 3.7). Five independent families yielded homozygous plants, including 1.3.3, 1.7.7, 4.2.8, 5.2.9 and 6.3.4. Unlike the reporter line populations, all five of these lines displayed strong, consistent, putatively nuclear GFP signal when screened for fluorescence on DEX containing media. To study induction in these lines in more detail five seedlings from each line, along with the reporters and *Col-0*, were transferred to GM microagar plates with either 0 μM or 100 μM DEX, four days after germination. This was higher than the concentration used for screening (Figure 3.3; Figure 3.7) of 60 μM DEX, as the signal for the reporter lines had often been relatively weak. Treatment was administered for 48 hours.

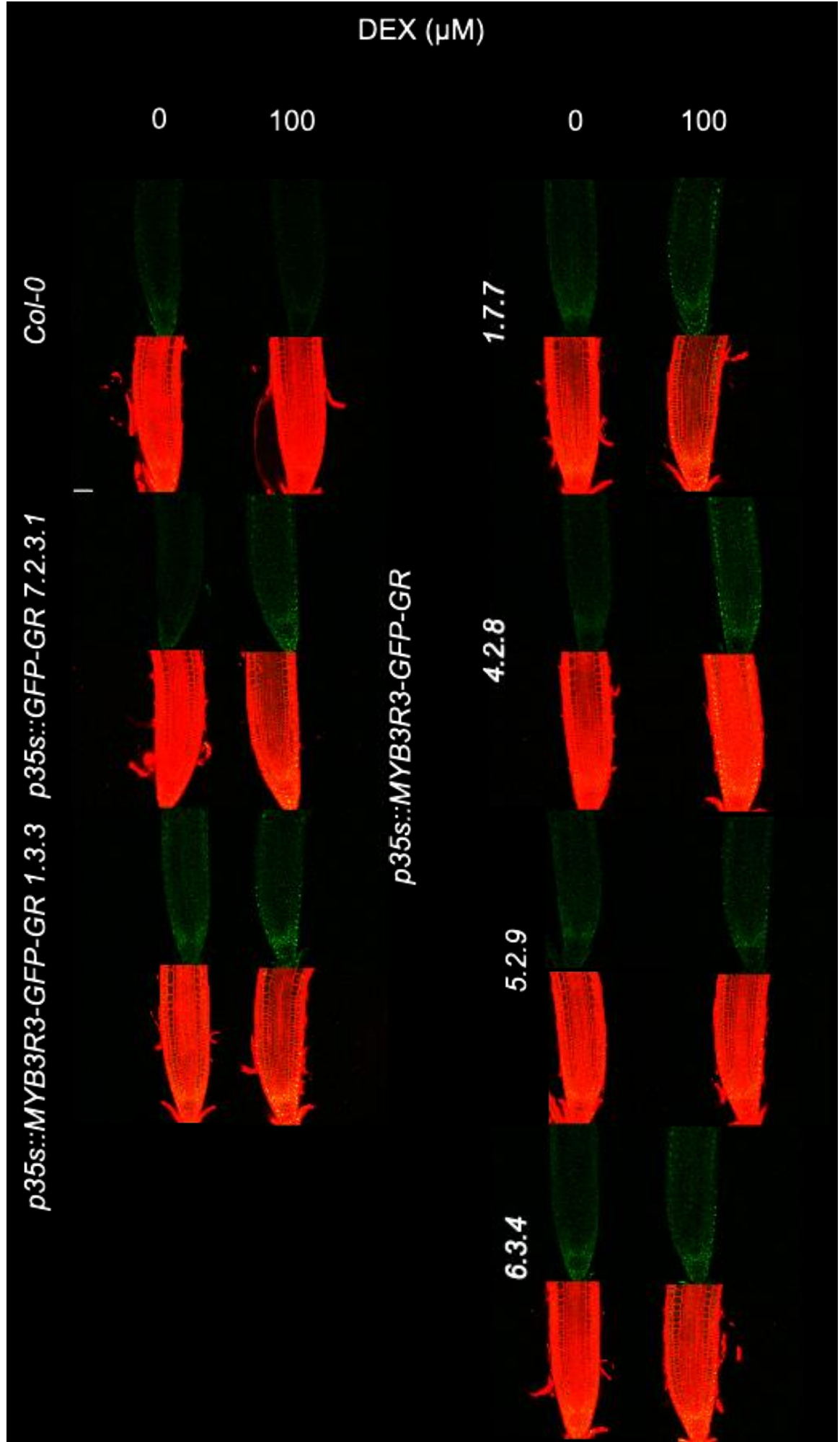
In order to get an approximate estimate of fluorescence intensity and therefore expression of GFP in the root apical meristem, five snaps were taken for each line by confocal microscopy, in the plane where the QC and cortex cells were visible, for both the induced and non-induced condition (Figure 3.9A). Prior to induction, most lines only showed very faint GFP signal. This was likely to be due to autofluorescence, as for some snaps *Col-0* showed a small amount of fluorescence within the emission spectrum of GFP close to the QC cells (Figure 3.9A). Upon induction, both the GFP reporter line, 7.2.3.1, and all five MYB3R3 inducible lines showed an increase in GFP expression. Again, post-induction signal was focused in subcellular structures of size and shape consistent with nuclei. In this plane, the punctate subcellular structures extended up the root meristem from the QC cells, and in the stele.

Subsequently, the genotypes were compared to each other by calculating the Corrected Total Cell Fluorescence (CTCF) values (Section 2.2.1; Figure 3.9C). All of the lines had higher CTCF values than *Col-0*, confirming the expression of GFP quantitatively. While the *p35s::GFP-GR* reporter (7.2.3.1) had a higher CTCF value compared to *Col-0*, it was still lower than all of the *p35s::MYB3R3-GFP-GR* lines, similar to observations while independently screening the transgenic seedlings. The

inducible MYB3R3 lines varied in expression, ranging from 76.03 – 87.99 AU. *p35s::MYB3R3-GFP-GR*'s GFP expression was comparatively in the middle.

To gain a deeper insight into the location and strength of transgene expression across the cell types of the root meristem, for each line under the induced condition, a three-dimensional confocal stack was obtained. Maximum intensity projects (Figure 3.7C) revealed that the reporter and all five *p35s::MYB3R3-GFP-GR* lines displayed putative nuclear GFP expression, across many cell types in the root meristem, in line with the chosen constitutive promoter. This pattern was consistent and distinct, as opposed to the induced wildtype (*Col-0*), which did not have any discernible expression besides autofluorescence.

A



B

Genotype	CTCF Value (AU)
<i>Col-0</i>	68.4323568
<i>p35s::GFP-GR: 7.2.3.1</i>	72.4046964
<i>p35s::GFP-GR: 1.3.3</i>	80.1972556
<i>p35s::GFP-GR: 1.7.7</i>	87.9858352
<i>p35s::GFP-GR: 4.2.8</i>	84.3198321
<i>p35s::GFP-GR: 5.2.9</i>	79.0567643
<i>p35s::GFP-GR: 6.3.4</i>	76.0329167

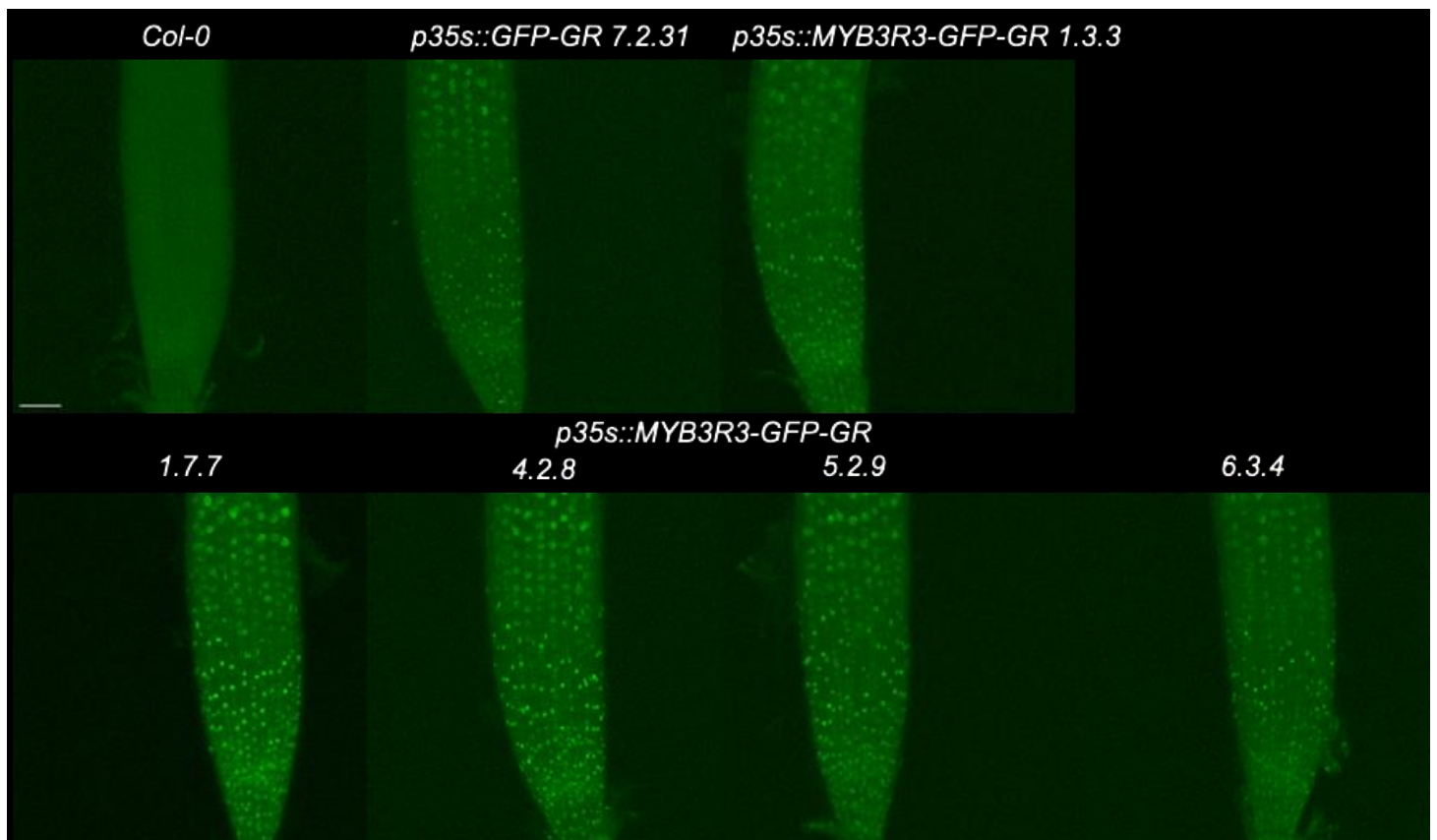
C

Figure 3.9: Profiles of five p35s::MYB3R3-GFP-GR lines (1.3.3, 1.7.7, 4.2.8, 5.2.9 and 6.3.4), compared to the control reporter line (p35s::GFP-GR T4: 7.2.3.1) and wildtype (Col-0). A: Individual snaps of all the lines before and after DEX induction. Scale bar is 50 μ m. Brightness 75%, contrast 44%. For each line, the left panel is non-induced and the right is induced, at 100 μ M DEX for 48 hours. Top rows show the GFP channel and the bottom rows contain the composite GFP and PI channel. B)CTCF values of the mean of five independent confocal snaps for each DEX induced genotype, relative to the mean of five uninduced snaps. Data is from one image corresponding to each genotype. This data was comprised of one biological replicate. C: Maximum intensity projections of the GFP channel for the lines, induced on 100 μ M DEX plates. GFP gain = 1156.

3.6 The five homozygous *p35s::MYB3R3-GFP-GR* lines showed differential responses to DEX induction in terms of root growth

In order to determine the optimum concentration for DEX induction, an experiment was planned, where the effect of various concentrations of DEX would be tested (Section 2.18). Four day old seedlings which had been grown on unsupplemented growth medium were transferred to plates containing either 0 μM , 10 μM , 30 μM , 50 μM , 100 μM or 200 μM DEX. The volume of DMSO was kept constant across all six concentrations. Two plates, each one containing ten seedlings, were prepared for each genotype at each concentration. This was carried out for each of the five *p35s::MYB3R3-GFP-GR* homozygous lines, the *p35s::GFP-GR T4: 7.2.3.1* reporter and Col-0.

Firstly, the effect of increases in DEX concentration on overall growth of the seedlings was assessed (Section 2.19). This was conducted by marking the position of each root tip upon transfer, and measuring how far each root grew three days after. Subsequently, this data was used to calculate the growth of the roots at each DEX concentration, relative to the growth of the roots transferred to the non-induced condition (0 μM DEX), independently for each genotype. Therefore, relative root growth (RRG), was determined by calculating the mean root length of the non-induced seedlings for each genotype (0 μM), and subtracting this value from each replicate at the various concentrations, for each individual genotype. Roots which did not embed into the media and therefore did not grow were coded as “NA” and discounted from the analysis. These values were plotted visually (Figure 3.10; Figure 3.11) to visualise the behaviour of and enable comparisons between the genotypes across the range of DEX concentrations.

To pick an optimum concentration that would show the genuine effects of MYB3R3 induction, the effect of DEX on the control lines was firstly analysed (Figure 3.10; Table 3.2; Table 3.3). The controls in this experiment, *Col-0* and *p35s::GFP-GR 7.2.3.1*, were predicted to have no response to DEX induction, in terms of root growth. However, when testing the effect of DEX induction from 0 to 200 μM , both genotypes had a significant response, determined by linear regression analysis ($p =$

7.16e-05 *** for DEX) (Figure 3.10). This was due to large decreases in RRG for seedlings transferred to 200 μM DEX, for both genotypes, indicating that this concentration of DEX was detrimental to plant growth. While there was a dip in relative growth for *Col-0* at 30 μM , followed by an increase at 50 μM , neither concentration was significantly different to induction at 10 μM and 100 μM , indicating this could be due to variation in the sample rather than a dose response to the DEX. As this is data from one biological replicate, it is possible that this observation would not be reproduced. RRG in the reporter, *p35s::GFP-GR 7.2.3.1* did not display any statistically significant differences, until the final concentration (200 μM) . Furthermore, regression analysis revealed that the lines were not statistically different from each other in terms of their responses to DEX. Based on these observations it was determined that DEX has an inhibitory effect on root growth at concentrations greater than 100 μM that is independent of any GOI, and thus only responses within the 0 – 100 μM range should be considered.

To ascertain the effects of DEX induction on RRG across the five *p35s::MYB3R3-GFP-GR* lines, boxplots of RRG over the range 0 – 100 μM root were compared (Figure 11). As MYB3R3 is a known inhibitor of the mitotic cell cycle, it was predicted that the induction would decrease root growth. The five inducible MYB3R3 showed different responses to DEX treatment, across the concentrations. RRG for 1.7.7 and 4.2.8 appeared to be fairly constant across all concentrations. On the other hand, 5.2.9 and 6.3.4 seemed to have increases in their RRGs, peaking at 50 μM and 100 μM respectively. 1.3.3, while initially displaying slight increases in RRG up until 50 μM , began to show a decrease 100 μM . As the lines belong to five independent T2 families, it was expected that they would show varied growth responses across the DEX concentrations, with respect to differences in the concentration of the transgene transcripts. Therefore, from this experiment it was determined that at the single time point of three days post DEX induction, of the lines, *p35s::MYB3R3-GFP-GR* showed a decrease in root growth at 100 μM DEX, relative to the growth of the roots under the non-induced condition.

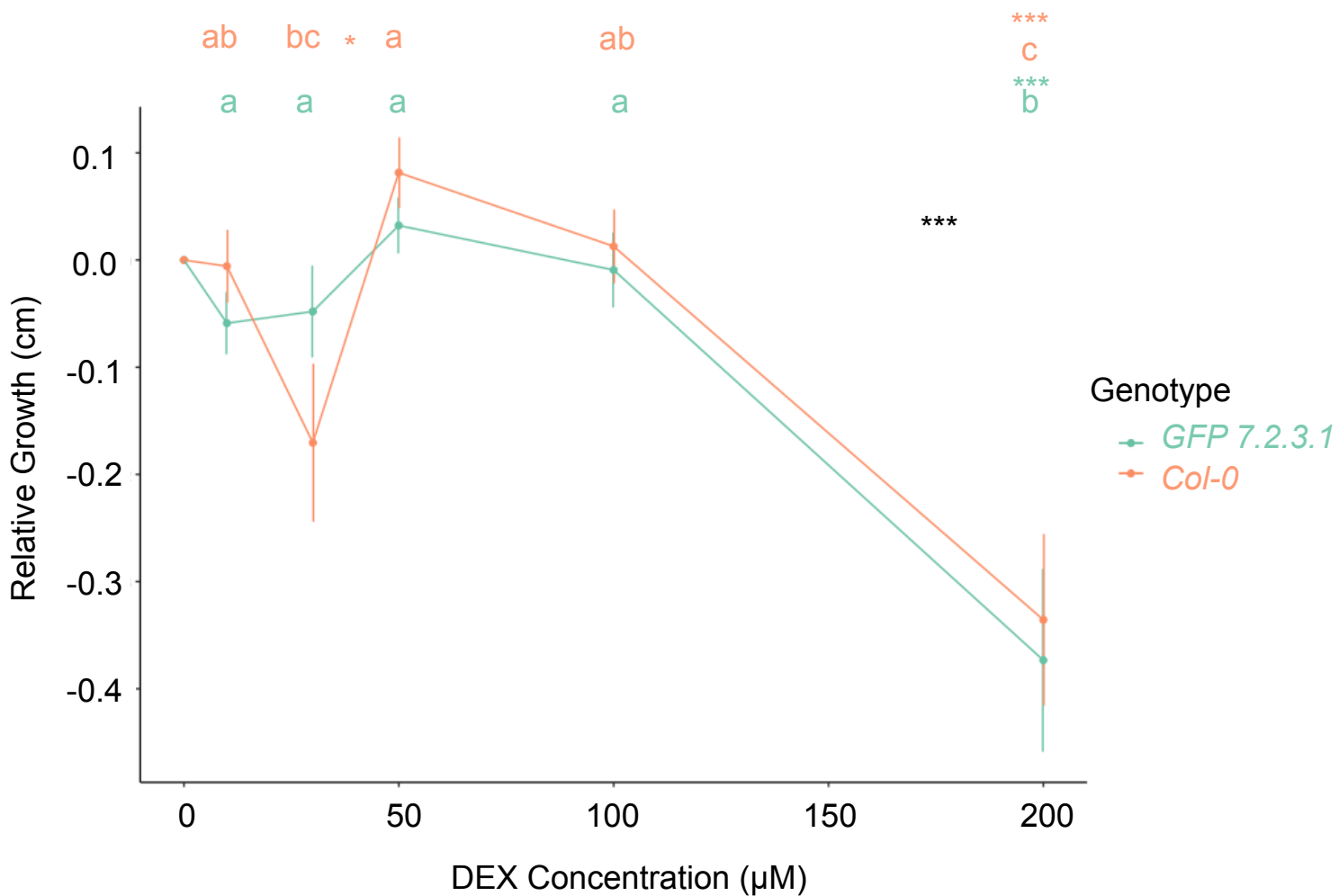


Figure 3.10: Line graph of RRG across DEX concentrations from 0 μM , 10 μM , 30 μM , 50 μM , 100 μM and 200 μM for Col-0 (orange) and p35s::GFP-GR 7.2.3.1 (green). Each point represents the mean of values-means_zero across 20 replicates, for each combination. Bars show standard error. The black *** corresponds to a Linear Regression: $lm = \text{Growth} \sim \text{Dex} + \text{Genotype} + \text{DEX}:\text{Genotype}$ where the statistic for DEX, $p = 7.16e-05$ *** is shown. The genotypes themselves, and the interaction of genotype with DEX do not return significant values ($p=0.821$, $p=0.619$) respectively. Letters correspond to Tukey's Post-Hoc HSD tests, tested separately for each genotype (Table 3.2, Table 3.3).

Table 3.2: Pairwise comparisons of DEX concentrations for Col-0 RRG. Tukey's Post-Hoc HSD Values for individual linear regressions of the Col-0 and 7.2.3.1 subsets, to show the pairwise comparisons of the different DEX concentrations for each genotype, individually. Codes of significance for p values: '***', 0.001 '**', 0.01 '*', 0.05. These values were used to generate letters shown on RRG graph (Figure 3.10).

DEX Concentration A (μM)	DEX Concentration B (μM)	p value	Significance
10	30	0.2235	
10	50	0.7963	
10	100	0.9993	
10	200	<0.001	***
30	50	0.0143	*
30	100	0.1386	
30	200	0.2208	
50	100	0.9032	
50	200	<0.001	***
100	200	<0.001	***

Table 3.3: Pairwise comparisons of DEX concentrations for p35s::GFP-GR 7.2.3.1 RRG. Tukey's Post-Hoc HSD Values for individual linear regressions of the Col-0 and 7.2.3.1 subsets, to show the pairwise comparisons of the different DEX concentrations for each genotype, individually. Codes of significance for p values: '***', 0.001 '**', 0.01 '*', 0.05. These values were used to generate letters shown on RRG graph (Figure 3.10).

DEX Concentration A (μM)	DEX Concentration B (μM)	p value	Significance
10	30	0.999854	
10	50	0.675367	
10	100	0.9550825	
10	200	0.000161	***
30	50	0.769605	
30	100	0.979962	
30	200	< 1e-04	***
50	100	0.97411	
50	200	< 1e-04	***
100	200	< 1e-04	***

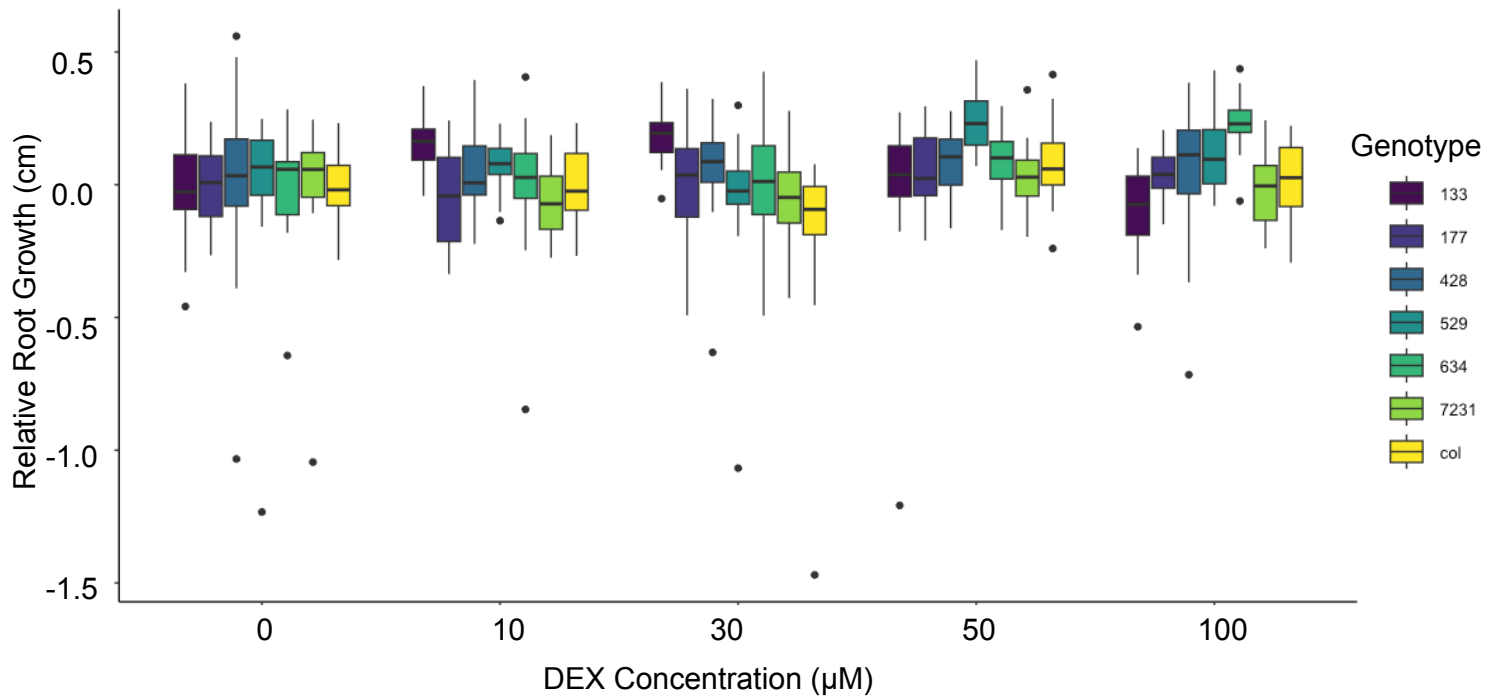


Figure 3.11: Boxplots of RGRs across 0 μM , 10 μM , 30 μM , 50 μM and 100 μM for each genotype. Numerical genotype codes refer to the five *p35s::MYB3R3* lines: 1.3.3, 1.7.7, 4.2.8, 5.2.9 and 6.3.4, *p35s::GFP-GR* 7.2.3.1 and *Col-0*. Each point represents the mean of values-means_zero across 20 replicates, for each combination.

3.7 Induction of MYB3R3 resulted in an increase in cortex cell size

To determine how DEX induced MYB3R3 translocation affected growth and division at a cellular level, the length of the cortex cells within roots were measured.

p35s::MYB3R3-GFP-GR T3 1.3.3 was selected out of the five homozygous inducible MYB3R3 lines, as its showed a moderate level of GFP expression relative to the other lines (Figure 9.B, C) and its root growth dipped at 100 μ M DEX, relative to the other concentrations (Figure 3.11) suggesting that induction was having a physiological effect. Wildtype *Col-0* was selected as a negative control, alongside *p35s::GFP-GR T4: 7.2.3.1* as the visually brighter control reporter line (Figure 3.5B).

From the above induction experiment used to obtain root length data, one plate for each of the above genotypes under each concentration was selected four days after transfer. All ten seedlings from each plate were imaged by confocal microscopy. For each seedling, snaps were taken that clearly showed cortical cell files to the left and right of the quiescent centre (QC) cells of the root meristem (Figure 3.12C). For each side, cells were measured from the first cell up from the QC, up to and including the end of the transition zone, where cells begin to elongate. In the absence of a marker, this was defined by the presence of a noticeably longer cell, which was usually double the length of the preceding cell (Section 2.20; Nieuwland et al., 2009).

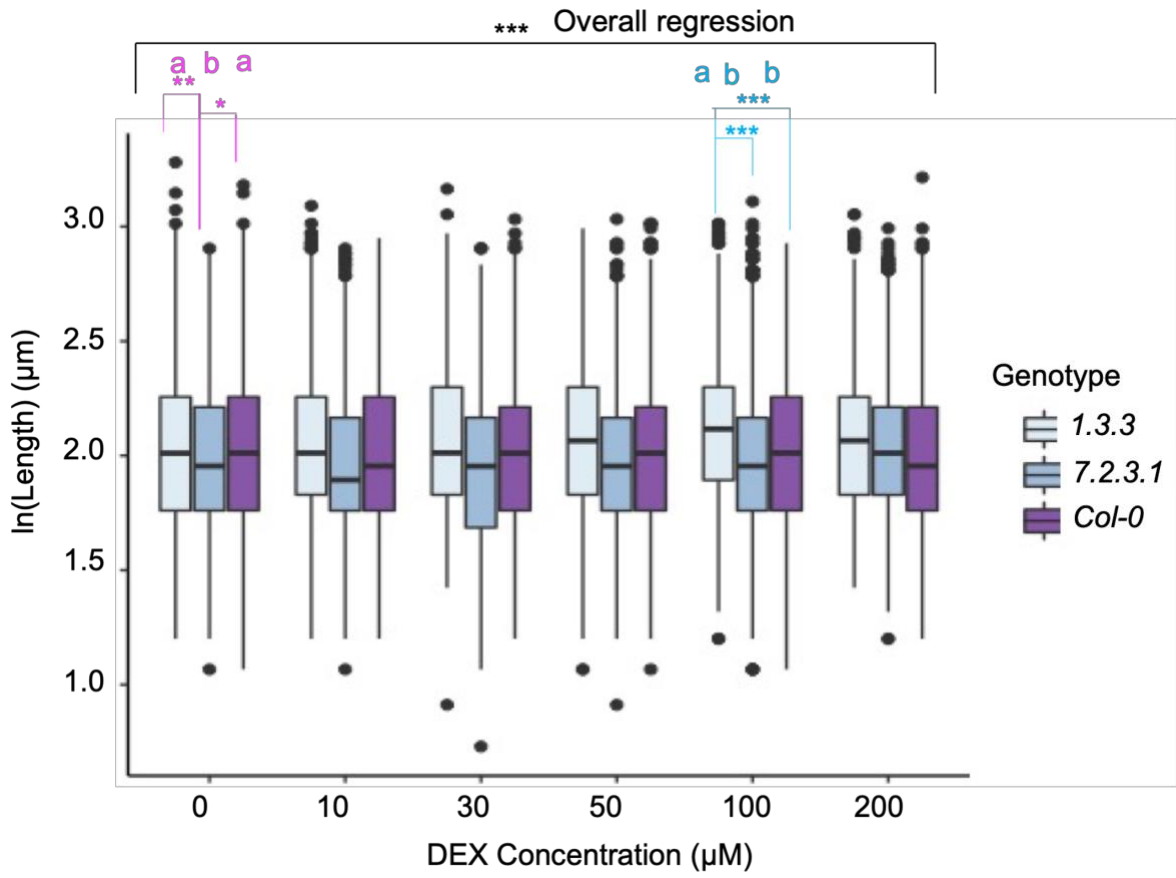
Across all DEX concentrations, cortex cell sizes of *Col-0* remained relatively constant (Figure 3.12; Figure 3.13C), and at all concentrations no statistical differences in length were found (Table 3.6). In contrast, induction of MYB3R3 increased cortex cell sizes at 50 μ M DEX, peaking at 100 μ M before decreasing slightly at 200 μ M (Figure 3.12A; Figure 3.13A; Table 3.4). Interestingly, the GFP-GR reporter, *7.2.3.1* also displayed altered cortex cell sizes in response to DEX (Figure 3.12A; Figure 13 B; Table 3.5) however, where DEX increased cell length in the MYB3R3 line, cell size in the GFP-GR reporter decreased significantly compared to uninduced roots at 30 μ M and 50 μ M, before increasing to similar levels again at 100 μ M, with a slight, non-significant increase at 200 μ M.

While wildtype and inducible MYB3R3 plants started off with comparable cortex cell sizes, interestingly, the cells of the reporter line were notably smaller (Figure 3.12A).

Linear regression revealed that both inducible lines were highly significantly different to wildtype, in terms of their response to DEX. However, as the reporter's cortex cells were smaller than the wildtype's and the MYB3R3's cells were larger, it was assumed that *p35s::MYB3R3-GFP-GR* T3: 1.3.3 accumulation of larger cells were due to the addition of MYB3R3, and not GFP-GR.

In terms of the effect of MYB3R3 translocation on cell size, cortex cell length became incrementally larger with increasing DEX concentrations for the *p35s::MYB3R3-GFP-GR* line, before decreasing in size again at 200 μ M (Figure 3.12A; Figure 13A). The difference in size between the uninduced condition and 100 μ M was highly significant ($p < 0.001$), therefore showing the greatest effect on cell size across the concentration (Table 3.4). At this concentration, the size of MYB3R3 induced cells was also highly significantly different to sizes observed for *p35s::GFP-GR* and *Col-0* ($p < 0.001$) (Figure 3.12B) which did not have statistically different sizes compared to each other, or to the sizes of their respective uninduced counterparts (Table 3.5; Table 3.6). Therefore, this was the concentration selected as optimum, to visualise the greatest effect of MYB3R3 induction, while no discernible effect was seen for the controls.

A



B

DEX Concentration (µM)	Genotype A	Genotype B	p value	Significance
0	<i>Col-0</i>	<i>1.3.3</i>	0.93236	
0	<i>Col-0</i>	<i>7.2.3.1</i>	0.01444	*
0	<i>1.3.3</i>	<i>7.2.3.1</i>	0.00922	**
100	<i>Col-0</i>	<i>1.3.3</i>	<1e-04	***
100	<i>Col-0</i>	<i>7.2.3.1</i>	0.2670	
100	<i>1.3.3</i>	<i>7.2.3.1</i>	<1e-04	***

C

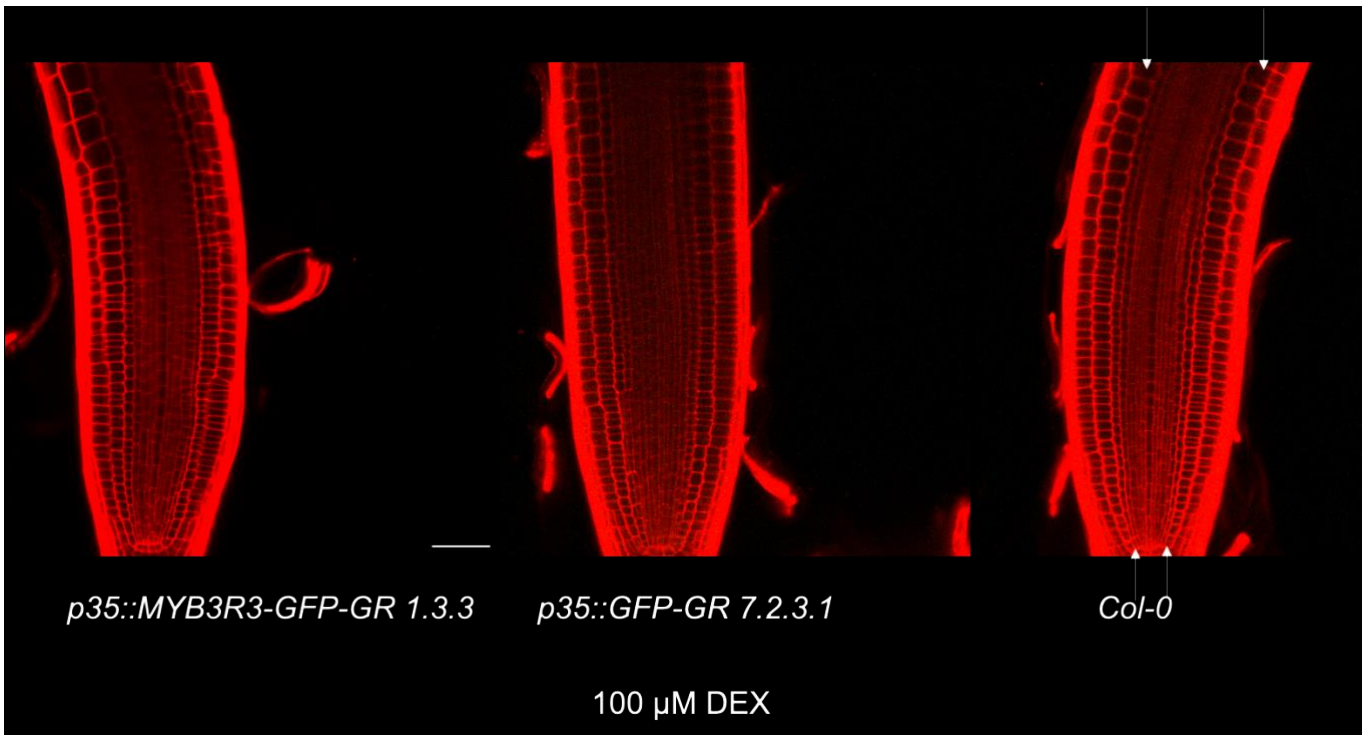
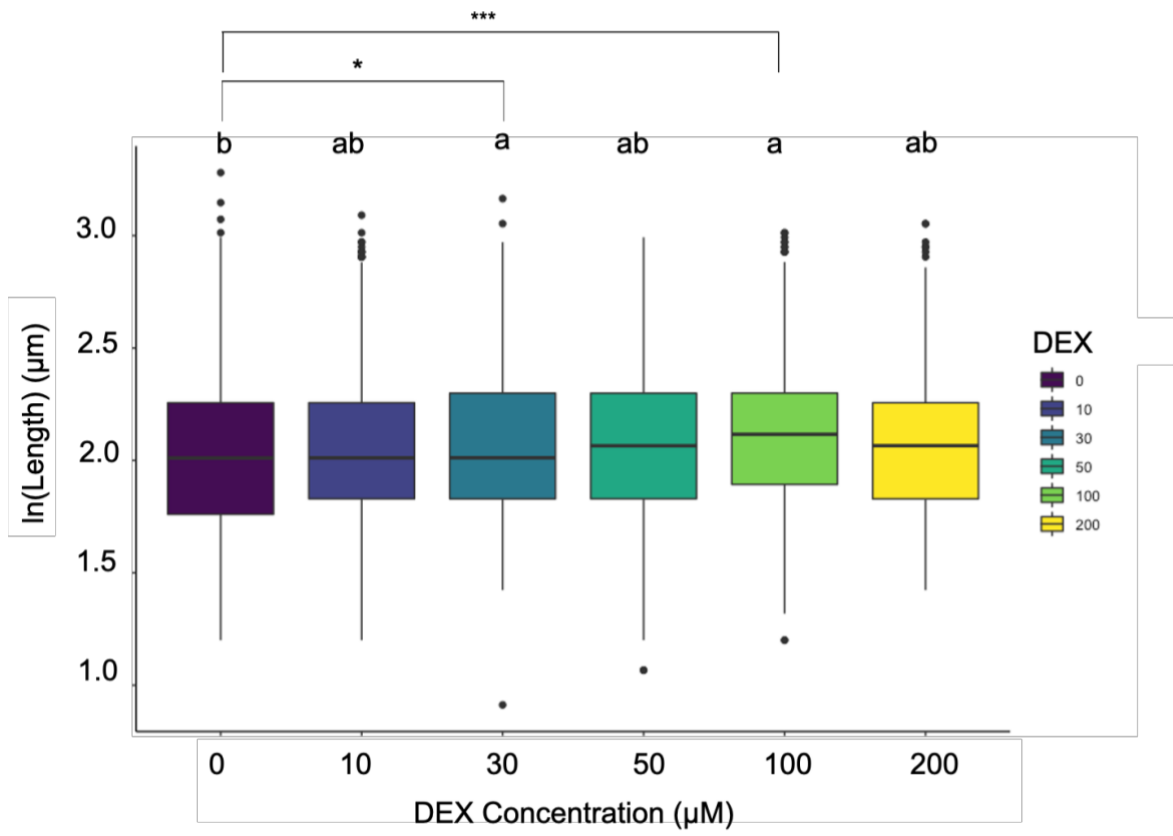


Figure 3.12: Comparison between the cortex cell length (CCL) of *p35s::MYB3R3-GFP-GR*, *p35s::GFP-GR* and *Col-0* upon increasing concentrations of DEX induction. A) Boxplots of all of the genotypes across all concentrations. The black bracket refers to the overall regression from the call where both transgenic lines were statistically different to *Col-0* in terms of their responses to DEX ($p < 2e-16$). The pink and blue letters and indents are from a Tukey's post-hoc test at 0 μM DEX and 100 μM DEX, respectively. Codes of significance for p values: '****', 0.001 '**', 0.01 '*', 0.05. B: Results from the Tukey's Post-HOC HSD tests, shown by letters on the boxplot, showing pairwise comparisons of genotypes at both 0 μM DEX and 100 μM DEX. C) Snaps of each genotype from the experiment, induced at 100 μM DEX. B) Propidium iodide channel, 100 $\mu\text{g/mL}$, white arrows point at the top and bottom of the cortex cells, measured in the image.

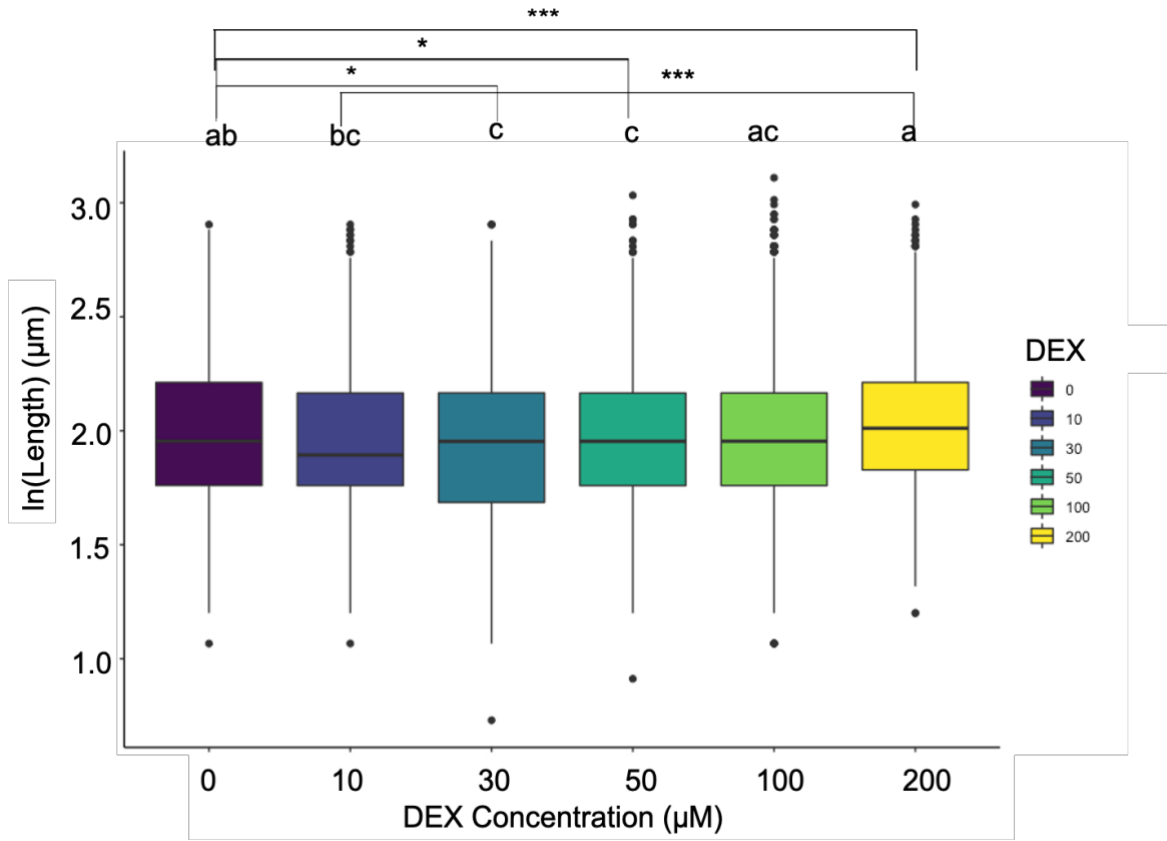
A

p35s::MYB3R3-GFP-GR



B

p35s::GFP-GR 7.2.3.1



C

Col-0

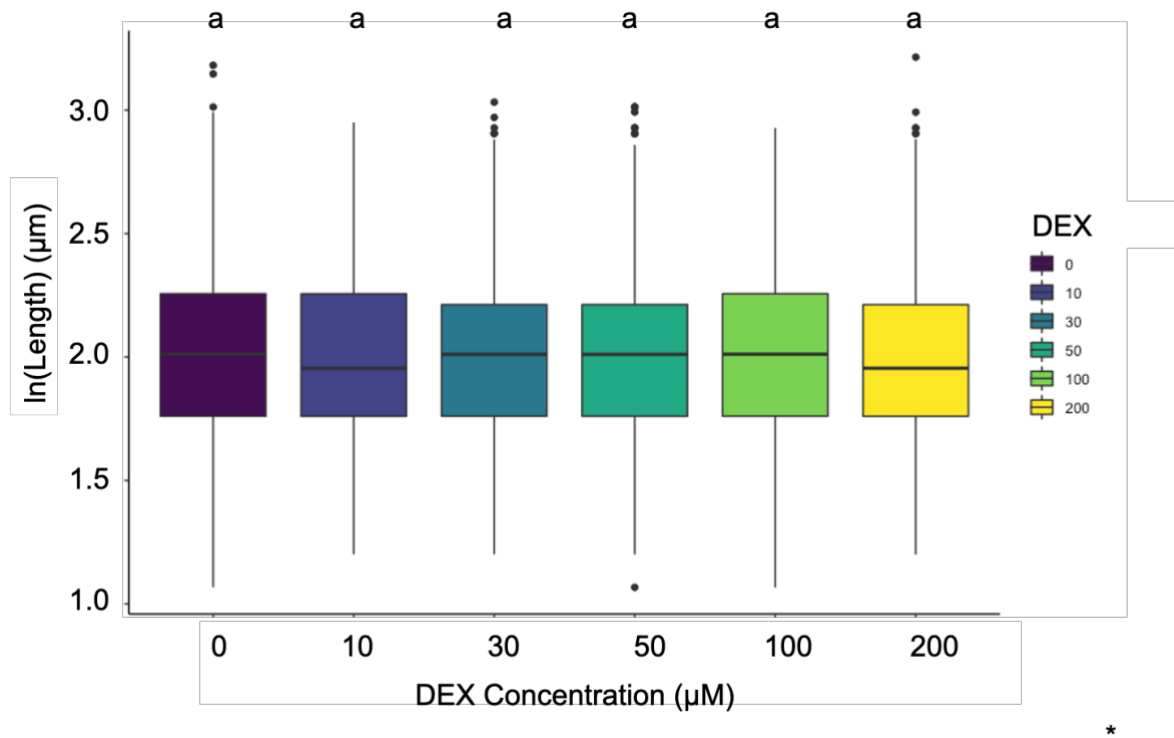


Figure 3.13: Boxplots showing the effect of DEX induction on the cortex cell length (CCL) of each genotype, separately. Data is from eight day old seedlings, transferred to various DEX four days prior to imaging. Values of length have been transformed, using the natural logarithm ($\ln(\text{length})$ where e is the base. (log. A) DEX induction of $p35s::MYB3R3\text{-GFP-GR}$. B) DEX induction of $p35s::GFP\text{-GR 7.2.31}$. C) DEX induction of $Col\text{-0}$. Each boxplot represents root cortex cell measurements from both sides of 10 seedlings, except for the last, $p35s::MYB3R3\text{-GFP-GR}$ at 200 μM , where only 7 seedlings could be measured due to damage. Letter values “a”, “b”, “c” and combinations are derived from Tukey’s Post-Hoc tests, where genotypes with different letter codes have statistically different cortex cell lengths. Codes of significance for p values: ‘***’, 0.001 ‘**’, 0.01 ‘*’, 0.05.

*Table 3.4: Pairwise comparisons of DEX concentrations for p35s::MYB3R3-GFP-GR 1.3.3 CCL. Table showing Tukey's Post-Hoc HSD values for the CCLs of each genotype with each possible combination, corresponding to the letters shown in the boxplots in Figure 3.13. Codes of significance for p values: '***', 0.001, '*', 0.05.*

DEX Concentration A (μM)	DEX Concentration B (μM)	p value	Significance
0	10	0.1443	
0	30	0.0498	*
0	50	0.0708	
0	100	<0.001	***
0	200	0.4419	
10	30	0.9977	
10	50	0.9994	
10	100	0.3860	
10	200	0.9988	
30	50	1.0000	
30	100	0.6773	
30	200	0.9681	
50	100	0.6159	
50	200	0.9829	
100	200	0.2710	

*Table 3.5: Pairwise comparisons of DEX concentrations for p35s::GFP-GR 7.2.3.1 CCL. Table showing Tukey's Post-Hoc HSD values for the CCLs of each genotype with each possible combination, corresponding to the letters shown in the boxplots in Figure 3.13. Codes of significance for p values: '****', 0.001, '**', 0.05.*

DEX Concentration A (μM)	DEX Concentration B (μM)	p value	Significance
0	10	0.1601	
0	30	0.0387	*
0	50	0.0325	*
0	100	0.9932	
0	200	0.5535	
10	30	0.9922	
10	50	0.9868	
10	100	0.3827	
10	200	<0.001	****
30	50	1.0000	
30	100	0.1199	
30	200	<0.001	****
50	100	0.1026	
50	200	<0.001	****
100	200	0.1718	

*Table 3.6: Pairwise comparisons of DEX concentrations for Col-0 CCL. Table showing Tukey's Post-Hoc HSD values for the CCLs of each genotype with each possible combination, corresponding to the letters shown in the boxplots in Figure 3.13. Codes of significance for p values: '****', 0.001, '**', 0.05.*

DEX Concentration A (μM)	DEX Concentration B (μM)	p value	*
0	10	0.323	
0	30	0.921	
0	50	0.199	
0	100	0.769	
0	200	0.509	
10	30	0.918	
10	50	1.000	
10	100	0.983	
10	200	1.000	
30	50	0.819	
30	100	1.000	
30	200	0.975	
50	100	0.941	
50	200	0.998	
100	200	0.998	

3.8 MYB3R3 induction resulted in decreased biomass accumulation over time

To observe the effects of MYB3R3 induction over time, the remaining plates containing ten seedlings from each genotype, at each concentration were left to grow for an additional week. The plates were then scanned, displaying growth phenotypes of the seedlings, 11 days after DEX induction (Figure 3.14). For *Col-0* and the inducible reporter, *p35s::GFP-GR T4: 2.1.4.16*, all seedlings appeared to have grown similarly, both at 0 and 100 μ M DEX, producing long roots which grew to the end of the plate. In contrast, for two of the homozygous inducible MYB3R3 lines, *1.7.7* and *4.2.8*, the roots of the induced seedlings were shorter, and did not reach the end of the plate. Furthermore, they showed the most prominent decrease in rosette size. Interestingly, these were the two lines which yielded the brightest GFP fluorescence throughout the layers of the root meristem when induced (Figure 3.9B). For *p35s::MYB3R3-GFP-GR 1.3.3*, the line selected to study, both induced and non-induced roots appeared to be shorter, relative to the wildtype. This indicates that there may be an excess of the transgene as opposed to HSP90, which allowed free protein to express and translocate to the nucleus under uninduced conditions. The two weaker lines, *5.2.9* and *6.3.4*, inferred by the fluorescence data (Figure 3.9B), did not show any obvious changes in root growth across the two concentrations, however *6.3.4*'s roots appeared to have smaller rosettes when treated with DEX. Interestingly, the reporter *p35s::GFP-GR T4: 7.2.3.1* appeared to have shorter roots than the other genotypes, when grown without DEX. However, when induced, the rosettes on the roots were the largest out of all of the lines at both concentrations, and its roots reached the bottom of the plate, suggesting that DEX induction could have improved its growth, in an opposite manner to what was seen with four out of the five *p35s::MYB3R3-GFP-GR* lines.

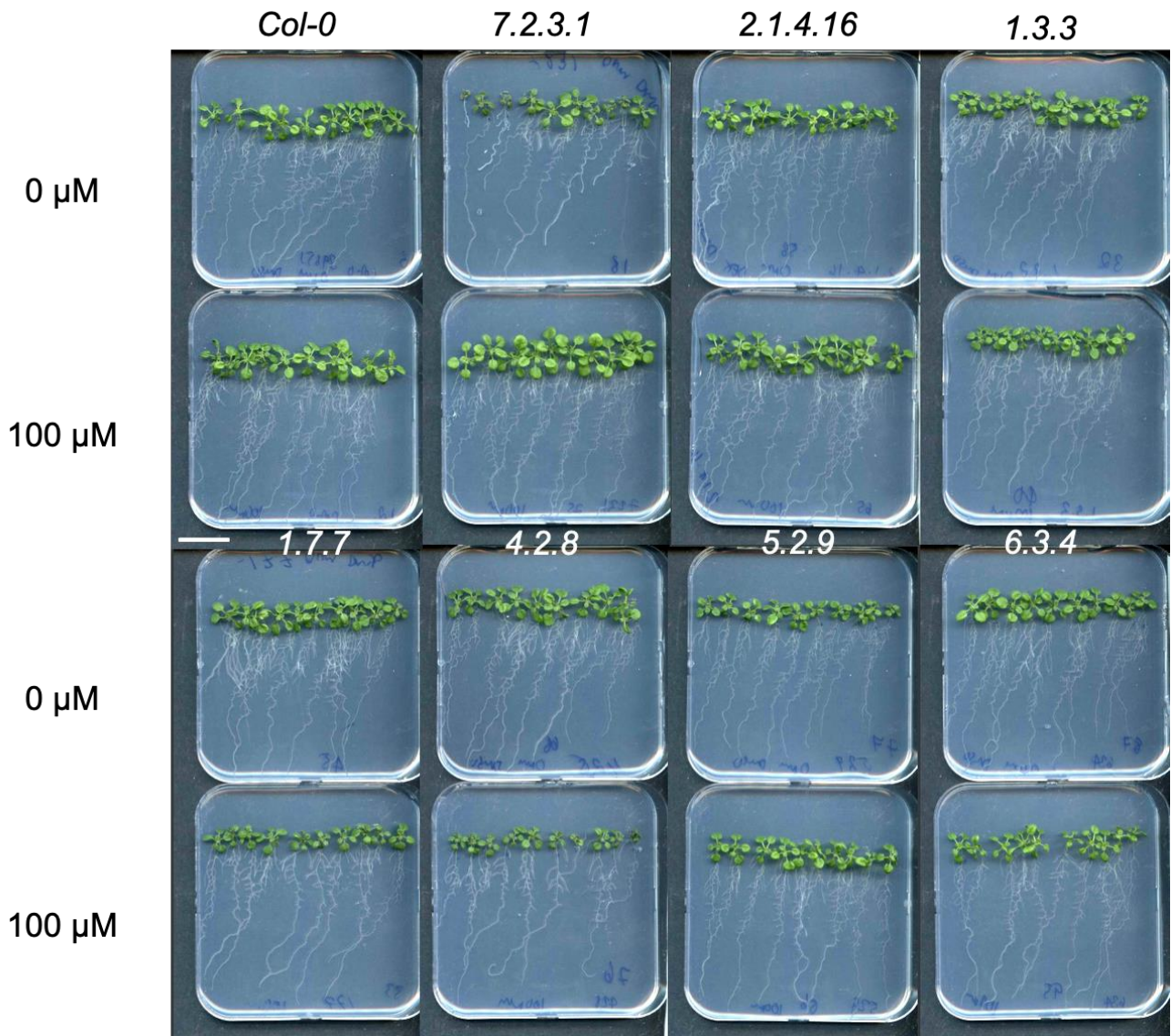


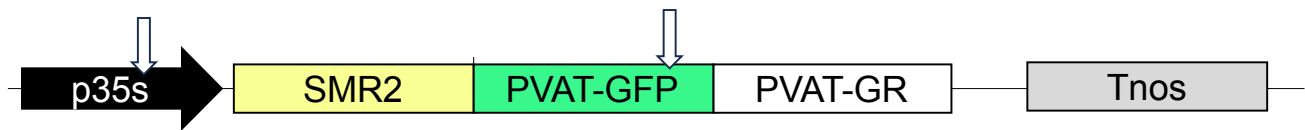
Figure 3.14: Collective scans of seedlings 14 DAG, transferred 4 DAG to either GM microagar (0 μ M) or 100 μ M DEX plates. The top two rows are wildtype (Col-0), p35s::GFP-GR T4: 7.2.31 and 2.1.4.16 reporters and p35s::MYB3R3-GFP-GR T3: 1.3.3. The lower two rows are the remaining four p35s::MYB3R3-GFP-GR T3 families, 1.7.7, 4.2.8, 5.2.9 and 6.3.4. Scale bar = 1 inch, resolution = 600 pixels per inch. Brightness increased 30%, contrast increased 63%, on PowerPoint.

3.9 Successful cloning of multiple candidate sizer molecules through use of the inducible expression cassette

Following the success of the use of the inducible system to study *MYB3R3*, the system was further applied to other cell cycle related proteins, hypothesised to be sizers. The *p35s::GFP-GR* reporter engineered by Gibson cloning was digested with *PacI* and ligated with a fragment of genomic DNA corresponding to *SMR2*. Plasmids were verified via Sanger sequencing and subsequently transformed into *Arabidopsis thaliana* via floral dipping procedures. *Agrobacterium tumefaciens* colonies were checked by colony PCR (Figure 3.15B).

Subsequently, transgenic seedlings, resistant to kanamycin were obtained. Both constructs were induced for three days on plates with 100 μ M DEX and visualised by confocal microscopy. *p35s::SMR2-GFP-GR* transgenics were mostly GFP positive, with GFP showing punctate subcellular localisation consistent with the size and shape of nuclei (Figure 3.16), and the lines appeared to be strong, ascertained by visually bright GFP signal. In total, 54 plants from each genotype were selected and grown to the next generation, to undergo the screening pipeline for retrieval of homozygous lines (Figure 3.7). Further analysis was not possible on these lines, but their identification at T1 is strong evidence for the reusability of the system for a range of different proteins.

A



B

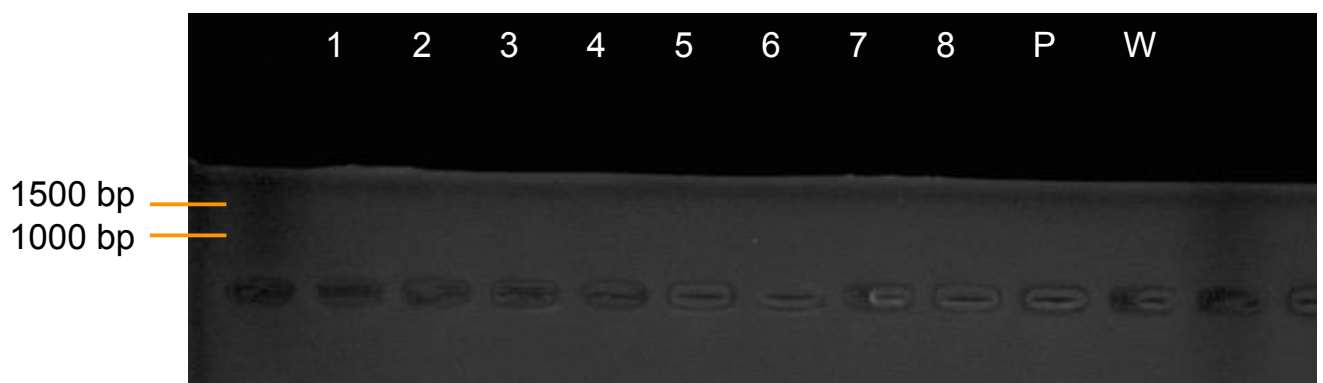


*Figure 3.15 Design and construction of p35s::SMR2-GFP-GR. A) Schematic diagram of the p35s::SMR2-GFP-GR cassette. Arrows indicate where cloning primers bind. Cassette was inserted into the *PacI* digested HIFI Assembly Vector (Figure 2.4) by NEB HIFI Assembly (Figure 2.5). B) *Agrobacterium tumefaciens* transformation of the completed p35s::SMR2-GFP-GR. 1-8 correspond to colonies selected and streaked onto a master plate. The ladder is SmartLadder, 200bp-10kb, (Eurogentec) P, the plasmid used for the transformation. W, the water control. The primers used were CaMV pro Seq 1 FP + GFP RP, producing an amplicon of 1293 bp. The extension time was 1 minute 30 seconds, annealing temperature 57°C.*

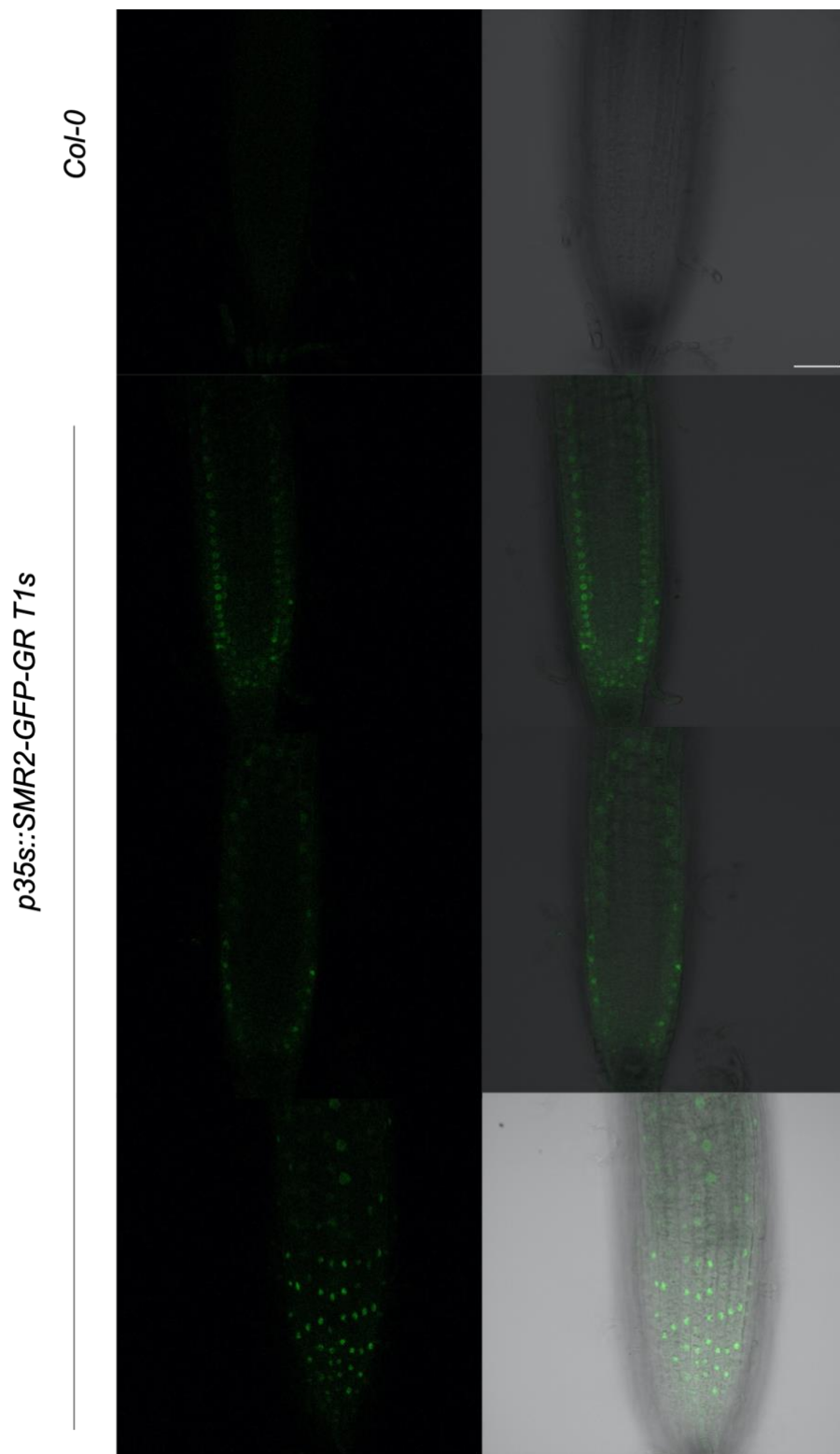


Figure 3.16: The root tips of three *p35s::SMR2-GFP-GR T1* transgenic seedlings, screened after being transferred to plates with 100 μ M DEX, compared to *Col-0*. Left column is the GFP channel, gain is 1156. The right channel is the composite of the GFP channel and transmitted light. Scale bar, 50 μ M.

4. Discussion

4.1 Golden Gate, a modular cloning strategy for large assemblies was successfully implemented to create a GR-based GFP reporter system

The first objective of the project was to produce a reusable, inducible GR system, which later would be applied to study hypothetical size proteins. To ensure the robustness of the system prior to its extensive use, it was firstly tested by creating GFP fusions as a visual reporter to evaluate DEX response. DEX induction systems have been widely used in plants, with the GR domain in both N (Craft et al., 2005) and C (Wildwater et al., 2005) terminals of the fusion. Consequently, a condition of the first aim was to generate GFP protein fusions in both possible positions. This would allow the functionality of the inducible expression cassette to be optimised prior to cloning GOIs and also provide essential control lines for subsequent induction experiments.

In order to make the constructs required to address the first aim, a cloning strategy was needed which would allow the combination of multiple parts to build several transcriptional units in a relatively quick, reusable and efficient manner. As traditional cloning is limited by its need for a variety of different Type II restriction enzymes, time consuming digestion and purification for each part, and ligations restricted to two parts at a time (Struhl, 1991), alternative modular assembly approaches were considered. Golden-Gate cloning using the MoClo toolkit (Engler et al., 2014), a well-established, highly efficient strategy which can build multi-fragment assemblies up of up to 35 parts with over 90% accuracy (Potapov et al., 2018; Pryor et al., 2020) was selected as the method of choice.

Golden Gate is advantageous over other methods of modular assembly such as Gateway cloning, a mechanism employing lambda phage integration (Hartley et al., 2000) during which excision leaves a considerable 25 bp scar (Hartley et al., 2000) that may be detrimental to protein folding and function. This is an area of particular concern in this study, due to its aim of constructing of double, and subsequently triple fusion proteins. Another strategy, BioBricks, leaves a smaller, 8bp scar (Cai et

al., 2010), but Golden Gate reduces this further, leaving only a 4 bp scar. The 4 bp scar is required as it allows complementarity of a chosen part with a Level 0 Acceptor plasmid, a vector supplied in the MoClo kit, to define the part's position in a transcription unit, which is built at the next level (Figure 2.2.). This is advantageous for single protein constructs as the addition of AATG to allow compatibility with the N terminal position Level 0, "NT1", provides a start codon for transcription, beginning at the second base (Figure 2.2). However, for fusion proteins, the scar at the beginning of the C terminal protein, in the Level 0 Acceptor "CDS1", resulted in a frame shift. While recent approaches such as Start-Stop Assembly have been designed to leave a three base pair overhang instead to prevent this, (Taylor et al., 2019), this would have required domestication of the vectors used, a time-consuming process. Instead, this issue was circumvented by careful planning. The 4 bp overhang used to incorporate a part into CDS1 had been designed for the addition of one base pair to code for a glycine residue (Bird et al., 2022). Therefore, codon optimisation specific to the *Arabidopsis* genome was employed to add only one base to the overhang, circumventing the frame shift via addition of a glycine residue.

A further advantage of using MoClo was that all four parts of the transcriptional units for the GFP-GR fusions could be ligated in a one-step reaction, and the promoter, both 5' and 3' UTRs and the terminator were already supplied in the kit (Table 2.2). This provides an advantage over other approaches such as Biobricks, which uses two different restriction endonucleases on each part to dictate order, and is thus limited to a maximum two-part max assembly (Chaudhari and Hanson, 2021) similar to traditional cloning and GoldenBraid (Sarrion-Perdigones et al., 2011), a theoretically similar approach for modular cloning.

The project was also well suited to the MoClo technique since there was a considerable degree of overlap between the parts used for each construct; all constructs shared the Nos terminator, fusion and single proteins shared the same promoter parts, GFP in CDS1 was shared amongst *p35s::GR-GFP* and all single GFP controls and all constructs were built into the same Level 2 Acceptor plant vector with a Kanamycin resistance cassette and LacZa acceptor site (Table 2.2; Figure 2.2; Figure 2.3; Weber et al., 2011). The multiple use of these parts was advantageous as it reduced expense, particularly since many of the required

components were already supplied in the kit (Engler et al., 2014). This also allowed the constructs to be comparable; with each of the constructs consisting of the same transcriptional units and differing only in positioning of the component parts within the final cassette (Figure 2.3). Furthermore, the incorporation of the LacZa gene into acceptor plasmids enabled optimised, efficient screening for correct assemblies (Table 2.4; Marillonnet and Grütznier, 2020).

The MoClo approach is theoretically quicker per construct than Biobricks and a novel method combining the two called GoldBricks (Chaudhari and Hanson, 2021). However, when comparing the assembly of seven genes in seven transcriptional units, each comprised of four parts, MoClo would require 50 reactions, compared to 10 for GoldBricks. Therefore, while all constructs used in the project were successfully cloned using Golden Gate there might be theoretical savings in efficiency through alternative strategies. However, it should also be noted that in practice time spent on cloning may also be significantly affected by other factors such as equipment availability and the potential for errors.

Overall, Golden Gate cloning was an appropriate choice and successful strategy to create multiple inducible GFP constructs to test and better understand the GR system used in this study.

4.2 Correct positioning of protein domains and inclusion of linkers are factors in the expression of fusion proteins

Planning the construction of functional fusion proteins is a challenging task; precise understanding of the relationship between their structure and function is mostly hypothetical. Genetic approaches include tandem fusion and domain insertion; where proteins are fused one after the other, or where one protein is inserted into a non-functional domain of its partner, respectively (Yu et al., 2014). The former was selected as it is easier to plan; inserting one protein into the domain of the other requires an existing cut site in one of the proteins and could have detrimental effect on protein folding and function unless placed in a non-functional domain (Yu et al., 2014). Further, there is a wealth of previous studies which have successfully used this approach to generate GR inducible tandem fusions (Craft et al., 2005; Wildwater et al., 2005; Günl et al., 2009; Yamaguchi et al., 2015). As the localisation and function of a tandem fusion protein can be dependent on orientation of the domains (Sachdev and Chirgwin, 1998), it was therefore essential to design cassettes with the GFP and GR proteins in both N and C terminal positions (Figure 2.1).

Upon selection of a tandem fusion protein design, a linker region to separate the domains of the two proteins was considered. This was good rationale, as direct fusion proteins can be frequently hindered by misfolding, deactivation, and hampered protein expression (Klein et al., 2014) as a consequence of steric hindrance, resulting in the production of non-functional proteins (Guo et al., 2017). A rigid linker was selected to prioritise separation of the two proteins, theoretically enabling them to fold properly (Chen et al., 2013). A PVAT (proline, valine, arginine, threonine) linker (<https://blog.addgene.org/gfp-fusion-proteins-making-the-right-connection>) was selected, which had been reported to assist in the expression of Protein Of Interest – fluorescent protein fusions, such as the ones designed in this study.

Upon construction of the fusion proteins, separated by the PVAT linker, at both the C and N terminus of GR, respective to its connection to GFP, constructs were transformed into *Arabidopsis* to test for expression. While most studies use the DEX system to ascertain the effects of transcription factor induction at normal levels of

expression and therefore use their chosen gene's endogenous promoter to drive expression (Yamaguchi et al., 2015), this study selected the CaMV 35s promoter (Table 2.2; Weber et al., 2011) to maximise nuclear concentration of cell cycle "sizers" and override normal concentration controls within the system. Therefore, as it was anticipated that the fusion protein would be ubiquitously expressed and sequestered in the cytoplasm via GR's interaction with HSP90, initial comparisons of the inducible reporter combinations were conducted in the absence of DEX (Figure 3.2). While *p35s::GFP-GR* yielded GFP fluorescence in 10% of kanamycin resistant T1 seedlings, *p35s::GR-GFP* transgenics were all negative for GFP. This indicated that the inducible reporter with the GR in the N terminal, but not C terminal position, translated into a functional protein. Interestingly, a study which compared fusions of the GR domain in both orientations for a transactivation system (Craft et al., 2005) found there to be higher fusion protein expression, uninduced in the absence of DEX when the GR domain was C terminally positioned, consistent with our findings.

While *p35s::GFP-GR* seedlings were positive for GFP (Figure 3.2D), displaying DEX induced nuclear localised GFP in the T2 generation (Figure 3.4), *p35s::GR-GFP* seedlings were not. This indicated that residues towards the C terminal end of the GR domain, or N terminal amino acids of GFP, or both, were critical to their function, and their interaction had prevented proper expression and folding of the protein. While Craft *et al.*, had selected their fusion protein with an N terminally positioned GR to be optimum, this was not the case in this study. Therefore, the lack of expression seen for *p35s::GR-GFP* could be specific to GFP. Potentially, GFP's C terminal could contain non-functional amino acids, which enable better separation of the two domains, irrespective of a linker protein.

While it can be concluded that the C terminal, rather than N terminal, GR induction protein was functional, as a *p35s::GFP-GR* construct without the linker had not been prepared, therefore it is inconclusive as to whether the linker improved folding, or if the orientation of the proteins was sufficient. While PVAT, a rigid linker was chosen to theoretically provide separation of the domains, a flexible, shorter linker, such as glycine, has also been favourably documented (Sabourin et al., 2007). This could have been advantageous as it has been reported that a shorter distance between active sites can increase the catalytic efficiency of the trans-protein domains (Guo et

al., 2017). On the other hand, the limitation could have been due to steric hindrance. If this is the case, a longer linker could be favourable to separate the proteins sufficiently to allow for more efficacious folding; the caveat of this being that highly homologous repeats of a multi-copy linker can reduce protein expression levels (Yu et al., 2014). To elucidate the nature of the relationship between a chosen linker and a fusion protein and to optimise expression, multiple reporter constructs could have been prepared with different linkers with contrasting characteristics. While this would have been informative, this would have been substantially more work and not necessarily feasible.

A more realistic, yet still enlightening approach would have been to use structural simulation programs to visualise tandem fusions and their linkers. Programs such as SWISS-MODEL can provide details about inter-protein secondary structure interactions (Guo et al., 2017) and FPMOD can also be used to generate hypothetical models (Chiang et al., 2006). This would have been a relatively feasible and informative strategy for the reporter fusion, as three-dimensional structures for GR and GFP have been determined. However, structural protein models are lacking for the G2/M phase specific GOIs, so could only have been applied to the reporter construct. While some software does exist which can predict protein structure based on the polypeptide sequence, it may not accurately predict the dynamics of the protein in a biological context (Rezaire et al., 2018). Moreover, due to the unique and unpredictable structural and functional characteristics of each individual fusion, a linker computationally optimised and experimentally verified could have different functional dynamics when universally applied to other bi or multi proteins.

The clear difference in functionality of the two reporter constructs tested in this study highlights the importance of empirically testing constructs with different conformations. This is particularly important given that further constructs were planned. For future inducible sizer design, it was hypothesised that simply avoiding joining a sizer to the C terminal end of the GR protein would be a good approach, as *p35s::GR-GFP* had been non-functional. Furthermore, several functional cell cycle-regulator- N terminal GFP fusion proteins have been reported including *pMYB3R3:MYB3R3-GFP* (Kobayashi et al., 2015), indicating that the approach would be compatible with GOIs.

4.3 While the functionality of the inducible *p35s::GFP-GR* protein was demonstrated, stability of the expression of the transgenic lines produced was variable

Upon selection of the *p35s::GFP-GR* orientation of the reporter, procedures aimed to obtain a homozygous line (Figure 3.3) that could be used to test and optimise the GR induction system. Interestingly, while strong signal was seen across a range of heterozygous lines in the T2 and T3 generations, the homozygous lines acquired had comparatively far weaker signal. Low expression of a fusion protein could be a consequence of protein misfolding, attributed to its orientation and its linker (Yu et al., 2014). However, this was an unlikely explanation as the fact that expression appeared to weaken, or in some cases completely disappear upon the lines becoming homozygous. This was indicative that issues beyond protein folding were at play.

Silencing of transgenes is a phenomenon which recurrently hinders genetic manipulation in plants, where transgene activity is diminished over time (Kooter et al., 1999). In line with observations in this study, transgene silencing has been reported to be one of the greatest issues for DEX induction constructs (Geng and Mackey, 2011). This is largely attributed to use of GR in the context of the GVG system (Gal4, VP16, GR) transactivation (Geng and Mackey, 2011), which was not used here. However, it can also be linked to the CaMV 35s promoter, which is a well-established target of silencing (Daxinger et al., 2008, Massunaga et al., 2019; Grob and Grossnikalus, 2019). Transgenes can be subject to the mechanisms of transcriptional gene silencing (TGS) and post-transcriptional gene silencing (PTGS). Both of these mechanisms can be mediated by methylation, which at the promoter can target the construct for TGS, and on DNA sequences encoding transgene, tend to target it for PTGS (Vaucheret et al., 1998).

In PTGS, mRNA belonging to the transgene is recognised by RNA-DEPENDENT RNA POLYMERASE 6 (RDR6), which begins to synthesise complementary strands of RNA (Morel et al., 2002). Subsequently, DICER-LIKE proteins (DCLs) facilitate the processing of these double stranded RNAs (dsRNAs) into several long small interfering siRNAs, transferring them to the slicer protein AGO1 for degradation (Baumberger and Baulcombe, 2005). This process is coordinated in development

and can result in systematic degradation of the transgene. Interestingly, it has been shown that the induction of DEX can cause subsequent degradation of transgenes, 24 h after induction (Ming et al., 2006). Furthermore, the use of a transactivation GR cassette based on the pOp/LhG4-GR system (Liang et al., 2012) observed silencing, by reduction in GFP expression in 90% of T2 seedlings. Compounding this, screening procedures in this study aimed to select lines with a high GFP signal and therefore abundance of transcript, which could have made them more likely to be silenced (Collier et al., 2018). This seems like a plausible mechanism; as PGTS is systemic, consistent with the systemic loss of expression seen in some of the stronger *p35s::GFP-GR* lines, and this method of silencing has also been frequently observed in studies using DEX induction procedures.

Equally, positional effects of the transgene in relation to the *Arabidopsis* genome could have been responsible for the diminished expression *p35s::GFP-GR* over time. *Agrobacterium* mediated floral dipping is widely regarded to be a major cause of genomic instability (Rajeevkumar et al., 2015); most transgene insertions cause deletions at their integration site (Forsbach et al., 2003), 21% have been reported to cause a large-scale rearrangement or deletion of chromosomal DNA (Latham et al., 2005) and between 23-67% of T-DNA insertions are estimated to perturb gene sequences (Latham et al., 2005). This can cause rearrangements of intrinsic promoter and coding sequences; it has been shown that the addition of non-native transcriptional units to *Arabidopsis* can link genes to multiple promoters, leading to disturbed expression (Latham et al., 2005). As a result, t-DNA insertions radical rearrangements can also occur in the three-dimensional chromatin architecture (Krispil et al., 2020) causing modifications of the nuclear landscape at the point of insertion (Grob and Grossniklaus et al., 2019). Novel high resolution chromosomal capture technologies have enabled further elucidation of epigenetically coordinated chromosomal changes (Grob and Grossniklaus, 2019; Krispil et al., 2020). Analysis of Hi-C data of SALK T-DNA insertion mutants revealed interactions between transgene integration sites and elements belonging to elements engaged with the *KNOT*; a conserved nuclear structure consisting of small RNAs and transposable elements (Grob and Grossniklaus et al., 2019). They reported in their study that these chromatin connections resulted in six out of eight T-DNA insertions displaying significantly different 4C profiles compared to wild type plants, indicating that

chromatin alterations are very common. Moreover, observation of plants carrying a NPTII transgene, which was also used in the plants in this study for kanamycin resistance (Figure 2.3; Figure 2.6) showed initial transcription, which was subsequently diminished over generations. This demonstrates that *KNOT*-linked silencing (KLS) is dynamic, its effects gaining prevalence over several generations, consistent with the decreased GFP expression observed in the T3 and T4 homozygous *p35s::GFP-GR* transgenics in this study. Therefore, this could also be a reason as to why protein expression dimmed across generations.

To circumvent transgene silencing, certain techniques have been devised in order to identify insertion points and select favourable sites. Previous approaches have included inverse PCR, TAIL PCR and the use of biotinylated primers in order to locate the left and right borders of the transgenic plasmid in the genome (Krispil et al., 2020). However, the caveat of this method is that 80% of T-DNA borders undergo deletions or insertions, hindering the binding ability of the designed primers. Recent strategies have utilised novel techniques; “Anchor” employs a ParB sequence fused to a fluorescent tag, followed by nanopore sequencing allow the tracking of a single transgenic locus (Meschichi et al., 2021) and 4SEE combines 4C-seq with computational analysis to further examine the effect a genome insertion has on the surrounding chromosomal landscape (Krispil et al., 2020). However, while these are informative, a consensus is still lacking about the exact effects of insertion points and chromatin. Moreover, their application to every T2 family would not necessarily be worthwhile when considering time and cost against the data received.

Additionally, an approach at the cloning level could be to use a promoter specific to cells in the root; the tissue used in this study for measurement of cell sizes. This would circumvent the use of the CaMV35s promoter, an element frequently vulnerable to epigenetic silencing. As this study later examined the cortex cells in the root apical meristem, *pPIN2* could have been an appropriate choice, as it would have localised expression to the cortex and epidermal cells (Marquès-Bueno et al., 2016). However, this would have limited cell size analysis to these cells only, negating the effects of sizer induction in the other stem cells in the meristem. Further, without their contribution, overall root phenotypes such as length could be harder to determine.

Therefore, while the CaMV 35S promoter is a target for silencing, its selection is still justified and an appropriate choice to test the effects of nuclear translocation of sizers.

Instead, in order to find lines that are not affected by silencing, the transformation could be done again on a new plant and at least 40 *p35::GFP-GR* T1 seedlings should be grown to the next generation (Schürholz et al., 2018). In the meantime, other members of the T2 families with Chi squared values indicative of a single T-DNA locus which hadn't yet been selected could be screened for GFP fluorescence and if positive, transferred to soil to see if silencing could be avoided in these lines. These transgenics would have independent genome integration sites respective to the homozygous lines used in this study, and therefore would perhaps be subject to fewer chromosomal rearrangements. However, while these lines represent independent integrations, they are from the same plant transformation, of which eight selected heterozygous 3:1 lines all showed decreased transgene activity upon gaining homozygosity. Consequently, a new transformation may be a better strategy (Albornoz et al., 2023). Additionally, screening approaches would be more informed for the new transgenics (Figure 3.3; Figure 3.7) while initially, seedlings with strong uninduced GFP signal were selected (Figure 3.2D), they may have been more prone to silencing than their weaker counterparts. It has been shown that there is a level of mRNA accumulation, specific to reporter genes which can trigger post-transcriptional silencing if exceeded (Schubert et al., 2004). As such, for new T1s, weaker lines would be selected and grown to the next generation.

Overall, while the lines did undergo silencing, three homozygous lines with detectable nuclear GFP expression were retrieved, displaying a response to DEX in line with the projects aims (Figure 3.5). Therefore, future experiments looked to use these lines and optimise the induction system.

4.4 A DEX induction protocol and screening procedures assisted in the selection of an inducible GFP-GR reporter protein for future optimisation of the system

The DEX induction optimisation protocol designed in this study was based on previous literature (Levesque et al., 2006; Schürholz et al., 2018). The parameters considered were mode of application, concentration and duration of DEX. While several methods of DEX application have been reported such as submersion in and spraying of DEX (Yamaguchi et al., 2015) here, transferring to plates was an appropriate choice, as it allowed uniform, precise treatment of the seedlings. Secondly, the concentration was considered. Previous DEX inductions found low concentrations to be sufficient such as 0.1 μM to show effects for GR-RBR (Wildwater et al., 2005) and even nanomolar concentrations (Aoyama and Chua, 1997). Others suggested using 5 μM to start (Yamaguchi et al., 2015). A study also performing a DEX optimisation protocol in the roots, five days after germination (DAG) used incremental concentrations between 0.1 μM and 100 μM , with each increment multiplying by ten (Schürholz et al., 2018). Here, an upper limit of 100 μM DEX was also applied, however as low GFP expression had been detected in the inducible reporter plants when screening at 60 μM DEX the following points were chosen: 0 μM , 25 μM , 50 μM , 75 μM , 100 μM ; to reach a high concentration via broad increments.

Lastly, the duration was decided. Quick inductions have been reported including detection of target gene activity 1 hour and 6 hours post treatment (William et al., 2004, Schürholz et al., 2018), and the goal of the project was to rapidly translocate hypothetical sizers to the nucleus, to break their cell size dependency. However, it was also a desirable characteristic of the system for this expression to prevail, to assess the effect of this over time, using root biomass of the plants as a convenient measure (Figure 3.10; Figure 3.11; Figure 3.14). Additionally, the age of the seedlings upon transfer to DEX could also affect their response. However, similar transgene activity has been reported for roots induced between 2 and 5 DAG (Schürholz et al., 2018), therefore the 4 DAG time point selected in this experiment should give consistent results.

While the methodology and planning behind the protocol was logical and based on previous studies, positive GFP signal for 8.1.4 across the range of concentrations tested was found to be inconsistent across seedlings, and as such could not be optimised. (Figure 3.5A). This could have been a consequence of variability in the uptake of DEX, relative to their position on the microagar plate, however this seems unlikely as efforts had been made to ensure DEX was well circulated in the media. A more likely explanation would be that silencing had occurred in some of the seedlings in the population.

Consequently, the DEX optimisation experiment led to the growth and retrieval of T4 homozygous lines, grown from different T3 families (Figure 3.5B). It is important to note that an optimised DEX system may need tweaking within and between different transgenic lines, based on strength and responsiveness. For example, a high-expressing line might require less DEX than a weakly-expressing line in order to accumulate the same concentration of fusion protein in the nucleus.

4.5 Profiling of homozygous *p35s::GFP-GR* T4 population found two lines with consistent GFP expression suitable for further DEX induction experiments

The retrieval of T4 homozygous *p35s::GFP-GR* lines led to the selection of two promising reporter lines, *2.1.4.16* and *7.2.3.1* (Figure 3.5B). The choice of these inducible reporters over *8.1.4* was justified; these two homozygous lines produced seedlings with detectable GFP, in over 20 seedlings each, when screened, displaying consistent expression, in contrast to GFP. This was desirable as it was a non-negotiable requirement of the system for transgene induction to be uniform (Zuro and Chua, 2003; Mortimer et al., 2015).

Interestingly, one line (*2.1.4.16*) showed faint apparently cytoplasmic GFP expression prior to induction (Figure 3.5B), indicating that the induction system is “leaky” (Craft et al., 2005). While most activation systems require no detection of the transgene prior to induction (Zuro and Chua, 2003; Albornoz et al., 2023), this is less important in this study, as the goal of DEX application is to elicit post-translational induction, rather than switch on their transcription (Figure 1.5), as hypothetical sizer proteins residing in the cytoplasm are likely to be inactive (Craft et al., 2005). Moreover, if future sizer constructs displayed expression before induction, it would be useful to use a reporter which behaved in the same way as a control.

However, in this study *p35s::GFP-GR 7.2.3.1* was prioritised, as upon DEX induction, it appeared to show brighter GFP expression, in more cell types. However, in the future it would be interesting to comparatively profile the reporter proteins in more detail. It would be interesting to not only quantify total signal before and after induction, and go a step further in terms of how readily expressed GFP translocates to the nucleus upon DEX treatment. This would be especially interesting with regards to *2.1.4.16*, in terms of seeing how rapidly the “leaky” GFP prior to induction moves to the nucleus, and if the fusion protein’s disengagement with HSP90 upon DEX application allows an overall higher rate of GFP translation, regardless of subcellular location.

4.6 A Gibson-based cloning approach was successful for cloning genes of interest into the inducible expression cassette, in a reusable manner

Having established the optimal arrangement of basic inducible expression cassette, *p35s::GFP-GR*, and verifying its functionality *in planta*, the third objective was to introduce GOIs relating to proteins hypothesised to be “sizers” in the plant cell cycle. As fusions to the C terminal end of GR had resulted in non-functionality, GOI incorporation was designed N terminal of GFP, using the same PVAT linker to separate the two domains (Figure 2.5B). Furthermore, as the first sizers cloned into the system belonged to the MYB family, which both contain an N terminally located DNA-binding domain comprised of three MYB motifs, highly critical to their function (Ito et al., 2005; Kobayashi et al., 2015), it made sense to avoid this region in the fusion.

A notable disadvantage of the Golden Gate system became apparent when planning to incorporate a gene of interest (GOI) into the selected *p35s::GFP-GR* base reporter. As the Level 1 Acceptor intermediate vector used was inflexible (Chaudhari and Hanson, 2021), the system could not be easily used to incorporate in an extra part between the promoter and GFP.

To circumvent this issue, NEBuilder HiFi Assembly was selected, an approach based on Gibson Assembly (Gibson et al., 2009; Sparkman et al., 2020) involving the design of overlapping primers, each extending 20 bp between the vector and insert respectively, followed by PCR to join regions by homologous end-joining (Thomas et al., 2015). This commercial product was chosen over standard Gibson Assembly as it has been shown to have higher efficiency when assembling constructs (Sultan et al., 2020). In this project, primers were initially designed to incorporate a *PacI* restriction site in between the promoter and GFP in the reporter cassette, which would act as the insertion site for the GOIs. From this point, primers were designed to amplify the GOI with complementary overlaps that allowed the GOI to be ligated into the vector and eliminate the *PacI* site (Figure 2.5). This approach was highly successful; for each construct only one reaction was required to produce a correctly assembled plasmid, as confirmed by Sanger sequencing. Altogether, this method was used to create constructs for six inducible, hypothetical sizer proteins,

ranging from 333 bp – 4230 bp demonstrating the efficiency and reusability of this cloning strategy.

Using a hybrid approach, where GOIs were introduced via HiFi Assembly instead of starting again at Level 0 Golden Gate plasmids was additionally beneficial as it negated the need to domesticate the GOIs; any *Bsal* and *Bpil* recognition sites in the GOI would need to be silently mutated before the sequence could be used in the Golden Gate system. The first G2-M phase GOIs selected to be cloned, *MYB3R3* and *MYB3R4*, had one and three such recognition sites respectively, so this step would have been essential for MoClo Assembly. This would have been detrimental in terms of time or expense since domesticating the parts would have required additional PCR steps. For *MYB3R4*, this would have meant the preparation of four separate PCR fragments, followed by their ligation into a Level -1 plasmid, an additional assembly step which had not been required for reporter assembly. Alternatively, ordering these altered parts directly in the form of gene blocks would be costly (Zhao et al., 2022). The incorporation of domestication steps also increases the risk of introducing sequence errors. Additionally, while the domestication would not alter the translated polypeptide chain, changes to the underlying genomic DNA sequence of the GOIs could disrupt interactions with DNA-binding proteins. As there is a high degree of characterised transcriptional regulation at G2/M, including the binding of MSA elements and associations of *MYB3R3* with components of G1/S (Kobayashi et al., 2015; Nomoto et al., 2022) any changes in these interactions could potentially mask their function.

While Gibson/Hi-Fi style cloning has been reported to have drawbacks such as difficulty cloning repetitive sequences (Zhao et al., 2022), the requirement for long primers which can form secondary structures, and the potential to amplify non-specific sequences (Chaudhari and Hanson, 2021), these issues did not present in this work, demonstrated by the six constructs that were successfully and easily cloned in this manner, including larger genes of up to 4230 bp (Table 2.5). While this approach can be expensive due to the need to use long primers and high-fidelity enzymes and parts are difficult to reuse (Lampropoulos et al., 2013) its efficiency and speed justifies its selection, particularly in the context of adding in the GOIs. It is

a ubiquitous system, applicable to any GOI, whereas other systems such as Golden Gate and may require additional alteration steps, respective to their sequence.

Overall, the use of Golden Gate combined with NEBuilder HiFi cloning successfully produced inducible sizer constructs, valuable for this study (Figure 2.6).

Consequently, post correct construction, independent inducible sizer constructs were transformed into *Arabidopsis* to test the system.

4.7 Inducible *p35s::MYB3R3-GFP-GR* and *p35s::SMR2-GFP-GR*, but not *p35s::MYB3R4-GFP-GR* plants were functional in *Arabidopsis thaliana*

Post verification of assembly, transformation of the inducible sizer constructs had varied success. For *p35s::MYB3R3-GFP-GR* T1 lines displayed strong nuclear signal after DEX treatment, across several families. This was encouraging in terms of the building of future GOI inducible constructs; as the fragment used for *MYB3R3* was 2592 bp in length, its success indicated that the plant binary vector, pAGM4673 supplied in the MoClo kit itself was stable enough to transform a large construct into *Arabidopsis*. As high copy number plasmids are prone to genomic instability (Polóniová et al., 2013), it was important to ensure the chosen plasmid in this study could correctly express a relatively large construct.

Interestingly, expression levels observed in *p35s::MYB3R3-GFP-GR* lines were consistently stronger than in the *p35s::GFP-GR* reporter alone, at T1, T2 and T3 generations. This could imply that the addition of *MYB3R3* to *p35s::GFP-GR* assisted with the overall folding or stability of the triple fusion, as its expression was qualitatively stronger than the reporter fusion. It has been reported that phosphorylation of three highly specific residues by CDKs target *MYB3R3* for degradation via the ubiquitin proteasome pathway (Chen et al., 2017). Therefore, if these residues are inactive in the multi-fusion protein, it could evade this mechanism, adding to stability of the unit. It has also been reported that proteins which have unstructured amino acids at the terminal end participating in the fusion can provide flexibility between trans-functional domains (Rizk et al., 2012) and as *MYB3R3* is a relatively large protein of 518 amino acids, it is not unreasonable to suggest it could have considerable amino acid regions with no vital or distinct function, able to act as an endogenous linker. Indeed, previous cloning of the large cell cycle transcription factor RBR, positioned C terminal in tandem with the GR domain has been reported and required no linker region for functionality (Wildwater et al., 2005).

Although the *MYB3R3* results demonstrate proof of concept for the expression cassette, it should be noted that there may be sequence-specific differences in the reusability of the system depending on the GOI. For example, here, while *p35s::MYB3R4-GFP-GR* was assembled correctly at the plasmid level (Figure 2.6C),

it did not produce any GFP positive transgenic seedlings with or without DEX despite screening in excess of 20 kanamycin resistant seedlings in the T1 generation. A possible explanation for this could be impairment of protein folding. While the PVAT linker had been reused in both MYB3R constructs, it was evidently not sufficient to enable proper folding or, potentially separation of the multi-protein domains. It could be that MYB3R4's C terminal caused steric hindrance when fused to GFP's N terminal domain, in a similar way to the interaction between NGR and CGFP. A previous study which looked at *pMYB3R3-MYB3R3-GFP* additionally used a GFP-MYB3R4 fusion, in the N to C terminal positions, respectively (Kobayashi et al., 2015). This indicated that they also could have had issues when using an N terminally positioned MYB3R4 GFP fusion, and consequently tried the fusion in the alternative orientation. Indeed, a functional GFP reporter construct of MYB3R4 under the control of its native promoter, where the MYB3R4 protein is C terminal, independent of a linker has also been reported (Yang et al., 2021). Here, they identified that MYB3R4 possesses a sequence in its carboxy-terminal, essential for cytosolic targeting, along with a conserved sequence hypothesised to act as a Nuclear Export Signal (Yang et al., 2021). Therefore, this sequence could have been disrupted in our study via fusion of MYB3R4 at its C terminal, masking the function of these amino acids. However, the use of a functional *pMYB3R4-MYB3R4-GFP* transgenic line has also been presented (Chen et al., 2017). While protein levels were barely detectable, they were able to quantify GFP fluorescence in response to a DNA damage inducing agent. However, details on the exact construction were lacking, and they may have used a different linker to the one used in this study. Equally, the insert for *MYB3R4* was 1638 bp larger than the one for *MYB3R3*. This could have been too large an insert for the Level 2 Acceptor vector, pAGM4673 (Engler et al., 2014) to tolerate.

On the other hand, this study was able to successfully clone and verify the functionality of *p35s::SMR2-GFP-GR* transgenic plants (Figure 3.15; Figure 3.16). Therefore, while an inducible MYB3R4 line was not generated, the verification of two constructs in plants demonstrated the reusability of the GR induction system.

4.8 Five homozygous *p35s::MYB3R3-GFP-GR* lines were obtained for comparison to and optimisation with *p35s::GFP-GR*

Selection procedures described in Figure 3.7 successfully identified five independent *p35s::MYB3R3-GFP-GR* homozygous T3 lines for further analysis. All five lines were found to show consistent nuclear GFP signal, after DEX induction for 48 hours, (Figure 3.9A), across a range of cell types in the root meristem (Figure 3.9C). This expression pattern was comparable to that of the *p35s::GFP-GR* homozygous reporter seedlings (Figure 3.5B). These results indicate that MYB3R3-GFP-GR was successfully released and translocated to the nucleus upon application of DEX, consistent with published mode of action of this system (Figure 1.5; Craft et al., 2005; Schürholz et al., 2018). Interestingly, given that GR-fusion proteins are expected to be bound to HSP90 and thus incompletely folded prior to induction (Kirschke et al., 2014), some GFP was visible prior to induction in some of the MYB3R3 lines (Figure 3.9A). This could have resulted from a higher ratio of the inducible protein to HSP90, allowing dissociated protein to express in the cytoplasm. Such “Leakiness” of uninduced GR fusion protein can be an issue; there is an argument to suggest that low levels of the target gene prior to DEX induction is a highly desirable quality of the activation system (Yamagichi et al., 2015; Albornoz et al., 2023). This is because of the system’s well characterised use of the study of transcription factors, where low basal transgene activity prior to treatment enables rapid gene activity upon DEX application, facilitating the identification of a genes’ downstream targets. However, while there was some discernible GFP background for some of the *p35s::MYB3R3-GFP-GR* lines, as visualised by snaps and z-stacks (Figure 3.9A; Figure 3.9C) it was very minimal, only presenting faintly in a few cells of the root meristem cells (Figure 3.9A). This could have been due to the strength of the lines or potential protection from phosphorylation-mediated degradation. Another explanation could be the use of the strong, constitutive promoter resulting in overexpression compared to expression under its native promoter which had been described to produce very faint GFP signals under normal conditions (Chen et al., 2017). This was not necessarily a problem as this study was interested in breaking the dependency between cell size and expression of the protein rather than recapitulating normal expression levels. Furthermore, later experiments could be planned to quantify cytoplasmic and nuclear pools of GFP to build detailed models of

the relationship between nuclear protein concentration and cell cycle progression. Therefore, all lines obtained were suitable for this, and to be optimised.

The five p35s::MYB3R3-GFP-GR lines qualitatively and quantitatively varied in GFP signal based on a preliminary analysis (Figure 3.9A). As is the case in many transgenic lines this could indicate a dosage effect where higher levels of the reporter gene correlate to increased GOI expression. Stronger lines can often result in more drastic phenotypes (Verkest et al., 2005), whereas weaker lines may behave more similarly to wildtype plants. Consequently, optimisation was conducted on all of the lines, to ascertain the effect of MYB3R3 induction and additionally, to take into account different requirements of inducible plants in relation to their strength.

4.9 An upper limit of DEX concentration was determined

The retrieval of the *p35s::MYB3R3-GFP-GR* lines enabled a second DEX optimisation experiment to be conducted, along with the selected *p35s::GFP-GR reporter* 7.2.3.1. This optimisation protocol had more points and closer intervals than the previous experiment, in order to closely pinpoint changes in size. The higher concentration, 200 μM was included to test the limits of the system and ensure that the maximal response had been identified.

Firstly, the effects of MYB3R3 translocation on root growth was ascertained. As the loss of function triple repressive MYB3R mutant, *myb3r1/3/5* had an increased meristem size and longer roots (Kobayashi et al., 2015), it was hypothesised that induction of MYB3R3 expression would result in shorter roots, compared to wildtype plants. Seedlings were induced for three days. This was good rationale as the cell cycle in *Arabidopsis* in the root apical meristem is estimated to be between 15 and 20 hours (Rahni and Birnbaum, 2019) increased to just over 24 hours in a G2/M protein loss of function mutant, *scl28*, hypothesised to be a positive cell cycle regulator (Goldy et al., 2021). Therefore, the selected course of DEX treatment would allow for cells in the root to undergo approximately three cycles, accounting for any potential delays attributed to MYB3R3 inhibition. This experiment was revealing in terms of the upper limit on DEX which could be applied to the system, as increasing the concentration to 200 μM dramatically decreased relative root length of both the reporter, and wildtype seedlings (Figure 3.10). While several studies found no effect of DEX treatment on wildtype plant vitality at concentrations including 50 μM (Albornoz et al., 2023); 10 mM and (Craft et al., 2005); and found that it did not cause DNA damage (Rodriguez et al., 2018) some studies have speculated that higher concentrations, such as 10 mg/L could exert toxicity on cells (Tang et al., 2016). This was useful information, as it was tempting to keep increasing concentration to try to observe greater GFP signal, and therefore maximise the accumulation of MYB3R3, and subsequently other sizer proteins, within the nucleus. However, this study clearly found that out of the concentrations used, 100 μM is the upper limit of DEX which can be applied for induction without affecting plant growth,

and any effects seen higher than this concentration cannot be solely attributed to the effect of the GOI.

Fortunately, there was no discernible effect of DEX induction root growth in either wild type Col-0 seedlings or the *p35s::GFP-GR* control reporter line when comparing non-induced seedlings to those induced at 100 μ M (Figure 3.10A; Table 3.2; Table 3.3), therefore, this concentration could confidently be selected when inducing size proteins. This was determined at a statistical level three days after treatment (DAT), and further concluded by comparing non-induced and induced (100 μ M DEX) seedlings at 11 DAT (Figure 3.14). Furthermore, both wildtype and *p35s::GFP-GR* plants' responses to DEX were found to be non-statistically different in relation to each other, in terms of their response to DEX. As such, it was assumed that any changes in root growth over this time period for the *p35s::MYB3R3-GFP-GR* lines were due to the effects of *MYB3R3*, rather than GFP induction.

4.10 No distinct trends were seen for MYB3R3 induction on root growth over a three-day period, however plant biomass was reduced after 15 days

Next, relative root growth (RRG) data was assessed for the five inducible MYB3R3 lines, in order to assess the effect of sustained MYB3R3 nuclear translocation on overall root organ length (Figure 3.11). Root growth, relative to the length at which each non-induced genotype had grown was examined for all concentrations except for 200 μM , due to its toxicity on control plants.

As the *myb3r1/3/5* mutant had been found to have longer roots than wild type (Kobayashi et al., 2015), it was expected that the induced MYB3R3 lines would have shorter roots as overexpression could reasonably be expected to have the opposite effect to the loss of function mutant. Interestingly, no consistent, distinct trends were seen across the genotypes and concentrations (Figure 3.11). Two of the lines, 1.7.7 and 4.2.8 were relatively constant in terms of their root growth across increases in DEX concentrations, relative to their non-induced counterparts. These were the two strongest lines, judged by fluorescence data (Figure 3.9B). Contrastingly, 5.2.9 and 6.3.4, the two weaker lines, had increased RRGs, which reached their maximum at 50 μM and 100 μM , which was not in line with experimental predictions. Strangely, all the lines had higher relative growth rates compared to the wildtype and reporter, at most concentrations. However, the means could have been heavily influenced by outliers; while efforts were made to discount any seedling which had not fully embedded in the media, this may have been difficult to determine for some seedlings. Furthermore, as this data consisted of one biological replicate only, future experiments could reduce intragenotype variability. It is also possible that three days may have been insufficient time for a subtle cell division phenotype to impact the overall length of the root. Indeed, studies reporting a change in overall organism size attributed to alterations in transcriptional MYB3R3 levels observed this after six days of growth (Kobayashi et al., 2015). Further, a study which investigated the effects of a loss of function mutant, *sc/28-3*, which acts downstream of MYB3R3 described shorter roots after 10 days of growth (Goldy et al., 2021).

To test whether longer induction resulted in a clearer phenotype, growth was visually inspected after induction at 100 μM for 11 days (Figure 3.14). After this longer

induction period, three out of the five lines had qualitatively shorter roots, and four had smaller shoots, relative to non-induced seedlings of the same genotypes. The same was not seen for the *p35s::GFP-GR* reporters (2.1.4.16 and 7.2.3.1) or the wildtype, indicating that the decreases in organ size were not due to DEX toxicity over this time period. This indicated that the translocation, accumulation, and sustained localisation of *MYB3R3* in the nucleus was able to inhibit tissue growth, at a time point between 3 and 11 days of treatment. This implies a role for *MYB3R3* in repressing organ growth, consistent with the findings of the *myb3r1/3/5* paper (Kobayashi et al., 2015), and with additional studies which have found that *MYB3R3* mediates reduction in root length under salt stress (Okumura et al., 2021), DNA damage (Chen et al., 2017) and high-temperature stress (Takahashi et al., 2019).

The reductions in root and shoot sizes could have been a consequence in decreases in transcriptional activity in G2/M genes. It has been found that loss of the three repressive MYBs led to a several fold upregulation of G2/M promoting genes in leaves produced 9 –15 days after germination (DAG) compared leaves produced 5 DAG (Kobayashi et al., 2015). While this finding is in differentiating leaf tissue as opposed to the meristematic roots and there may be tissue specific differences, it does imply that transcriptional alterations in *MYB3R3* may require a certain number of cell cycles to significantly alter G2/M phase promoting gene expression. This could explain the reduction in root growth observed after 11 days of DEX treatment (Figure 3.14) but not after three (Figure 3.11).

To gain a deeper insight into the effects of DEX induction on root growth of the inducible lines, the experiment should be repeated. A time course could be done, scanning the plates every 24 hours from the point of transfer. This would reveal the exact day at which the sustained translocation of *MYB3R3* to the nucleus results in a detectable decrease in the lengths of the roots. This would also allow for later quantification of root length, as this was not possible to do at the 11 day time period, as roots for some plants had reached the bottom of the dish and were therefore not measurable.

Interestingly, there was one of the inducible *p35s::MYB3R3-GFP-GR* lines, which, after three days, behaved in the way in which we predicted in terms of root growth.

p35s::MYB3R3-GFP-GR 1.3.3, after a very small increase in RRG across concentrations from 0 μM – 50 μM DEX, showed a decrease at 100 μM (Figure 3.11). This was also lower than that of the control *p35s::GFP-GR* reporters, indicating that this was a specific effect of MYB3R3 induction, rather than an effect of the interaction between DEX and GR alone. While this data needed to be repeated, it did suggest that this line could have a more rapid response to induction than the other families, at the higher concentration.

4.11 Nuclear translocation of *p35s::MYB3R3-GFP-GR* increased cortex cell sizes in the root apical meristem

As examining the relationship between biomass accumulation and cell size is highly elucidating when understanding proliferation and division, root cell size analysis was also performed (Section 2.20). For initial cell length measurements, the proliferating cortex cells were selected to enable comparisons with other cell cycle regulatory studies (Nomoto et al., 2022). For analysis, *p35s::MYB3R3-GFP-GR T3: 1.3.3* had been selected out of the inducible MYB3R3 lines, as its expression seemed to be moderate in comparison to other lines, and its response to DEX after three days in terms of root growth had aligned with expectations based on previous literature (Kobayashi et al., 2015). Cells in both the apical and basal meristem prior to rapid elongation in the transition zone were measured, in order to account for all dividing cells. As cell size increases exponentially when entering the basal meristem (Nieuwland et al., 2009), data was transformed logarithmically for analysis, using the natural logarithm transformation (Figure 3.12; Figure 3.13).

Increasing DEX concentrations produced *p35s::MYB3R3-GFP-GR* seedlings with cortex cell sizes incrementally larger, peaking at 100 μM . At this point, cell sizes were statistically different compared to non-induced cortex cells, at a degree where $p=0.001$. While 30 μM DEX cells were also statistically different to the base level, the level was much lower ($p=0.05$). On the other hand, the wildtype control was unresponsive to increases DEX; although there was a dip in the median of its cortex cells at 200 μM DEX, this was not significantly different to any of the other concentrations, and this point had been discounted by its strong effects in terms of inhibiting root growth. The control reporter line *p35s::GFP-GR 7.2.3.1* interestingly, did show a response to DEX. This was highly statistically significant ($p < 0.001$) based on a linear model evaluating the effect of increasing DEX concentrations on the different genotypes, with *Col-0* as the reference level. However, upon closer comparisons of each point with each other, within the *p35s::GFP-GR 7.2.3.1* population, much of this resulted from increases in cortex cell sizes at 200 μM , which was highly statistically significant when compared to the lowest concentrations (0 μM and 10 μM). To a lesser degree ($p=0.05$), differences were observed between non-

induced and induced cells. However, this could have been due to sample variation. Importantly, no significant difference was found between 0 μ M and 100 μ M, and while the wildtype and GFP reporter cortex cell sizes were not statistically different at 100 μ M, they both were in relation to *p35s::MYB3R3-GFP-GR* at this concentration, to a degree of 0.001. Overall, this experiment produced a cellular phenotype for MYB3R3 translocation to the nucleus, and provided an optimum concentration for DEX for this response without altering growth of the control reporter or wildtype. This correlated with the findings for root growth analysis three days after DEX treatment for *p35s::MYB3R3-GFP-GR 1.3.3*; 100 μ M DEX produced larger cortex cell sizes in the root apical meristem, which could have contributed to the observed decreased root growth.

While other literature has reported the relationship between MYB3R3 and nuclear size, (Chen et al., 2017) in accordance to current understanding, this is the first study which has attributed a cell size phenotype to MYB3R3. However, while it was identified that the translocation of MYB3R3 to the nucleus produced larger cells in the root meristem, cell cycle length was not measured. Previous studies have correlated MYB3R3 function with a slower cell cycle; using nuclear content as a proxy for cell cycle progression, they determined that MYB3R3 can arrest the cell cycle at G2/M in response to abiotic and biotic stresses, such as salt (Okumura et al., 2021) and DNA damage (Chen et al., 2017). As such, future experiments using the inducible MYB3R3 lines will aim to determine cell cycle length, with an aim to correlate the increase in cell sizes observed with a longer cell cycle, specifically at G2/M. As the repressive triple MYB mutant, *myb3r1/3/5* was shown to have a much faster cell cycle, (Kobayashi et al., 2015), it is predicted that the overexpression and induction of MYB3R3 would have the opposite effect. This would be consistent with the increase cell length presented here as increased cell cycle length would allow cells to reach a greater length before dividing. The inducible system will be particularly useful for these experiments as it would allow detailed characterisation of the dynamics between MYB3R3 expression and changes in cell cycle progression; for example, allowing the effect of induction in cells in different phases of the cell cycle to be compared.

Further, these results provide a line of evidence to suggest that MYB3R3 is a possible candidate for an inhibitor dilutor. The observed increase in cell size could indicate that a new larger critical size threshold at which the cell can divide has been set due to the need to dilute out the inhibitory effect of the additional MYB3R3 protein within the nucleus. This could be compounded by MYB3R3 circumventing degradation mechanisms if its phosphorylation sites are protected in the multi-fusion protein. This could be further evidenced by quantification of GFP protein levels and performing future experiments to relate this to cell cycle progression. Using these results, detailed predictive simulations could be made using the model, to determine MYB3R3's role in the size control of asymmetric daughter cells.

4.12 Evaluation of the overall success of the induction system

Overall, this study has demonstrated that the design and execution of the GR induction tool was successful in meeting elements of all three aims of the project. MoClo cloning was able to produce a GFP-GR reporter of the system, and subsequent transformation and analysis highlighted the optimal positioning of the fusion proteins within the construct. Initial screening and analysis of transgenic seedlings with this construct enabled testing of the system, and its validation facilitated the design of inducible sizer protein constructs using a hybrid cloning approach. This was also largely effective; six correctly assembled cassettes were produced, three of which were transformed to *Arabidopsis* and two of which were found to be expressed. Although the reporter line did undergo silencing, this is a common issue in the obtaining of a homozygous plant transformant and could be likely circumvented by another transformation event in the future.

The efficiency of the cloning processes enabled for the retrieval of five homozygous *p35s::MYB3R3-GFP-GR* lines alongside a reliable *p35s::GFP-GR* control reporter line, all of which behaved in a similar way in terms of fluorescent expression. Subsequently, this allowed for the GR system to be optimised, while simultaneously studying the effects of breaking MYB3R3's cell size dependency.

In further experiments a DEX dependent increase in cortex cell size length was observed upon MYBR3 translocation. This was significantly different to non-induced *p35s::MYB3R3-GFP-GR*, and to control wildtype and *p35s::GFP-GR* reporter plants, showing that this was a true effect of MYB3R3 induction, and not a response to DEX alone. This result demonstrated a notable achievement of the project, and highlighted the capacity of the GR system in terms of revealing the effects of breaking cell size dependency, with relation to hypothetical sizer proteins. Additionally, while not quantified, there was notable reduction in root length and shoot size in most of the inducible MYB3R3 lines 11 DAT on 100 mM DEX. This demonstrated that the system had the potential to elicit long term effects on growth and development, in multiple plant organs. Further, the reusability of the system was demonstrated by the return of nuclear localised GFP positive DEX treated *p35s::SMR2-GFP-GR* T1 seedlings. However, the system did require an

uncharacteristically high concentration of DEX to optimise the system. Although this study did not find any adverse effects in relation to root growth or cell size at the chosen concentration of 100 mM, several studies have reported DEX toxicity, including those greater than 20 mM for seedlings grown on agar (Samalova et al., 2005), the same application in this study. This could be an issue when administering DEX to see the effect of breaking protein cell size dependency in the shoot apical meristem. However, DEX toxicity has been linked to the induction of genes involved in defence by the GVG system (Böhner et al., 1999) indicating that this may have been an issue more applicable to transactivation studies, rather than simple GR-GOI fusions, such as the one used in this study.

In light of the high concentrations of DEX required, alternative chemical induction systems could be used. These include the Estrogen Receptor (ER), induced by oestradiol (Bruce et al., 2000) and the AlcA system, induced by ethanol (Caddick et al., 1998; Roslan et al., 2001), where respective chemicals can be administered to receptor fusions to GOIs, resulting in overexpression. In line with the requirements of the system for studying cell cycle proteins, both systems have shown rapid increases in protein concentration, at low concentrations of inducer. The ER system could be advantageous, as it has a higher binding affinity of 0.05 nM, compared to 10 nM for DEX (Zuo and Chau, 2000). The AlcA system on the other hand, has been reported to be optimal at 2% ethanol (Roslan et al., 2001). It is clear that regardless of the system, the range of concentrations for different chemicals are vastly different, demonstrating that optimum concentrations are highly construct specific. Moreover, observations different family members of each respective *p35s::MYB3R3-GFP-GR* and *p35s::GFP-GR* lines showed that inducer responses are subjective even within transformation events. Therefore, it is difficult to say whether a different system could have elicited more of a response at a lower concentration.

In addition, a justification of the GR system was its endogenous nuclear localisation tag, which enabled the shutting of the GR fusion into the nucleus, post DEX application. While the AlcA and GR systems have been combined (Roberts et al., 2005) and a nuclear localisation tag can be incorporated to the ER domain (Davis et al., 2012), this would involve more cloning steps for an approach which is not guaranteed to be successful, or even more efficient. Furthermore, as this system has

been widely used, downstream applications are available, such as Chromatin Immunoprecipitation to reveal binding sites, using an antibody for the GR domain (Yamaguchi et al., 2015).

While the results for *p35s::MYB3R3-GFP-GR* are promising, it is worth noting that while MYB3R3 is a transcription factor (Kobayashi et al., 2015), other cell cycle proteins used in this study, such as SMR2, are not. Therefore, the future application of the GR system to *p35s::SMR2-GFP-GR* will be novel, and will be based solely on the subcellular manipulation of proteins, as opposed to transcriptional activation. This will be revealing for other types of protein and represents a potential broadening of the use of the system.

In conclusion the GR/DEX system is presented here is considered to be a suitable choice for studying the breaking of cell size dependency of regulatory cell cycle proteins.

5. Future work and perspectives

5.1 Continued optimisation of the DEX system

While induction experiments performed in this study demonstrated an effect of MYB3R3 translational induction on cortex cell size, it would be informative to understand exactly when and how the MYB3R3 protein is translocated to the nucleus. Firstly, a time course should be done over the course of several days, using the selected concentration of 100 μ M. As the larger induced MYB3R3 cells were seen after treatment for four days, it would be interesting to image every 24 hours over this time period, to see at which point nuclear GFP signal appears, and whether this is maintained. If the signal diminishes, it could be that mechanisms internal to the cell are degrading the protein. Whichever way, it would be interesting to see how the signal changes over time, and how this relates to phenotypes seen.

Subsequently, a time course should be conducted every 1 hour for 24 hours, to determine speed and saturation of initial induction. A fast response time would be desirable (Zuo and Chua, 2000), allowing for rapid breaking of cell size dependency. Additionally, it would be interesting to assess differences in days at which the seedlings were transferred to DEX, or even germinating on media with DEX. This would help elucidate the roles of MYB3R3 at different stages in development.

In order to ascertain the dynamics of the MYB3R3 localisation before and after DEX treatment, quantification could be carried out on GFP fluorescence before and after induction in different subcellular compartments. To achieve this, a cross could be performed with a nuclear membrane marker line, such as *pKAKU4-KAKU4-RFP* (Goto et al., 2014) to definitively mark the boundary between the nucleus and the cytoplasm. This boundary would allow the ratio of nuclear to cytoplasmic GFP to be quantified. If this cross is successful, the above procedures could be carried out in combination with the optimised induction protocol for fluorescence described above, over a period of time, to reveal the temporal and spatial dynamics of the system in a highly detailed manner.

5.2. Optimise cell analysis procedures to determine cell lengths of all of the cells in the root

This study used cell-o-tape (Section 2.20; French et al., 2012) to semi-autonomously measure cortex cells from confocal microscopy snaps. However, the various other cell types of the root meristem (RM) were not measured. As some cell cycle regulatory proteins have been shown to only affect cell dynamics in certain cell types, as is the case for CYCD4;1 with regard to the pericycle (Nieuwland et al., 2009), it would be a more informative approach to measure all cell types in the RM.

Various technology optimised for RM cell analysis exists to carry this out. Of particular note is iROCS software (Schmidt et al., 2014). The programme has a range of applications including a module for DAPI staining that can be used to measure nuclear size, a common proxy for cell cycle stage (Chen et al., 2017; Takatsuka et al., 2022). Additionally, segmentation analysis can be performed to generate volumes for all stem cells in the RM. However, this requires complex sample preparation which is time limiting, and studies which used different sample preparation methods can give contradictory results as in the analysis of SCL28 (Goldy et al., 2021; Nomoto et al., 2022). Therefore, in order to measure all the cell types in the RM, MorphographX (Barbier de Reuille et al, 2015) could be used instead, to create a 2.5 D projection from a Z-stack, and perform segmentation analysis.

Conducting this analysis could provide important information. Firstly, it would give a clearer and more detailed analysis of the expression of the inducible constructs throughout the root. While in this study, GFP fluorescence was measured (Figure 3.9B), this was only conducted in the plane where the QC and cortex cells were visible (Figure 3.9A). Maximum intensity projections of three-dimensional z stacks did show expression throughout different cell types of the RM (Figure 3.9C), however this was not quantified, and only showed the brightest regions of GFP fluorescence throughout the slices of the stack. Therefore, the optimised programs would provide a much deeper insight into the localisation and intensity of GFP throughout the root. This, correlated with cell size measurements, would indicate the sensitivity of different cell types to the induction system.

5.3 Elucidate the relationship between large induced MYB3R3 cells and cell cycle length

It is expected that the larger cortex cells observed upon MYB3R3 translocation, and the reduction in root biomass over time was a consequence of delays in the cell cycle. Indeed, MYB3R3 activity has been previously linked to longer cell cycle duration in response to salt stress (Okumura et al., 2021), DNA damage (Chen et al., 2017). Under these conditions, plants develop shorter roots, compared to normal conditions, due to a shorter root meristem, as cells enter the elongation zone earlier (Okumura et al., 2021).

As changes in the size of the root meristem could be attributed to two possibilities; reductions in the production of cells, or increases in cell elongation (Nieuwland et al., 2004), kinematic analysis could be performed on the inducible MYB3R3 lines to quantify the number of cells and identify the position relative to the QC in which elongation begins (Nomoto et al., 2022). Furthermore, it would be interesting to examine the overall length of the root meristem, and to correlate this information with the observed increases in cell size, and reduction in root growth.

In order to prepare for measuring cell cycle length, inducible *p35s::MYB3R3-GFP-GR* and *p35s::GFP-GR* lines were crossed with a cell cycle reporter, consisting of a fluorescent plasma membrane marker and a nuclear S-G2-M marker. This cross was performed using Wave131-YFP from the Geldner Lab (Geldner et al., 2009) and pH4::DB-CHERRY which was created in the same manner as PH4:DB:VENUS (Jones et al., 2017). This will not only allow direct measurement of the duration of the cell cycle via timelapse microscopy but will additionally allow size to be measured in dividing cells, compared to those which are not currently in the cell cycle. This could help elucidate the size at which mitosis occurs, but also the size at which cells transition from G1/S, to G2/M. This data together with mass and concentration data of sizer proteins would provide valuable information and links in elucidating cell size control at G2/M.

As tight size control at G1/S has been reported (Jones et al., 2017; D'Ario et al., 2021), it could be possible that any delay in the cell cycle at G2/M could be

compensated for in the subsequent cell cycle, at G1/S. Therefore, to control for this, inducible constructs could be transformed into the background of cell cycle mutants known to have a delayed G1/S phase, such as the *cyclin-d3;1-3* triple loss of function mutant (Jones et al., 2017). This would help ensure that any compensatory changes in the length of the G1 phase of the cell cycle that might mask the effect of delaying the G2/M transition were removed, providing a clearer picture of cell size control at G2/M.

Following on from this, in order to gain deeper insight into the transcriptional network, single cell RNA-seq could be performed (Dorrity et al., 2021) on induced lines in both the mutant and wildtype background, crossed with the cell cycle marker. This would produce individual transcriptomic profiles for cells in different stages of the cell cycle, with and without increased MYB3R3 concentrations. This would also enable comparisons of different cell types across proliferating and differentiating tissues (Zhang et al., 2021). This would be a valuable technique when investigating G2/M phase inhibitors which act in a tissue specific manner, such as the SMR family (Nomoto et al., 2022).

5.4 Further candidate sizer testing using the DEX inducible system

While there is an abundance of important proteins which contribute to regulation at G2/M, this study focused on inhibitors of the cell cycle. *p35s::SMR2-GFP-GR* was screened at T1, and was shown to be functional when induced. Therefore, this construct would logically be the next inducible protein to investigate. As the loss of function mutant, *smr1/2/13* has been shown to have significantly smaller cells in the root and leaves (Nomoto et al., 2022), it would be interesting to see if the opposite is true in the inducible system. Furthermore, SMR2 is of interest due to its association with *SCARECROW-LIKE28 (SCL28)*, a G2/M phase specific GRAS transcription factor (Goldy et al., 2021; Nomoto et al., 2022), which itself is regulated by the binding of upstream MYB proteins to its promoter (Goldy et al., 2021; Nomoto et al., 2022). This protein is of particular interest as there have been contradictory findings in the literature, with an estradiol induction system finding SCL28 to increase cell cycle lengths, indicating it to be an activator (Goldy et al., 2021) and another study reporting that SCL28 overexpression delayed the cell cycle (Nomoto et al., 2022). Therefore, it would be interesting to study a protein downstream of SCL28, such as SMR2 in order to elucidate the network at G2/M further. Additionally, as MYB3R3 and SCL28 are both transcription factors, their manipulation in induction systems aligns with traditional use. On the other hand, the application of GR induction to SMR2 would be a novel use, examining how the trans-localisation of a cell cycle inhibitor, which is not a transcription factor, could have an effect on cell cycle or cell length.

References.

- Albornoz, K., Zhou, J., Beckles, D.M., 2023. Chemical induction of the *Arabidopsis thaliana* CBF1 gene in transgenic tomato fruit to study postharvest chilling injury. *Current Plant Biology* 33, 100275. <https://doi.org/10.1016/j.cpb.2023.100275>.
- Allen, G.C., Flores-Vergara, M.A., Krasynanski, S., Kumar, S., Thompson, W.F., 2006. A modified protocol for rapid DNA isolation from plant tissues using cetyltrimethylammonium bromide. *Nat Protoc* 1, 2320–2325. <https://doi.org/10.1038/nprot.2006.384>.
- Andersen, S.U., Buechel, S., Zhao, Z., Ljung, K., Novák, O., Busch, W., Schuster, C., Lohmann, J.U., 2008. Requirement of B2-Type Cyclin-Dependent Kinases for Meristem Integrity in *Arabidopsis thaliana*. *Plant Cell* 20, 88–100. <https://doi.org/10.1105/tpc.107.054676>
- Aoyama, T. and Chua, N.H. (1997) 'A glucocorticoid-mediated transcriptional induction system in transgenic plants', *The Plant Journal: For Cell and Molecular Biology*, 11(3), pp. 605–612. Available at: <https://doi.org/10.1046/j.1365-313x.1997.11030605.x>.
- Baumberger, N., Baulcombe, D.C., 2005. *Arabidopsis* ARGONAUTE1 is an RNA Slicer that selectively recruits microRNAs and short interfering RNAs. *Proceedings of the National Academy of Sciences* 102, 11928–11933. <https://doi.org/10.1073/pnas.0505461102>.
- Barbier de Reuille, P., Routier-Kierzkowska, A.-L., Kierzkowski, D., Bassel, G.W., Schüpbach, T., Tauriello, G., Bajpai, N., Strauss, S., Weber, A., Kiss, A., Burian, A., Hofhuis, H., Sapala, A., Lipowczan, M., Heimlicher, M.B., Robinson, S., Bayer, E.M., Basler, K., Koumoutsakos, P., Roeder, A.H.K., Aegerter-Wilmsen, T., Nakayama, N., Tsiantis, M., Hay, A., Kwiatkowska, D., Xenarios, I., Kuhlemeier, C., Smith, R.S., 2015. MorphoGraphX: A platform for quantifying morphogenesis in 4D. *Elife* 4, 05864. <https://doi.org/10.7554/eLife.05864>

Beemster, G.T.S., De Veylder, L., Vercruyssen, S., West, G., Rombaut, D., Van Hummelen, P., Galichet, A., Gruijsem, W., Inzé, D., Vuylsteke, M., 2005. Genome-wide analysis of gene expression profiles associated with cell cycle transitions in growing organs of *Arabidopsis*. *Plant Physiol* 138, 734–743.

<https://doi.org/10.1104/pp.104.053884>

Bird, J.E., Marles-Wright, J. and Giachino, A. (2022) 'A User's Guide to Golden Gate Cloning Methods and Standards', *ACS Synthetic Biology*, 11(11), pp. 3551–3563.

Available at: <https://doi.org/10.1021/acssynbio.2c00355>.

Bohner, S., Lenk, I., Rieping, M., Herold, M., Gatz, C., 1999. Technical advance: transcriptional activator TGV mediates dexamethasone-inducible and tetracycline-inactivatable gene expression. *Plant J* 19, 87–95. <https://doi.org/10.1046/j.1365-313x.1999.00503.x>

Boniotti, M.B. and Gutierrez, C. (2001) 'A cell-cycle-regulated kinase activity phosphorylates plant retinoblastoma protein and contains, in *Arabidopsis*, a CDKA/cyclin D complex', *The Plant Journal*, 28(3), pp. 341–350. Available at: <https://doi.org/10.1046/j.1365-313X.2001.01160.x>.

Boruc, J., Mylle, E., Duda, M., De Clercq, R., Rombauts, S., Geelen, D., Hilson, P., Inzé, D., Van Damme, D., Russinova, E., 2010. Systematic Localization of the *Arabidopsis* Core Cell Cycle Proteins Reveals Novel Cell Division Complexes. *Plant Physiology* 152, 553–565. <https://doi.org/10.1104/pp.109.148643>

Boruc, J., Van den Daele, H., Hollunder, J., Rombauts, S., Mylle, E., Hilson, P., Inzé, D., De Veylder, L., Russinova, E., 2010. Functional Modules in the *Arabidopsis* Core Cell Cycle Binary Protein–Protein Interaction Network[W]. *Plant Cell* 22, 1264–1280. <https://doi.org/10.1105/tpc.109.073635>

Boudolf, V., Barrôco, R., Engler, J. de A., Verkest, A., Beeckman, T., Naudts, M., Inzé, D., De Veylder, L., 2004. B1-Type Cyclin-Dependent Kinases Are Essential for the Formation of Stomatal Complexes in *Arabidopsis thaliana*. *The Plant Cell* 16, 945–955.

Bruce, W., Folkerts, O., Garnaat, C., Crasta, O., Roth, B., Bowen, B., 2000. Expression profiling of the maize flavonoid pathway genes controlled by estradiol-inducible transcription factors CRC and P. *Plant Cell* 12, 65–80. <https://doi.org/10.1105/tpc.12.1.65>

Caddick, M.X., Greenland, A.J., Jepson, I., Krause, K.P., Qu, N., Riddell, K.V., Salter, M.G., Schuch, W., Sonnewald, U., Tomsett, A.B., 1998. An ethanol inducible gene switch for plants used to manipulate carbon metabolism. *Nat Biotechnol* 16, 177–180. <https://doi.org/10.1038/nbt0298-177>

Cadepond, F., Schweizer-Groyer, G., Segard-Maurel, I., Jibard, N., Hollenberg, S.M., Giguère, V., Evans, R.M., Baulieu, E.E., 1991. Heat shock protein 90 as a critical factor in maintaining glucocorticosteroid receptor in a nonfunctional state. *Journal of Biological Chemistry* 266, 5834–5841. [https://doi.org/10.1016/S0021-9258\(19\)67673-8](https://doi.org/10.1016/S0021-9258(19)67673-8)

Cai, Y., Wilson, M.L. and Peccoud, J. (2010) ‘GenoCAD for iGEM: a grammatical approach to the design of standard-compliant constructs’, *Nucleic acids research*, 38(8), pp. 2637–2644. Available at: <https://doi.org/10.1093/nar/gkq086>.

Chang, W., Guo, Y., Zhang, H., Liu, X., Guo, L., 2020. Same Actor in Different Stages: Genes in Shoot Apical Meristem Maintenance and Floral Meristem Determinacy in Arabidopsis. *Frontiers in Ecology and Evolution* 8.

Chaudhari, V.R. and Hanson, M.R. (2021) ‘GoldBricks: an improved cloning strategy that combines features of Golden Gate and BioBricks for better efficiency and usability’, *Synthetic Biology*, 6(1), p. ysab032. Available at: <https://doi.org/10.1093/synbio/ysab032>.

Chen, P., Takatsuka, H., Takahashi, N., Kurata, R., Fukao, Y., Kobayashi, K., Ito, M., Umeda, M., 2017. Arabidopsis R1R2R3-Myb proteins are essential for inhibiting cell division in response to DNA damage. *Nat Commun* 8, 635. <https://doi.org/10.1038/s41467-017-00676-4>

Chen, X., Zaro, J.L., Shen, W.-C., 2013. Fusion protein linkers: property, design and functionality. *Adv Drug Deliv Rev* 65, 1357–1369.

<https://doi.org/10.1016/j.addr.2012.09.039>

Chiang, J., Li, I., Pham, E., Truong, K., 2006. FPMOD: A Modeling Tool for Sampling the Conformational Space of Fusion Proteins, in: 2006 International Conference of the IEEE Engineering in Medicine and Biology Society. Presented at the 2006 International Conference of the IEEE Engineering in Medicine and Biology Society, pp. 4111–4114. <https://doi.org/10.1109/IEMBS.2006.259224>

Clough, S.J. and Bent, A.F. (1998) 'Floral dip: a simplified method for *Agrobacterium*-mediated transformation of *Arabidopsis thaliana*', *The Plant Journal: For Cell and Molecular Biology*, 16(6), pp. 735–743. Available at:

<https://doi.org/10.1046/j.1365-313x.1998.00343.x>.

Collier, R., Thomson, J.G., Thilmony, R., 2018. A versatile and robust *Agrobacterium*-based gene stacking system generates high-quality transgenic *Arabidopsis* plants. *The Plant Journal* 95, 573–583. <https://doi.org/10.1111/tpj.13992>

Coudreuse, D. and Nurse, P. (2010) 'Driving the cell cycle with a minimal CDK control network', *Nature*, 468(7327), pp. 1074–1079. Available at:

<https://doi.org/10.1038/nature09543>.

Craft, J., Samalova, M., Baroux, C., Townley, H., Martinez, A., Jepson, I., Tsiantis, M., Moore, I., 2005. New pOp/LhG4 vectors for stringent glucocorticoid-dependent transgene expression in *Arabidopsis*. *Plant J* 41, 899–918.

<https://doi.org/10.1111/j.1365-313X.2005.02342.x>

Cruz-Ramírez, A., Díaz-Triviño, S., Blilou, I., Grieneisen, V.A., Sozzani, R., Zamioudis, C., Miskolczi, P., Nieuwland, J., Benjamins, R., Dhonukshe, P., Caballero-Pérez, J., Horvath, B., Long, Y., Mähönen, A.P., Zhang, H., Xu, J., Murray, J.A.H., Benfey, P.N., Bako, L., Marée, A.F.M., Scheres, B., 2012. A bistable circuit involving SCARECROW-RETINOBLASTOMA integrates cues to inform asymmetric stem cell division. *Cell* 150, 1002–1015.

D'Ario, M. and Sablowski, R. (2019) 'Cell Size Control in Plants', *Annual Review of Genetics*, 53(1), pp. 45–65. Available at: <https://doi.org/10.1146/annurev-genet-112618-043602>.

D'Ario, M., Tavares, R., Schiessl, K., Desvoyes, B., Gutierrez, C., Howard, M., Sablowski, R., 2021. Cell size controlled in plants using DNA content as an internal scale. *Science* 372, 1176–1181. <https://doi.org/10.1126/science.abb4348>

Davis, A.M., Hall, A., Millar, A.J., Darrah, C., Davis, S.J., 2009. Protocol: Streamlined sub-protocols for floral-dip transformation and selection of transformants in *Arabidopsis thaliana*. *Plant Methods* 5, 3. <https://doi.org/10.1186/1746-4811-5-3>

Davis, V.L., Newbold, R.R., Couse, J.F., Rea, S.L., Gallagher, K.M., Hamilton, K.J., Goulding, E.H., Jefferson, W., Eddy, E.M., Bullock, B.C., Korach, K.S., 2012. Expression of a dominant negative estrogen receptor alpha variant in transgenic mice accelerates uterine cancer induced by the potent estrogen diethylstilbestrol. *Reprod Toxicol* 34, 512–521. <https://doi.org/10.1016/j.reprotox.2012.08.005>

Daxinger, L., Hunter, B., Sheikh, M., Jauvion, V., Gascioli, V., Vaucheret, H., Matzke, M., Furner, I., 2008. Unexpected silencing effects from T-DNA tags in *Arabidopsis*. *Trends Plant Sci* 13, 4–6. <https://doi.org/10.1016/j.tplants.2007.10.007>

De Veylder, L., Beeckman, T., Beemster, G., Krols, L., Terras, F., Landrieu, I., Van Der Schueren, E., Maes, S., Naudts, M., Inzé, D., 2001. Functional analysis of cyclin-dependent kinase inhibitors of *Arabidopsis*. *PLANT CELL* 13, 1653–1667. <https://doi.org/10.1105/tpc.13.7.1653>

del Pozo JC, Diaz-Trivino S, Cisneros N, Gutierrez C. 2006. The balance between cell division and endoreplication depends on E2FC-DPB, transcription factors regulated by the ubiquitin-SCFSKP2A pathway in *Arabidopsis*. *Plant Cell* 18(9):2224–35

Desvoyes, B., de Mendoza, A., Ruiz-Trillo, I., Gutierrez, C., 2014. Novel roles of plant RETINOBLASTOMA-RELATED (RBR) protein in cell proliferation and asymmetric cell division. *Journal of Experimental Botany* 65, 2657–2666. <https://doi.org/10.1093/jxb/ert411>

Dorrity, M.W., Alexandre, C.M., Hamm, M.O., Vigil, A.-L., Fields, S., Queitsch, C., Cuperus, J.T., 2021. The regulatory landscape of *Arabidopsis thaliana* roots at single-cell resolution. *Nat Commun* 12, 3334. <https://doi.org/10.1038/s41467-021-23675-y>

Engler, C., Youles, M., Gruetzner, R., Ehnert, T.-M., Werner, S., Jones, J.D.G., Patron, N.J., Marillonnet, S., 2014. A golden gate modular cloning toolbox for plants. *ACS Synth Biol* 3, 839–843. <https://doi.org/10.1021/sb4001504>

Facchetti, G., Chang, F. and Howard, M. (2017) ‘Controlling cell size through sizer mechanisms’, *Current Opinion in Systems Biology*, 5, pp. 86–92. Available at: <https://doi.org/10.1016/j.coisb.2017.08.010>.

Fantes, P.A. (1977) ‘Control of cell size and cycle time in *Schizosaccharomyces pombe*’, *Journal of Cell Science*, 24(1), pp. 51–67. Available at: <https://doi.org/10.1242/jcs.24.1.51>.

Ferreira, P.C. *et al.* (1991) ‘The *Arabidopsis* functional homolog of the p34cdc2 protein Ferreira, P.C., Hemerly, A.S., Villarroel, R., Van Montagu, M., Inzé, D., 1991. The *Arabidopsis* functional homolog of the p34cdc2 protein kinase. *The Plant Cell* 3, 531–540. <https://doi.org/10.1105/tpc.3.5.531>

Forsbach, A., Schubert, D., Lechtenberg, B., Gils, M., Schmidt, R., 2003. A comprehensive characterization of single-copy T-DNA insertions in the *Arabidopsis thaliana* genome. *Plant Mol Biol* 52, 161–176. <https://doi.org/10.1023/a:1023929630687>

French, A.P., Wilson, M.H., Kenobi, K., Dietrich, D., Voß, U., Ubeda-Tomás, S., Pridmore, T.P., Wells, D.M., 2012. Identifying biological landmarks using a novel cell measuring image analysis tool: Cell-o-Tape. *Plant Methods* 8, 7. <https://doi.org/10.1186/1746-4811-8-7>

Geng, X., Mackey, D., 2011. Dose-response to and systemic movement of dexamethasone in the GVG-inducible transgene system in *Arabidopsis*. *Methods Mol Biol* 712, 59–68. https://doi.org/10.1007/978-1-61737-998-7_6

Gibson, D.G., Young, L., Chuang, R.-Y., Venter, J.C., Hutchison, C.A., Smith, H.O., 2009. Enzymatic assembly of DNA molecules up to several hundred kilobases. *Nat Methods* 6, 343–345. <https://doi.org/10.1038/nmeth.1318>

Goto, C., Tamura, K., Fukao, Y., Shimada, T., Hara-Nishimura, I., 2014. The Novel Nuclear Envelope Protein KAKU4 Modulates Nuclear Morphology in *Arabidopsis*[W]. *Plant Cell* 26, 2143–2155. <https://doi.org/10.1105/tpc.113.122168>

Guo, H., Yang, Y., Xue, F., Zhang, H., Huang, T., Liu, W., Liu, H., Zhang, F., Yang, M., Liu, C., Lu, H., Zhang, Y., Ma, L., 2017. Effect of flexible linker length on the activity of fusion protein 4-coumaroyl-CoA ligase::stilbene synthase. *Molecular BioSystems* 13, 598–606. <https://doi.org/10.1039/C6MB00563B>

Günl, M., Liew, E.F., David, K., Putterill, J., 2009. Analysis of a post-translational steroid induction system for GIGANTEA in *Arabidopsis*. *BMC Plant Biology* 9, 141. <https://doi.org/10.1186/1471-2229-9-141>

Green, Michael R. and Joseph Sambrook., 2012. *Molecular Cloning NEW EDITION A Laboratory Manual*, 4th edition, Cold Spring Harbour Laboratory Press.

Grob, S., Grossniklaus, U., 2019. Invasive DNA elements modify the nuclear architecture of their insertion site by KNOT-linked silencing in *Arabidopsis thaliana*. *Genome Biol* 20, 120. <https://doi.org/10.1186/s13059-019-1722-3>

Haga, N., Kato, K., Murase, M., Araki, S., Kubo, M., Demura, T., Suzuki, K., Müller, I., Voß, UJürgens, G., Ito, M., 2007. R1R2R3-Myb proteins positively regulate cytokinesis through activation of KNOLLE transcription in *Arabidopsis thaliana*. *Development* 134, 1101–1110. <https://doi.org/10.1242/dev.02801>

Haga, N., Kobayashi, K., Suzuki, T., Maeo, K., Kubo, M., Ohtani, M., Mitsuda, N., Demura, T., Nakamura, K., Jürgens, G., Ito, M., 2011. Mutations in MYB3R1 and MYB3R4 Cause Pleiotropic Developmental Defects and Preferential Down-Regulation of Multiple G2/M-Specific Genes in *Arabidopsis*1[C][W]. *Plant Physiol* 157, 706–717. <https://doi.org/10.1104/pp.111.180836>

Harashima, H., Dissmeyer, N. and Schnittger, A. (2013) 'Cell cycle control across the eukaryotic kingdom', *Trends in Cell Biology*, 23(7), pp. 345–356. Available at: <https://doi.org/10.1016/j.tcb.2013.03.002>.

Hartley, J.L., Temple, G.F. and Brasch, M.A. (2000) 'DNA cloning using in vitro site-specific recombination', *Genome Research*, 10(11), pp. 1788–1795. Available at: <https://doi.org/10.1101/gr.143000>.

Hemerly, A., Engler, J.deA., Bergounioux, C., Van Montagu, M., Engler, G., Inzé, D., & Ferreira, P. (1995). Dominant negative mutants of the Cdc2 kinase uncouple cell division from iterative plant development. *The EMBO journal*, 14(16), 3925–3936. <https://doi.org/10.1002/j.1460-2075.1995.tb00064.x>

Himanen K, Boucheron E, Vanneste S, de Almeida Engler J, Inzé D, Beekman T. 2002. Auxin-mediated cell cycle activation during early lateral root initiation. *Plant Cell* 14(10):2339–51

Kirschke, E., Goswami, D., Southworth, D., Griffin, P.R., Agard, D.A., 2014. Glucocorticoid receptor function regulated by coordinated action of the Hsp90 and Hsp70 chaperone cycles. *Cell* 157, 1685–1697. <https://doi.org/10.1016/j.cell.2014.04.038>

Ito M. Conservation and diversification of three-repeat Myb transcription factors in plants. *J Plant Res* 2005; 118:61-9; PMID:15703854; [http://dx.doi.org/ 10.1007/s10265-005-0192-8](http://dx.doi.org/10.1007/s10265-005-0192-8)

Jones, A.R., Band, L.R., Murray, J.A.H., 2019. Double or Nothing? Cell Division and Cell Size Control. *Trends in Plant Science* 24, 1083–1093. <https://doi.org/10.1016/j.tplants.2019.09.005>

Jones, A.R., Forero-Vargas, M., Withers, S.P., Smith, R.S., Traas, J., Dewitte, W., Murray, J.A.H., 2017. Cell-size dependent progression of the cell cycle creates homeostasis and flexibility of plant cell size. *Nat Commun* 8, 15060. <https://doi.org/10.1038/ncomms15060>

Klein, J.S., Jiang, S., Galimidi, R.P., Keeffe, J.R., Bjorkman, P.J., 2014. Design and characterization of structured protein linkers with differing flexibilities. *Protein Eng Des Sel* 27, 325–330. <https://doi.org/10.1093/protein/gzu043>

Kobayashi, K., Suzuki, Toshiya, Iwata, E., Nakamichi, N., Suzuki, Takamasa, Chen, P., Ohtani, M., Ishida, T., Hosoya, H., Müller, S., Leviczky, T., Pettkó-Szandtner, A., Darula, Z., Iwamoto, A., Nomoto, M., Tada, Y., Higashiyama, T., Demura, T., Doonan, J.H., Hauser, M.-T., Sugimoto, K., Umeda, M., Magyar, Z., Bögre, L., Ito, M., 2015. Transcriptional repression by MYB3R proteins regulates plant organ growth. *EMBO J* 34, 1992–2007. <https://doi.org/10.15252/embj.201490899>

Konagaya, K., Nanasato, Y. and Taniguchi, T. (2020) 'A protocol for Agrobacterium-mediated transformation of Japanese cedar, Sugi (*Cryptomeria japonica* D. Don) using embryogenic tissue explants', *Plant Biotechnology*, 37(2), pp. 147–156. Available at: <https://doi.org/10.5511/plantbiotechnology.20.0131a>.

Kooter, J.M., Matzke, M.A., Meyer, P., 1999. Listening to the silent genes: transgene silencing, gene regulation and pathogen control. *Trends Plant Sci* 4, 340–347. [https://doi.org/10.1016/s1360-1385\(99\)01467-3](https://doi.org/10.1016/s1360-1385(99)01467-3)

Kumar, N., Harashima, H., Kalve, S., Bramsiepe, J., Wang, K., Sizani, B.L., Bertrand, L.L., Johnson, M.C., Faulk, C., Dale, R., Simmons, L.A., Churchman, M.L., Sugimoto, K., Kato, N., Dassanayake, M., Beemster, G., Schnittger, A., Larkin, J.C., 2015. Functional Conservation in the SIAMESE-RELATED Family of Cyclin-Dependent Kinase Inhibitors in Land Plants. *Plant Cell* 27, 3065–3080.

Krispil, R., Tannenbaum, M., Sarusi-Portuguez, A., Loza, O., Raskina, O., Hakim, O., 2020. The Position and Complex Genomic Architecture of Plant T-DNA Insertions Revealed by 4SEE. *Int J Mol Sci* 21, 2373. <https://doi.org/10.3390/ijms21072373>

Latham, J.R., Wilson, A.K., Steinbrecher, R.A., 2006. The Mutational Consequences of Plant Transformation. *Journal of Biomedicine and Biotechnology* 2006, 1–7. <https://doi.org/10.1155/JBB/2006/25376>

Levesque MP, Vernoux T, Busch W, Cui H, Wang JY, Blilou I, Hassan H, Nakajima K, Matsumoto N, Lohmann JU, Scheres B, Benfey PN. Whole-genome analysis of the SHOOT-ROOT developmental pathway in Arabidopsis. *PLoS Biol.* 2006;4:e249. [PMC free article] [PubMed] [Google Scholar]

Liang, D., White, R.G., Waterhouse, P.M., 2012. Gene Silencing in Arabidopsis Spreads from the Root to the Shoot, through a Gating Barrier, by Template-Dependent, Nonvascular, Cell-to-Cell Movement. *Plant Physiology* 159, 984–1000. <https://doi.org/10.1104/pp.112.197129>

Magyar, Z., Horváth, B., Khan, S., Mohammed, B., Henriques, R., De Veylder, L., Bakó, L., Scheres, B., Bögre, L., 2012. Arabidopsis E2FA stimulates proliferation and endocycle separately through RBR-bound and RBR-free complexes. *EMBO J* 31, 1480–1493. <https://doi.org/10.1038/emboj.2012.13>

Marillonnet, S. and Grützner, R. (2020) ‘Synthetic DNA Assembly Using Golden Gate Cloning and the Hierarchical Modular Cloning Pipeline’, *Current Protocols in Molecular Biology*, 130(1), p. e115. Available at: <https://doi.org/10.1002/cpmb.115>.

Matsunaga, W., Shimura, H., Shirakawa, S., Isoda, R., Inukai, T., Matsumura, T., Masuta, C., 2019. Transcriptional silencing of 35S driven-transgene is differentially determined depending on promoter methylation heterogeneity at specific cytosines in both plus- and minus-sense strands. *BMC Plant Biology* 19, 24.

<https://doi.org/10.1186/s12870-019-1628-y>

Marquès-Bueno, M. del M., Morao, A.K., Cayrel, A., Platre, M.P., Barberon, M., Caillieux, E., Colot, V., Jaillais, Y., Roudier, F., Vert, G., 2016. A versatile Multisite Gateway-compatible promoter and transgenic line collection for cell type-specific functional genomics in *Arabidopsis*. *Plant J* 85, 320–333.

<https://doi.org/10.1111/tpj.13099>

Menges, M. *et al.* (2005) 'Global analysis of the core cell cycle regulators of *Arabidopsis* identifies novel genes, reveals multiple and highly specific profiles of expression and provides a coherent model for plant cell cycle control', *The Plant Journal: For Cell and Molecular Biology*, 41(4), pp. 546–566. Available at:

<https://doi.org/10.1111/j.1365-313X.2004.02319.x>

Meschichi, A., Ingouff, M., Picart, C., Mirouze, M., Desset, S., Gallardo, F., Bystricky, K., Picault, N., Rosa, S., Pontvianne, F., 2021. ANCHOR: A Technical Approach to Monitor Single-Copy Locus Localization in *Planta*. *Front Plant Sci* 12, 677849.

<https://doi.org/10.3389/fpls.2021.677849>

Lampropoulos, A., Sutikovic, Z., Wenzl, C., Maegele, I., Lohmann, J.U., Forner, J., 2013. GreenGate - A Novel, Versatile, and Efficient Cloning System for Plant Transgenesis. *PLoS One* 8, e83043. <https://doi.org/10.1371/journal.pone.0083043>

Levesque, M.P., Vernoux, T., Busch, W., Cui, H., Wang, J.Y., Blilou, I., Hassan, H., Nakajima, K., Matsumoto, N., Lohmann, J.U., Scheres, B., Benfey, P.N., 2006.

Whole-Genome Analysis of the SHORT-ROOT Developmental Pathway in *Arabidopsis*. *PLOS Biology* 4, e143. <https://doi.org/10.1371/journal.pbio.0040143>

Li, M., Jiang, S., Wang, Y., Liu, G., 2006. Post-transcriptional gene silencing signal could move rapidly and bidirectionally in grafted *Arabidopsis thaliana*. CHINESE SCI BULL 51, 313–319. <https://doi.org/10.1007/s11434-006-0313-3>

Magyar, Z., Horváth, B., Khan, S., Mohammed, B., Henriques, R., Veylder, L.D., Bakó, L., Scheres, B., Bögre, L., 2012. *Arabidopsis* E2FA stimulates proliferation and endocycle separately through RBR-bound and RBR-free complexes. The EMBO Journal. <https://doi.org/10.1038/emboj.2012.13>

Morel, J.-B., Godon, C., Mourrain, P., Béclin, C., Boutet, S., Feuerbach, F., Proux, F., Vaucheret, H., 2002. Fertile Hypomorphic ARGONAUTE (*ago1*) Mutants Impaired in Post-Transcriptional Gene Silencing and Virus Resistance. The Plant Cell 14, 629–639. <https://doi.org/10.1105/tpc.010358>

Mortimer, C.L., Dugdale, B., Dale, J.L., 2015. Updates in inducible transgene expression using viral vectors: from transient to stable expression. Current Opinion in Biotechnology, Food Biotechnology • Plant Biotechnology 32, 85–92. <https://doi.org/10.1016/j.copbio.2014.11.009>

Nieuwland, J. *et al.* (2009) 'The D-type cyclin CYCD4;1 modulates lateral root density in *Arabidopsis* by affecting the basal meristem region', *Proceedings of the National Academy of Sciences*, 106(52), pp. 22528–22533. Available at: <https://doi.org/10.1073/pnas.0906354106>.

Nomoto, Y. *et al.* (2022) 'A hierarchical transcriptional network activates specific CDK inhibitors that regulate G2 to control cell size and number in *Arabidopsis*'. Nat Commun 13, 1660. <https://doi.org/10.1038/s41467-022-29316-2>

Nowack, M.K., Grini, P.E., Jakoby, M.J., Lafos, M., Koncz, C., Schnittger, A., 2006. A positive signal from the fertilization of the egg cell sets off endosperm proliferation in angiosperm embryogenesis. Nat Genet 38, 63–67. <https://doi.org/10.1038/ng1694>

Nowack, M.K., Harashima, H., Dissmeyer, N., Zhao, X., Bouyer, D., Weimer, A.K., De Winter, F., Yang, F., Schnittger, A., 2012. Genetic Framework of Cyclin-Dependent Kinase Function in Arabidopsis. *Developmental Cell* 22, 1030–1040. <https://doi.org/10.1016/j.devcel.2012.02.015>

Okumura, T., Nomoto, Y., Kobayashi, K., Suzuki, T., Takatsuka, H., Ito, M., 2021. MYB3R-mediated active repression of cell cycle and growth under salt stress in *Arabidopsis thaliana*. *J Plant Res* 134, 261–277. <https://doi.org/10.1007/s10265-020-01250-8>

Okushima Y, Shimizu K, Ishida T, Sugimoto K, Umeda M. 2014. Differential regulation of B2-type CDK accumulation in *Arabidopsis* roots. *Plant Cell Rep.* 33(7):1033–40

Polóniová, Z., Dubnický, P., Gálová, Z., Libantova, J., Ildikó, Matušíková, Moravčíková, J., 2013. PLANT TRANSFORMATION VECTORS AND THEIR STABILITY IN *AGROBACTERIUM TUMEFACIENS*.

Porceddu A, Stals H, Reichheld J-P, Segers G, De Veylder L, De Pinho Barrôco R, Casteels P, Van Montagu M, Inzé D, Mironov V (2001) A plant-specific cyclin-dependent kinase is involved in the control of G2/M progression in plants. *J Biol Chem* 276 : 36354–36360.

Potapov, V., Ong, J.L., Kucera, R.B., Langhorst, B.W., Bilotti, K., Pryor, J.M., Cantor, E.J., Canton, B., Knight, T.F., Evans, T.C.Jr., Lohman, G.J.S., 2018. Comprehensive Profiling of Four Base Overhang Ligation Fidelity by T4 DNA Ligase and Application to DNA Assembly. *ACS Synth. Biol.* 7, 2665–2674. <https://doi.org/10.1021/acssynbio.8b00333>

Pryor, J.M., Potapov, V., Kucera, R.B., Bilotti, K., Cantor, E.J., Lohman, G.J.S., 2020. Enabling one-pot Golden Gate assemblies of unprecedented complexity using data-optimized assembly design. *PLoS One* 15, e0238592. <https://doi.org/10.1371/journal.pone.0238592>

Proulx-Giraldeau, F., Skotheim, J.M. and François, P. (no date) 'Evolution of cell size control is canalized towards adders or sizers by cell cycle structure and selective pressures', *eLife*, 11, p. e79919. Available at: <https://doi.org/10.7554/eLife.79919>.

Rahni, R., Birnbaum, K.D., 2019. Week-long imaging of cell divisions in the Arabidopsis root meristem. *Plant Methods* 15, 30. <https://doi.org/10.1186/s13007-019-0417-9>

Riou-Khamlichi, C., Huntley, R., Jacquard, A., Murray, J.A.H., 1999. Cytokinin Activation of Arabidopsis Cell Division Through a D-Type Cyclin. *Science* 283, 1541–1544. <https://doi.org/10.1126/science.283.5407.1541>

Rizk, M., Antranikian, G., Elleuche, S., 2016. Influence of Linker Length Variations on the Biomass-Degrading Performance of Heat-Active Enzyme Chimeras. *Mol Biotechnol* 58, 268–279. <https://doi.org/10.1007/s12033-016-9925-2>

Roberts, G.R., Garoosi, G.A., Koroleva, O., Ito, M., Laufs, P., Leader, D.J., Caddick, M.X., Doonan, J.H., Tomsett, A.B., 2005. The alc-GR System. A Modified alc Gene Switch Designed for Use in Plant Tissue Culture. *Plant Physiol* 138, 1259–1267. <https://doi.org/10.1104/pp.105.059659>

Rodriguez, E., Chevalier, J., Ghoul, H.E., Voldum-Clausen, K., Mundy, J., Petersen, M., 2018. DNA damage as a consequence of NLR activation. *PLOS Genetics* 14, e1007235. <https://doi.org/10.1371/journal.pgen.1007235>

Roslan, H.A., Salter, M.G., Wood, C.D., White, M.R., Croft, K.P., Robson, F., Coupland, G., Doonan, J., Laufs, P., Tomsett, A.B., Caddick, M.X., 2001. Characterization of the ethanol-inducible alc gene-expression system in Arabidopsis thaliana. *Plant J* 28, 225–235. <https://doi.org/10.1046/j.1365-313x.2001.01146.x>

Sabourin, M., Tuzon, C.T., Fisher, T.S., Zakian, V.A., 2007. A flexible protein linker improves the function of epitope-tagged proteins in Saccharomyces cerevisiae. *Yeast* 24, 39–45. <https://doi.org/10.1002/yea.1431>

Sachdev, D., Chirgwin, J.M., 1998. Solubility of proteins isolated from inclusion bodies is enhanced by fusion to maltose-binding protein or thioredoxin. *Protein Expr Purif* 12, 122–132. <https://doi.org/10.1006/prep.1997.0826>

Samalova, M., Brzobohaty, B., Moore, I., 2005. pOp6/LhGR: a stringently regulated and highly responsive dexamethasone-inducible gene expression system for tobacco. *The Plant Journal* 41, 919–935. <https://doi.org/10.1111/j.1365-313X.2005.02341.x>

Sanz L, Dewitte W, Forzani C, Patell F, Nieuwland J, et al. 2011. The Arabidopsis D-type cyclin CYCD2;1 and the inhibitor ICK2/KRP2 modulate auxin-induced lateral root formation. *Plant Cell* 23(2):641–60

Sarrion-Perdigones, A., Falconi, E.E., Zandalinas, S.I., Juárez, P., Fernández-del-Carmen, A., Granell, A., Orzaez, D., 2011. GoldenBraid: an iterative cloning system for standardized assembly of reusable genetic modules. *PLoS One* 6, e21622. <https://doi.org/10.1371/journal.pone.0021622>

Schmidt, T., Pasternak, T., Liu, K., Blein, T., Aubry-Hivet, D., Dovzhenko, A., Duerr, J., Teale, W., Ditengou, F.A., Burkhardt, H., Ronneberger, O., Palme, K., 2014. The iRoCS Toolbox – 3D analysis of the plant root apical meristem at cellular resolution. *The Plant Journal* 77, 806–814. <https://doi.org/10.1111/tpj.12429>

Schmoller, K.M. *et al.* (2015) ‘Dilution of the cell cycle inhibitor Whi5 controls budding- Schmoller, K.M., Turner, J.J., Kõivomägi, M., Skotheim, J.M., 2015. Dilution of the cell cycle inhibitor Whi5 controls budding-yeast cell size. *Nature* 526, 268–272. <https://doi.org/10.1038/nature14908>

Schlücking, K., Edel, K.H., Köster, P., Drerup, M.M., Eckert, C., Steinhorst, L., Waadt, R., Batistič, O., Kudla, J., 2013. A New β -Estradiol-Inducible Vector Set that Facilitates Easy Construction and Efficient Expression of Transgenes Reveals CBL3-Dependent Cytoplasm to Tonoplast Translocation of CIPK5. *Molecular Plant* 6, 1814–1829. <https://doi.org/10.1093/mp/sst065>

Schubert, D., Lechtenberg, B., Forsbach, A., Gils, M., Bahadur, S., Schmidt, R., 2004. Silencing in Arabidopsis T-DNA Transformants: The Predominant Role of a Gene-Specific RNA Sensing Mechanism versus Position Effects. *The Plant Cell* 16, 2561–2572.

Schürholz, A.-K., López-Salmerón, V., Li, Z., Forner, J., Wenzl, C., Gaillochet, C., Augustin, S., Barro, A.V., Fuchs, M., Gebert, M., Lohmann, J.U., Greb, T., Wolf, S., 2018. A Comprehensive Toolkit for Inducible, Cell Type-Specific Gene Expression in Arabidopsis. *Plant Physiology* 178, 40–53. <https://doi.org/10.1104/pp.18.00463>

Serrano-Mislata, A., Schiessl, K. and Sablowski, R. (2015) 'Active Control of Cell Size Generates Spatial Detail during Plant Organogenesis', *Current biology: CB*, 25(22), pp. 2991–2996. Available at: <https://doi.org/10.1016/j.cub.2015.10.008>.

Spakman, D., King, G.A., Peterman, E.J.G., Wuite, G.J.L., 2020. Constructing arrays of nucleosome positioning sequences using Gibson Assembly for single-molecule studies. *Sci Rep* 10, 9903. <https://doi.org/10.1038/s41598-020-66259-4>

Struhl, K. (1991) 'Subcloning of DNA Fragments', *Current Protocols in Molecular Biology*, 13(1), p. 3.16.1-3.16.2. Available at: <https://doi.org/10.1002/0471142727.mb0316s13>.

Tang, W., Collver, H., Kinken, K., 2004. Dexamethasone-Inducible Green Fluorescent Protein Gene Expression in Transgenic Plant Cells. *Genomics Proteomics Bioinformatics* 2, 15–23. [https://doi.org/10.1016/S1672-0229\(04\)02003-0](https://doi.org/10.1016/S1672-0229(04)02003-0)

Sugiyama, H., Goto, Y., Kondo, Y., Coudreuse, D., Aoki, K., 2023. Live-cell imaging provides direct evidence for a threshold in CDK activity at the G2/M transition. <https://doi.org/10.1101/2023.03.26.534249>

Sultan, I., Keawsompong, S., 2020. Formulation of an Efficient Combinatorial Cellulase Cocktail by Comparative Analysis of Gibson Assembly and NEBuilder HiFi DNA Assembly Modus Operandi.

Takahashi, N., Ogita, N., Takahashi, T., Taniguchi, S., Tanaka, M., Seki, M., Umeda, M., 2019. A regulatory module controlling stress-induced cell cycle arrest in Arabidopsis. *eLife* 8, e43944. <https://doi.org/10.7554/eLife.43944>

Takatsuka, H., Ohno, R. and Umeda, M. (2009) 'The Arabidopsis cyclin-dependent kinase-activating kinase CDKF;1 is a major regulator of cell proliferation and cell expansion but is dispensable for CDKA activation', *The Plant Journal*, 59(3), pp. 475–487. Available at: <https://doi.org/10.1111/j.1365-313X.2009.03884.x>.

Taylor, G.M., Mordaka, P.M. and Heap, J.T. (2019) 'Start-Stop Assembly: a functionally scarless DNA assembly system optimized for metabolic engineering', *Nucleic Acids Research*, 47(3), p. e17. Available at: <https://doi.org/10.1093/nar/gky1182>.

Thomas, S., Maynard, N.D., Gill, J., 2015. DNA library construction using Gibson Assembly®. *Nat Methods* 12, i–ii. <https://doi.org/10.1038/nmeth.f.384>

Van Leene, J., Hollunder, J., Eeckhout, D., Persiau, G., Van De Slijke, E., Stals, H., Van Isterdael, G., Verkest, A., Neiryneck, S., Buffel, Y., De Bodt, S., Maere, S., Laukens, K., Pharazyn, A., Ferreira, P.C.G., Eloy, N., Renne, C., Meyer, C., Faure, J.-D., Steinbrenner, J., Beynon, J., Larkin, J.C., Van de Peer, Y., Hilson, P., Kuiper, M., De Veylder, L., Van Onckelen, H., Inzé, D., Witters, E., De Jaeger, G., 2010. Targeted interactomics reveals a complex core cell cycle machinery in Arabidopsis thaliana. *Mol Syst Biol* 6, 397. <https://doi.org/10.1038/msb.2010.53>

Verkest, A., Manes, C.-L. de O., Vercruyssen, S., Maes, S., Van Der Schueren, E., Beeckman, T., Genschik, P., Kuiper, M., Inzé, D., De Veylder, L., 2005. The Cyclin-Dependent Kinase Inhibitor KRP2 Controls the Onset of the Endoreduplication Cycle during Arabidopsis Leaf Development through Inhibition of Mitotic CDKA;1 Kinase Complexes. *Plant Cell* 17, 1723–1736. <https://doi.org/10.1105/tpc.105.032383>

Vaucheret, H., Béclin, C., Elmayan, T., Feuerbach, F., Godon, C., Morel, J.-B., Mourrain, P., Palauqui, J.-C., Vernhettes, S., 1998. Transgene-induced gene silencing in plants. *The Plant Journal* 16, 651–659. <https://doi.org/10.1046/j.1365-313x.1998.00337.x>

Weber, E., Engler, C., Gruetzner, R., Werner, S., Marillonnet, S., 2011. A modular cloning system for standardized assembly of multigene constructs. *PLoS One* 6, e16765. <https://doi.org/10.1371/journal.pone.0016765>

Weimer, A.K., Biedermann, S., Harashima, H., Roodbarkelari, F., Takahashi, N., Foreman, J., Guan, Y., Pochon, G., Heese, M., Van Damme, D., Sugimoto, K., Koncz, C., Doerner, P., Umeda, M., Schnittger, A., 2016. The plant-specific CDKB1-CYCB1 complex mediates homologous recombination repair in Arabidopsis. *EMBO J* 35, 2068–2086. <https://doi.org/10.15252/embj.201593083>

Wildwater, M., Campilho, A., Perez-Perez, J.M., Heidstra, R., Blilou, I., Korthout, H., Chatterjee, J., Mariconti, L., Grissem, W., Scheres, B., 2005. The RETINOBLASTOMA-RELATED Gene Regulates Stem Cell Maintenance in Arabidopsis Roots. *Cell* 123, 1337–1349. <https://doi.org/10.1016/j.cell.2005.09.042>

William, D.A., Su, Y., Smith, M.R., Lu, M., Baldwin, D.A., Wagner, D., 2004. Genomic identification of direct target genes of LEAFY. *Proc Natl Acad Sci U S A* 101, 1775–1780. <https://doi.org/10.1073/pnas.0307842100>

Williamson, D., Tasker-Brown, W., Murray, J.A.H., Jones, A.R., Band, L.R., 2023. Modelling how plant cell-cycle progression leads to cell size regulation. *PLOS Computational Biology* 19, e1011503. <https://doi.org/10.1371/journal.pcbi.1011503>

Willis, L., Jönsson, H. and Huang, K.C. (2019) 'Limits and constraints on mechanisms of cell-cycle regulation imposed by cell size homeostasis measurements'. *bioRxiv*, p. 720292. Available at: <https://doi.org/10.1101/720292>.

Yamada, K.J., Takatsuka, H., Hirota, J., Mineta, K., Nomoto, Y., Ito, M., 2022. Members of SIAMESE-RELATED Class Inhibitor Proteins of Cyclin-Dependent Kinase Retard G2 Progression and Increase Cell Size in *Arabidopsis thaliana*. *Life (Basel)* 12, 1356. <https://doi.org/10.3390/life12091356>

Yamaguchi, N., Winter, C.M., Wellmer, F., Wagner, D., 2015. Identification of Direct Targets of Plant Transcription Factors Using the GR Fusion Technique. *Methods Mol Biol* 1284, 123–138. https://doi.org/10.1007/978-1-4939-2444-8_6

Yi, D., Alvim Kamei, C.L., Cools, T., Vanderauwera, S., Takahashi, N., Okushima, Y., Eekhout, T., Yoshiyama, K.O., Larkin, J., Van den Daele, H., Conklin, P., Britt, A., Umeda, M., De Veylder, L., 2014. The *Arabidopsis* SIAMESE-RELATED Cyclin-Dependent Kinase Inhibitors SMR5 and SMR7 Regulate the DNA Damage Checkpoint in Response to Reactive Oxygen Species. *The Plant Cell* 26, 296–309. <https://doi.org/10.1105/tpc.113.118943>

Yu, K., Liu, C., Kim, B.-G., Lee, D.-Y., 2015. Synthetic fusion protein design and applications. *Biotechnology Advances* 33, 155–164. <https://doi.org/10.1016/j.biotechadv.2014.11.005>

Zatulovskiy, E., Zhang, S., Berenson, D.F., Topacio, B.R., Skotheim, J.M., 2020. Cell growth dilutes the cell cycle inhibitor Rb to trigger cell division. *Science* 369, 466–471. <https://doi.org/10.1126/science.aaz6213>

Zhang, T.-Q., Chen, Y., Wang, J.-W., 2021. A single-cell analysis of the *Arabidopsis* vegetative shoot apex. *Developmental Cell* 56, 1056-1074.e8. <https://doi.org/10.1016/j.devcel.2021.02.021>

Zhao X, Harashima H, Dissmeyer N, Pusch S, Weimer AK, Bramsiepe J, et al. A general G1/S-phase cell-cycle control module in the flowering plant *Arabidopsis thaliana*. *PLoS Genet.* 2012; 8(8):e1002847. pmid:22879821

Zhao, Y., Han, J., Tan, J., Yang, Y., Li, S., Gou, Y., Luo, Y., Li, T., Xiao, W., Xue, Y., Hao, Y., Xie, X., Liu, Y.-G., Zhu, Q., 2022. Efficient assembly of long DNA fragments and multiple genes with improved nickase-based cloning and Cre/loxP recombination. *Plant Biotechnology Journal* 20, 1983–1995.
<https://doi.org/10.1111/pbi.13882>

Zuo, J. and Chua, N.-H. (2000) 'Chemical-inducible systems for regulated expression of plant genes', *Current Opinion in Biotechnology*, 11(2), pp. 146–151. Available at: [https://doi.org/10.1016/S0958-1669\(00\)00073-2](https://doi.org/10.1016/S0958-1669(00)00073-2).

Zuo, J., Niu, Q.-W. and Chua, N.-H. (2000) 'An estrogen receptor-based transactivator XVE mediates highly inducible gene expression in transgenic plants', *The Plant Journal*, 24(2), pp. 265–273. Available at: <https://doi.org/10.1046/j.1365-313x.2000.00868.x>.

Appendices.

1.1 Libraries used for boxplots on R studio

```
# Libraries
library(ggplot2)
library(tidyverse)
library(hrbrthemes)
library(viridis)
```

1.2 Boxplot command for all cortex cell sizes

```
# Command to code DEX concentration as a categorical factor
```

```
> dframe1$Factordex <- as.factor(dframe1$dex)
```

```
# Command for boxplot of all genotypes at all concentraions using natural logarithm
of cortex cell length, where e is the base
```

```
> ggplot(data = dframe1, mapping = aes(x = Factordex, y = log(length), fill =
factor(line))) +
+ geom_boxplot() +
+ labs(fill = "Line") +
+ scale_x_discrete(name = "Dex", limits=c("0","10","30","50", "100", "200")) +
+ scale_y_continuous(name ="Length") +
+ scale_fill_brewer(palette="BuPu") +
+ theme_classic() +
+ theme(text=element_text(size=14))
```

1.3 Commands used for individual cortex cell size boxplots

Commands to subset the data

```
> dframe2 <- subset(dframe1, line=="col")
> dframe2 <- subset(dframe1, line=="7231")
> dframe2 <- subset(dframe1, line=="133")
```

Command used for cortex cell boxplots for individual genotype

```
> ggplot(data = dframe2, mapping = aes(x = Factordex, y = log(length),
fill=Factordex)) +
+ geom_boxplot() +
+ scale_x_discrete(name = "Dex", limits=c("0","10","30","50", "100", "200")) +
+ scale_fill_viridis_d() +
+ theme_classic()
```

1.4 Libraries used for One-Way ANOVA and Tukey's post hoc HSD tests

```
library(lme4)
library(lmerTest)
library(multcomp)
```

1.5 Linear regression for cortex cell boxplots, all genotypes and DEX concentrations

make Col-0 the base

```
> dframe1$line=relevel(factor(dframe1$line),"col")
```

Analysis

```
> model <- lm(log(length) ~ line + dex + line:dex, data=dframe1)
> summary(model)
> plot(model)
```

1.6 Linear regression for subset cortex cell sizes

```
# subset the data to look at each line and condition individually
```

```
> dframe2 = subset(dframe1, dex=="0")
```

```
> dframe2 = subset(dframe1, dex=="100")
```

```
# Analysis
```

```
dframe2$Factorline <- as.factor(dframe2$line)
```

```
model <- lm(formula = log(length) ~ Factorline, data = dframe2)
```

```
> summary(model)
```

```
> plot(model)
```

```
> posthoc = glht(model,  
  linfct = mcp(Factorline="Tukey"))
```

```
> mcs = summary(posthoc,  
  test=adjusted("single-step"))
```

```
> mcs
```

```
> cld(mcs, level=0.05,  
  decreasing=TRUE)
```

1.7 Linear regression for subset cortex cell sizes

```
> dframe2 <- subset(dframe1, line=="col")
```

```
> dframe2 <- subset(dframe1, line=="7231")
```

```
> dframe2 <- subset(dframe1, line=="133")
```

```
> dframe2$Factordex <- as.factor(dframe2$dex)
model <- lm(formula = log(length) ~ Factordex, data = dframe2)
```

```
summary(model)
```

```
plot(model)
```

```
> posthoc = glht(model,
  linfct = mcp(Factorline="Tukey"))
```

```
> mcs = summary(posthoc,
  test=adjusted("single-step"))
```

```
> mcs
```

```
> cld(mcs, level=0.05,
  decreasing=TRUE)
```

1.8 Calculation of relative root growth (RRG)

```
# upload data
> dt=read.csv(file.choose(), header=TRUE, stringsAsFactors=TRUE)

# calculate the means for each combination of line and dex
> means=tapply(dt$length, list(dt$dex,dt$line), mean, na.rm=TRUE, simplify=TRUE)

# list means
> print(means)

# calculate the means at the zero point for each genotype
> means_zero = means[1,]

# make table of lengths

> tab=xtabs(length~Rep+line+factor(dex), dt)

> tab=xtabs(Growth~Genotype+factor(Dex), dt)

# change zeroes to NAs

> tab[tab==0]<- NA

> print(tab)

# subtract means_zero away from each value

> deviations=sweep(tab, MARGIN=c(2,3), STATS=means_zero, FUN="-")
> print(deviations)

# change array to data.frame
```

```
> devDF=as.data.frame(deviations)
```

1.9 Calculating error bars

```
library(Rmisc)
```

```
library(plyr)
```

```
> devDF=as.data.frame(tab)
```

```
> summarySE(dt, measurevar="Growth", groupvars=c("Dex, Genotype"),  
na.rm=TRUE)
```

```
> devDFc <- summarySE(devDF, measurevar="Growth", groupvars=c("Dex",  
"Genotype"))
```

```
> data=dframe1
```

```
> summarySE(data=dframe1, measurevar="Growth", groupvars=c("Dex",  
"Genotype"))
```

```
> summarySE(data=dframe1, dataNA, measurevar="Growth", groupvars=c("Dex",  
"Genotype"), na.rm=TRUE)
```

```
> cdt <- ddply(dt, c("Dex", "Genotype"), summarise,  
  N = length(Growth),  
  mean = mean(Growth),  
  sd = sd(Growth),  
  se = sd/sqrt(N)
```

```
cdt
```

```
dtNA <- dt
```

```
dtNA$Growth[]
```

```
> summarySE(data=dtNA, measurevar="Growth", groupvars=c("Dex", "Genotype"),  
na.rm=TRUE)
```

```
# code for standard error final
```

```
> dt=read.csv(file.choose(), header=TRUE, stringsAsFactors=TRUE)
```

```
> summary(dt)
```

```
> dtc <- summarySE(data=dtNA, measurevar="Growth", groupvars=c("Dex",  
"Genotype"), na.rm=TRUE)
```

```
summary(dtc)
```

```
print(dtc)
```

1.10 Plotting line graph for RRG

```
> ggplot(dtc, aes(x=Dex, y=Growth, colour=Genotype)) +  
  geom_errorbar(aes(ymin=Growth-se, ymax=Growth+se), width=0.1) +  
  geom_line() +  
  geom_point()
```

1.11 Linear regression for RRG values

```
model<-lm(Growth ~ Dex + Genotype, Dex:Genotype, data = dframe1)
```

1.12 Subset linear regressions

```
> dframe2 = subset(dframe1, Genotype=="7231")
```

```
> dframe2 = subset(dframe1, Genotype=="col")
```

```
> model <- lm(Growth ~ FactorDex, data=dframe2)
```

Tukeys post-hoc HSD tests conducted as in 1.5

1.13 Plotting Boxplot Graph of RRG

Using packages in Appendices 1.1

```
> ggplot(data = devDF, mapping = aes(x = dex, y =length, fill=line)) +  
  geom_boxplot() +  
  scale_x_discrete(name = "Dex", limits=c("0","10","30","50", "100")) +  
  scale_fill_viridis_d() +  
  theme_classic() +  
  theme(legend.key.size = unit(0.9, 'cm'),  
        legend.key.height = unit(0.9, 'cm'), #change legend key height  
        legend.key.width = unit(0.9, 'cm'), #change legend key width  
        legend.title = element_text(size=14), #change legend title font size  
        legend.text = element_text(size=10))
```